IODP
INTERNATIONAL OCEAN DISCOVERY PROGRAM

# International Ocean Discovery Program Expedition 402 Preliminary Report

## Tyrrhenian Continent–Ocean Transition: Tyrrhenian Magmatism and Mantle Exhumation (TIME)

**9 February–8 April 2024**

Alberto Malinverno, Nevio Zitellini, Emily R. Estes, and the Expedition 402 Scientists

## Publisher's notes

Core samples and the wider set of data from the science program covered in this report are under moratorium and accessible only to Science Party members until 8 April 2025.

This publication was prepared by the *JOIDES Resolution* Science Operator (JRSO) at Texas A&M University (TAMU) as an account of work performed under the International Ocean Discovery Program (IODP). This material is based upon work supported by the JRSO, which is a major facility funded by the National Science Foundation Cooperative Agreement Number OCE1326927. Funding for IODP is provided by the following international partners:

National Science Foundation (NSF), United States
Ministry of Education, Culture, Sports, Science and Technology (MEXT), Japan
European Consortium for Ocean Research Drilling (ECORD)
Ministry of Science and Technology (MOST), People's Republic of China
Australia-New Zealand IODP Consortium (ANZIC)
Ministry of Earth Sciences (MoES), India

Portions of this work may have been published in whole or in part in other IODP documents or publications.

### Disclaimer



### Copyright



### Citation

Malinverno, A., Zitellini, N., and Estes, E.R., 2025. Expedition 402 Preliminary Report: Tyrrhenian Continent–Ocean Transition. International Ocean Discovery Program. https://doi.org/10.14379/iodp.pr.402.2025

### ISSN

World Wide Web: 2372-9562

January 2025

# Expedition 402 participants

## Expedition 402 scientists


**Alberto Malinverno**
**Co-Chief Scientist**
Lamont-Doherty Earth Observatory
Columbia University
USA
**alberto@ldeo.columbia.edu**

**Nevio Zitellini**
**Co-Chief Scientist**
Institute of Marine Sciences (ISMAR)
National Research Council
Italy
**nevio.zitelllini@bo.ismar.cnr.it**

**Emily R. Estes**
**Expedition Project Manager/Staff Scientist**
International Ocean Discovery Program
Texas A&M University
USA
**estes@iodp.tamu.edu**

**Noriaki Abe**
**Physical Properties Specialist**
Tono Geoscience Center
Japan Atomic Energy Agency (JAEA)
Japan
**abe.noriaki@jaea.go.jp**

**Norikatsu Akizawa**
**Igneous Geochemist**
Atmosphere and Ocean Research Institute
University of Tokyo
Japan
**akizawa@aori.u-tokyo.ac.jp**

**Manon Bickert**
**Structural Geologist/Petrologist**
Geo-Ocean
University Brest, CNRS, Ifremer
France
**manon.bickert@ifremer.fr**

**Emily H. Cunningham**
**Igneous Geochemist**
Department of Geology and Geophysics
University of Utah
USA
**emily.h.cunningham@utah.edu**

**Agata Di Stefano**
**Micropaleontologist/Nannofossils**
Department of Biological, Geological and Environmental Science
Earth Science Division
University of Catania
Italy
**agata.distefano@unict.it**

**Irina Y. Filina**
**Physical Properties Specialist**
Earth and Atmospheric Sciences
University of Nebraska, Lincoln
USA
**ifilina2@unl.edu**

**Qi Fu**
**Inorganic Geochemist**
Department of Earth and Atmospheric Sciences
University of Houston
USA
**qfu5@central.uh.edu**

**Swanne Gontharet**
**Organic Geochemist**
Laboratoire d'Océanographie et du Climat: Expérimentations et Approches Numériques
Sorbonne Université
France
**swanne.gontharet@locean.ipsl.fr**

**Lorna E. Kearns**
**Sedimentologist**
Institute for Geophysics
University of Texas at Austin
USA
**lorna.kearns@austin.utexas.edu**

**Ravi Kiran Koorapati**
**Micropaleontologist/Planktic Foraminifera**
Department of Earth Sciences
Binghamton University
USA
**rkoorap1@binghamton.edu**

**Chao Lei**
**Structural Geologist/Petrologist**
College of Marine Science and Engineering
China University of Geosciences, Wuhan
China
**clei@cug.edu.cn**

**Maria Filomena Loreto**
**Physical Properties Specialist**
Institute of Marine Sciences (ISMAR)
National Research Council
Italy
**filomena.loreto@bo.ismar.cnr.it**

**Luca Magri**
**Sedimentologist**
Institute for Marine and Antarctic Studies (IMAS)
University of Tasmania
Australia
**luca.magri@utas.edu.au**

**Walter Menapace**
**Sedimentologist**
Marine Geotechnics
MARUM-University of Bremen
Germany

Also at
Department of Marine Geosciences
ICM-CSIC
Spain
**wmenapace@marum-alumni.de**

**Tomoaki Morishita**
**Igneous Petrologist**
School of Geosciences and Civil Engineering
College of Science and Engineering
Kanazawa University
Japan
**moripta@staff.kanazawa-u.ac.jp**

**Ashutosh Pandey**
**Igneous Petrologist**
School of Earth, Environmental and Sustainability Sciences
Indian Institute of Science Education and Research
Thiruvananthapuram
India
**ashutp@iisertvm.ac.in**

**Victoria L. Pavlovics**
**Paleomagnetist**
Department of Geology and Geophysics
University of Utah
USA
**v.pavlovics@utah.edu**

**Philippe A. Pezard**
**Petrophysicist**
Geosciences Montpellier, CNRS
France
**philippe.pezard@umontpellier.fr**

**Eirini M. Poulaki**
**Metamorphic Petrologist**
Rosenstiel School of Marine and Atmospheric Sciences
University of Miami
USA
**epoulaki@miami.edu**

**Milena A. Rodriguez-Pilco**
**Microbiologist**
Marine Biology
Texas A&M University at Galveston
USA
**mrodriguezp@tamu.edu**

**Alessio Sanfilippo**
**Igneous Petrologist/Observer**
Department of Earth and Environmental Science
University of Pavia
Italy
**alessio.sanfilippo@unipv.it**

**Brandon D. Shuck**
**Physical Properties Specialist/Downhole Measurements**
Lamont-Doherty Earth Observatory
Columbia University
USA
**bshuck@ldeo.columbia.edu**

**Paola Vannucchi**
**Structural Geologist/Petrologist/Observer**
Earth Sciences Department
University of Florence
Italy
**paola.vannucchi@unifi.it**

**Xiangyu Zhao**
**Paleomagnetist**
School of Oceanography
Shanghai Jiao Tong University
China
**xy.zhao@sjtu.edu.cn**

## Outreach

**Tessa L. Peixoto**
**Outreach Officer**
USA
**tessa.peixoto@gmail.com**

**Larkin Bohn**
**Outreach Officer**
USA
**larkin.bohn@gmail.com**

# Operational and technical staff

## Siem Offshore AS officials

**Jacob Robinson**
Master of the Drilling Vessel

**Glenn Barrett**
Drilling Supervisor

## JRSO shipboard personnel and technical representatives

**Alejandro Avila Santis**
Marine Laboratory Specialist

**James Brattin**
Applications Developer

**Kristin Bronk**
Marine Laboratory Specialist

**William Cary**
Applications Developer

**Lisa Crowder**
Laboratory Officer

**Anthony Eason**
Publications Specialist

**Fabricio Ferreira**
Marine Laboratory Specialist

**Clayton Furman**
Schlumberger Engineer

**Randy Gjesvold**
Marine Instrumentation Specialist

**Kevin Grigar**
Operations Superintendent

**James Kowalski**
Curatorial Specialist

**Aidan Leetz**
Marine Laboratory Specialist

**Tiffany Liao**
Marine Laboratory Specialist

**Chang Liu**
Marine Laboratory Specialist

**Nicholas Logan**
Marine Computer Specialist

**Daniel Marone**
Assistant Laboratory Officer

**Aaron Mechler**
Marine Laboratory Specialist

**Beth Novak**
Assistant Laboratory Officer

**Claudio Robustelli Test**
Marine Laboratory Specialist

**Steven Thomas**
Marine Computer Specialist

**Garrick Van Rensburg**
Marine Instrumentation Specialist

**Max Witek**
Marine Laboratory Specialist

# Abstract

In a classical view of tectonic rifting, divergent lithospheric plates cause the asthenospheric mantle to ascend, decompress, and melt, eventually producing new magmatic crust. This view has been updated by drilling results that found exhumed mantle at the continent–ocean transition (COT), leading to the definition of magma-poor continental margins. Obtaining samples and data from drilling in magma-poor COTs is a challenge because the exposed mantle is typically buried under a thick sediment cover. The Tyrrhenian Sea provides an optimal location to test COT formation models by drilling because it has a comparatively thin sediment cover, allows for studying a conjugate pair of COT margins in a single drilling expedition, and has been mapped in unprecedented detail with recent geophysical measurements.

The key objective of International Ocean Discovery Program Expedition 402 was to determine the nature of the geological basement in the central Vavilov Basin, where exhumed mantle peridotites were expected, and in the conjugate margins to the west (Cornaglia Terrace) and east (Campania Basin). In the Vavilov Basin, Sites U1614 and U1616 recovered an exceptional variety of mantle rocks, including lherzolites, harzburgites, plagioclase-bearing lherzolites and harzburgites, dunites, and minor amounts of pyroxenites and mantle intrusions. The mantle peridotites are significantly hydrated and weathered, resulting in the formation of low-temperature serpentine and carbonate veins. In contrast, Site U1612 recovered at the sediment/basement interface an unconsolidated breccia with clasts of basalt, peridotite, and granite, followed by variably deformed mylonitic gneisses that transition downhole to granitoid quartz-diorite rocks. On the western Tyrrhenian margin (Cornaglia Terrace), Site U1613 sampled a sediment sequence dating back to the Messinian (late Miocene), resting on much older sedimentary rocks akin to those outcropping in Sardinia, supporting the hypothesis that the margin consists of extended continental crust. On the conjugate margin to the east (Campania Terrace), Site U1617 did not reach the basement but recovered a complete sequence of Messinian evaporites, including halite.

The samples and data collected during Expedition 402 provide an extensive new data set to determine the heterogeneity of the mantle, the nature and history of melt production and impregnation, and the extent and evolution of serpentinization and carbonate formation; to constrain the geometry and timing of the deformation that led to mantle exhumation; to study the fluid-rock interactions between seawater, sediment, and the serpentinizing mantle; and to constrain geodynamic models of rifting and COT formation.


# Plain language summary

The Earth's mantle rocks, known as peridotites, are generally inaccessible to direct sampling because they are buried tens of kilometers below the Earth's crust. Consequently, even though the Earth's mantle makes up 84% of the volume of our planet, our direct knowledge of it is still inadequate. In some continental margins, faults active during the separation of the continents uplifted the deep mantle rocks to the seafloor. However, access to these peridotites is still a challenge because, after continental separation, the margins are buried by sediments that can be several kilometers thick. The geologically young Tyrrhenian Sea is an ideal target for attempting to sample these mantle rocks because not enough time has passed to deposit thick sediments.

Recent seismological surveys predict that peridotites make up most of the basement in a 3600 m deep central Tyrrhenian Basin under a 200–300 m thick sedimentary cover. International Ocean Discovery Program (IODP) Expedition 402 succeeded in drilling through about 150 m of basement rocks at two sites in the central basin, recovering a wide variety of peridotites and some granitoid rocks belonging to the continental crust. Moreover, a drill site on the western margin of the Tyrrhenian Basin reached continental rocks similar to those that outcrop on the island of Sardinia. Another site on the eastern margin sampled deposits of gypsum and salt that formed when the Mediterranean Sea dried up about 5.5 million years ago.

The samples and data collected during IODP Expedition 402 will be used to understand the history of magma generation in the mantle peridotites, the chemical interactions between seawater

and the mantle rocks, and the deformation processes that unroofed the deep mantle and led to the formation of the continent–ocean transition.

# 1. Introduction and background

In a long-established plate tectonic view of continent–ocean transitions (COTs), diverging plates initially create a rift with extended continental crust, leading to continental breakup and the formation of magmatic ocean crust through partial melting of an upwelling, decompressing mantle. However, this view had to be revised after the discovery of COTs with exhumed mantle peridotite such as those found in the Galicia Atlantic margin (Boillot and Winterer, 1988). The geometry of the exhumation process in these magma-poor COTs is not well known, but the mantle rocks were expected to form the footwall of long-offset, low-angle normal detachment faults. Faults of this type have been proposed to expose deep-seated continental crust in metamorphic core complexes (Lister and Davis, 1989) and mantle peridotites at the axis of the Mid-Atlantic Ridge (Tucholke et al., 1998). The formation of magma-poor COTs is currently explained by a series of processes: after breakup, the mantle is exhumed first, gradually exposing deeper lithospheric levels. Eventually, the shoaling asthenosphere produces melt (e.g., Pérez-Gussinyé et al., 2006; Davis and Lavier, 2017). However, this idealized sequence has not been convincingly documented by sampling in any COT so far. This is due to sparse drilling in old continental margins where the basement is buried under a thick sediment cover.

## 1.1. Geologic setting

The Tyrrhenian Sea is an ideal location to investigate a COT by drilling: due to its young age, it has a thin sedimentary cover and it displays a 3D variation that allows for sampling the conjugate margins and the central area with exhumed mantle during a single expedition. The sediment stratigraphy and bedrock lithology of the Tyrrhenian Sea are well documented by decades of investigations. Dredging has recovered a variety of continental basement rocks from nonmagnetic seamounts and steep escarpments, including granite, phyllite, quartzite, schist, marble, and shallow-water carbonates (Colantoni et al., 1981). The Tyrrhenian Sea also contains several prominent basaltic volcanoes of Late Pliocene to present-day age (Argnani and Savelli, 1999; Peccerillo, 2017). The Tyrrhenian Sea has been surveyed with thousands of kilometers of seismic reflection lines and dense measurements of gravity, magnetic anomalies, and heat flow (Morelli, 1971; Fabbri and Curzi, 1979; Della Vedova et al., 1984; Caratori Tontini et al., 2004). Scientific ocean drilling visited the Tyrrhenian for Deep Sea Drilling Project (DSDP) Leg 13 Site 132 (The Shipboard Scientific Party, 1973), DSDP Leg 42 Site 373 (Shipboard Scientific Party, 1978), Ocean Drilling Program (ODP) Leg 107 Sites 650–656 (Kastens and Mascle, 1990), and ODP Leg 161 Site 974 (Shipboard Scientific Party, 1996).

This extensive data set shows that the Tyrrhenian is the youngest basin in the Western Mediterranean. Its rifting began in the Middle-Late Miocene as the Calabrian arc migrated away from Corsica and Sardinia, driven by slab rollback of the east-southeast migrating Apennine subduction (Malinverno and Ryan, 1986; Faccenna et al., 2001). The greatest amounts of extension occurred in the central and southeastern Tyrrhenian, whose margins (e.g., the Cornaglia and Campania Terraces; Figure **F1**) were interpreted as stretched continental crust, whereas the deepest central areas (e.g., the Vavilov Basin) were inferred to be oceanic crust (Duschenes et al., 1986; Kastens and Mascle, 1990).

There is, however, clear evidence of exhumed mantle in the central Tyrrhenian (Sartori et al., 2004). A 30 m thick section of serpentinized peridotites was sampled during Leg 107 at the base of Site 651 beneath 135 m of island arc basalts (Beccaluva et al., 1990; Bonatti et al., 1990) (Figure **F1**). More recently, extensive seismic reflection and refraction experiments conducted during the Mediterranean overturning circulation (MEDOC) project shed new light on the composition of the Tyrrhenian basement. Analyses of these data show a seismic velocity structure in the Vavilov basin similar to that of COTs where peridotitic mantle has been exhumed by low-angle normal faults and serpentinized by interaction with seawater (Prada et al., 2014). This finding led to the suggestion that most of the basement in the deep Vavilov Basin consists of mantle peridotite (Prada et al., 2015) rather than basaltic oceanic crust.

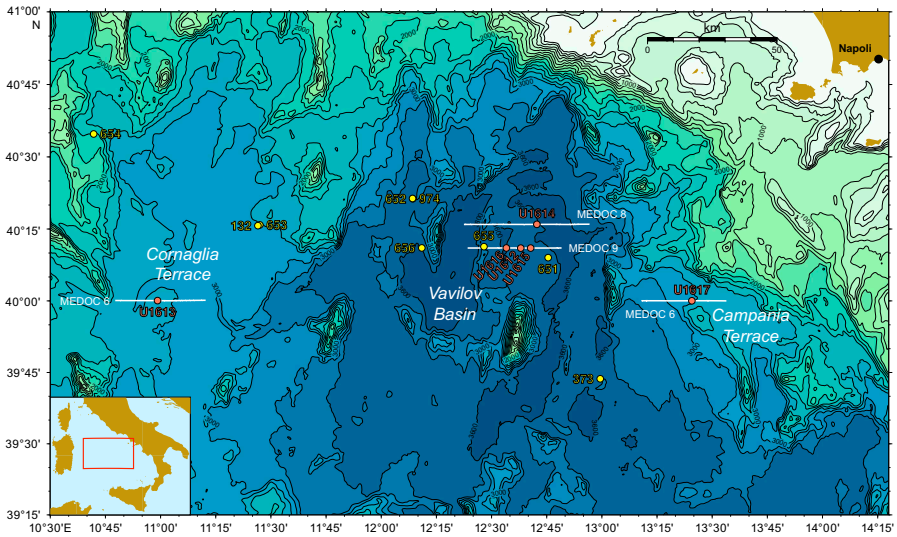


**Figure F1.** Location map of IODP Expedition 402 sites (red) and sites previously drilled during DSDP Leg 42, ODP Leg 107 and ODP Leg 161 (yellow). White lines = location of seismic reflection lines in Figures F2, F7, F8, and F11. The map was created using the Generic Mapping Tools software (Wessel et al., 2019).

Prada et al. (2014) also proposed that the crust in the Cornaglia and Campania Terraces is oceanic, based on their velocity structure. Prada et al. (2015) later noted that the velocity structure of these areas is also quite similar to that of thinned continental crust; however, they still preferred the oceanic crust hypothesis because the normal fault offsets observed in seismic reflection profiles seemed insufficient to account for the amount of extension necessary to thin the original continental crust. Existing models of magma-poor COT development predict that mantle exhumation should precede ocean crust formation. However, if magmatic oceanic crust formed in the Cornaglia and Campania Terraces before mantle exhumation took place in the Vavilov basin, existing magma-poor COT models would have to be turned around (Prada et al., 2014).

# 2. Scientific objectives

The main hypothesis motivating Expedition 402 is that the COT variability present in the Tyrrhenian Sea was created by similar processes occurring at COTs worldwide. In particular, the sequence of events that formed the Tyrrhenian COT may be significantly related to mantle heterogeneities during the segmented opening of the basin. We propose that the 3D variation observed in the Tyrrhenian Sea is typical of COT formation processes rather than the 2D amagmatic mantle exhumation inferred from comparatively lower resolution studies. This hypothesis will be explored by addressing five scientific objectives, only achievable by drilling the basement at multiple locations.

## 2.1. Objective 1: to determine the kinematics and geometry of the extensional deformation in space and time

Determining the ages of faulting, mantle deformation, and melting is key to understanding the kinematics of deformation and constraining numerical simulations that relate deformation and melting. ODP Leg 107 confirmed the essential features of the Tyrrhenian seismic stratigraphy, anchored to the Messinian salinity crisis deposits (5.33–5.96 Ma), and demonstrated that the Vavilov and Marsili Basins formed in the Pliocene (Kastens and Mascle, 1990). Sediment coring during Expedition 402 will refine the Tyrrhenian Pliocene–Pleistocene stratigraphy with biostratigraphy, magnetostratigraphy, and tephrochronology. In particular, determining the age of sediment immediately above the Vavilov basin basement will allow for dating extensional deformation along the detachment faults that exhumed the mantle. Also, the age of the oldest sediments above basement or continental basement in the Cornaglia and Campania Terraces will help to date the formation of the Tyrrhenian margins, and data from micropaleontology will constrain paleodepth.

Volcanic tephras in the sediment section and magmatic events in the basement rocks will be dated with radioisotopes. Ar/Ar and K/Ar geochronology will be applied to lava glasses and basalt groundmasses. Gabbroic inclusions in the peridotites are excellent for dating by K/Ar on amphiboles and feldspars and U/Th on zircon and xenotime. Radioisotope geochronology will be critical to determine the age and sequence of brittle and ductile deformation.

## 2.2. Objective 2: to determine the heterogeneity of the mantle source and establish the timing and origin of the associated magmatism

We aim to characterize the spatial and temporal variations of the mantle source through the coupled study of melting products and residual mantle. Analyses of the chemistry of peridotite samples (major and trace elements and Re-Os isotopes) and of ortho/clinopyroxene mineral separates (major and trace elements and isotopes of Sr-Nd and Hf-Pb) will constrain the provenance, exhumation process, and lateral extent of mantle heterogeneities.

Preliminary analyses of Leg 107 peridotites highlight the potential of Expedition 402 core samples to unravel the melting and melt extraction history of the Tyrrhenian mantle through detailed trace element analyses of peridotite orthopyroxene, clinopyroxene, and olivine. The mantle rocks recovered during Expedition 402 will be compared to the Leg 107 peridotites, which are markedly more depleted than the subcontinental and oceanic mantle peridotites exposed in circum-Tyrrhenian ophiolites and the Iberian COT.

To constrain the sequence of events recorded in the basement rocks, we will use radioisotopes to date basalt lavas, magmatic rocks intruded in peridotites, and mylonites in shear bands. During Expedition 402, we will also attempt to sample the basaltic magmatic crust inferred in the Cornaglia and Campania Terraces. The composition of these basalts will be compared to that of the various basalt types that have been found on Tyrrhenian volcanoes, which range in composition from mid-ocean ridge basalts to back-arc and ocean-island basalts (Argnani and Savelli, 1999; Peccerillo, 2017).

## 2.3. Objective 3: to establish the rheology, deformation patterns, and timing of mantle exhumation

Mantle exhumation in the Tyrrhenian can be compared to that occurring in slow- or ultraslow-spreading centers. In these settings, exhumation occurs either by (1) asymmetric detachment faulting, where deformation is localized in a ~100 m thick fault zone on top of a topographic high and there is appreciable associated magmatism (Tucholke et al., 2007), or (2) polarity change in a symmetric detachment fault system, where the deformation style is poorly resolved and the magmatic supply is very limited (Sauter et al., 2013). Observations at mid-ocean ridges show that deformation mechanisms in exhumed mantle areas are heterogeneous and can vary with time depending on the evolution of the extension rate and magmatic supply and on variations in the intensity and type of hydrothermal processes (e.g., Cannat et al., 2008).

The current limited sampling of Tyrrhenian peridotites does not allow for the identification of exhumation mechanisms and deformation modes because no clear fault plane material has been recovered. Drilling peridotites at Expedition 402 sites will increase the likelihood of sampling fault material from the principal slip surface and the damage zone associated with the detachment. Recovery of fault plane material will allow for identifying the exhumation mechanism. In particular, we will be able to test whether deformation is localized in areas of peridotites impregnated by magmatism and later altered to talc-chlorite-amphibole, minerals with low friction coefficients. Physical properties measurements will also provide constraints on the rheology of mantle rocks.

## 2.4. Objective 4: to determine the fluid-rock interactions in the peridotite basement

The search for low-temperature (past or active) serpentinization or alteration in general is key to better constrain the seawater-lithosphere chemical exchange through time. Drilling the Tyrrhenian peridotite provides an opportunity to quantify long-term alteration processes and test

whether serpentinization is still active in the upper section of a peridotite that was exhumed sometime between 2 and 5 Ma and is currently covered by sediment.

Serpentinization can take place at 300°–350°C, resulting in the formation of serpentine rich in magnetite, as seen in mid-ocean ridge environments. Serpentinization can also occur at lower temperatures of <150°–200°C, producing less magnetite; this process is seen in ophiolites and rifted continental margins. Measurements of magnetic susceptibility (MS) and a suite of geochemical analyses (e.g, stable oxygen isotopes) will help clarify the details of the serpentinization process. We will also attempt to detect the presence of active serpentinization products, such as abiotic methane.

## 2.5. Objective 5: to test models of rifting and COT formation

Expedition 402 results that address Objectives 1–4 will also provide a unique data set, not available in other systems in the world, that will allow for evaluating current COT formation models. Numerical models have shown that serpentinized mantle is exhumed at the COT when either the extension velocity is slow or the mantle was originally depleted. The rich and diverse data set obtained during Expedition 402 will provide important constraints to numerical models of lithospheric deformation, melt production, and mantle exhumation. Numerical models will also incorporate hydrothermal circulation and the thermodynamics of fluid-rock interactions. The combination of modeling and observations will allow us to analyze the influence of fluids on the deformation mode and the role of fluid-rock interaction in element exchange. The focus of the modeling will be on reproducing the conditions of the Tyrrhenian system, but the results will also improve our understanding of the key parameters controlling COT formation in other environments worldwide.

To achieve these scientific objectives, two transects of sites were drilled during Expedition 402 (Figure **F1**):

1. An east–west transect to determine the nature of the basement and define the timing and relationships of mantle deformation, melting, and magmatic events. This transect consists of five sites, located (from west to east) in the Cornaglia Terrace (U1613), the Vavilov Basin (U1616, U1612, and U1615), and the Campania Terrace (U1617). The sites in the Cornaglia and Campania terraces are over a basement of either extended continental crust or oceanic crust; the sites in the Vavilov basin are between Sites 651 and 655 and are planned to reach the exhumed mantle.
2. A north–south transect to determine the lateral variability in the mechanisms and kinematics of mantle exhumation. Mantle exhumation appears to follow the general southward increase in crustal extension in the Tyrrhenian Sea, from a relatively small amount in the northernmost Vavilov Basin to an about 100 km wide unroofing at 40°N. The original plan for Expedition 402 had three proposed sites in this transect, roughly aligned from north to south. As explained in the site summaries below, major drilling difficulties in the unstable volcaniclastic sediments and tectonized peridotites of the Vavilov basin severely limited our options, and in the north–south transect only Site U1614, located ~10 km north of the east–west transect sites, could be completed.

## 2.6. Relationship with the Scientific Ocean Drilling 2050 Science Framework

The data collection and scientific activities of Expedition 402 will directly address a strategic objective and a flagship initiative defined in the comprehensive 2050 Science Framework. For the strategic objective of "the oceanic life cycle of tectonic plates," Expedition 402 will explore the early evolution of oceanic lithosphere following continental rifting in a favorable location with a thin sediment cover, including the initial stage of ocean crust formation, the variation of fundamental rifting modes (from magma-rich to magma-deprived), and the serpentinization of mantle rocks exhumed at COTs. For the flagship initiative "probing the deep Earth," Expedition 402 will complement efforts to characterize the oceanic lithosphere by providing samples and measurements of mantle rocks such as those exposed in oceanic core complexes at slow-spreading mid-ocean ridges

and investigating the fluid exchange in the subseafloor between sediments, oceanic crust, and mantle.

# 3. Site summaries

## 3.1. Site U1612, Vavilov Basin

### 3.1.1. Background and objectives

Site U1612 (water depth = 3574 m) is one of the four drill sites in the Vavilov Basin that target exhumed mantle peridotites. It was considered the highest priority site because of its location near the intersection of the planned east–west and north–south transects across the Tyrrhenian Sea, and it was the first site visited during Expedition 402 (Figures **F1**, **F2**). As for the other sites in the Vavilov Basin, the scientific objectives for Site U1612 were to date with biostratigraphy and magnetostratigraphy the oldest sediment above the basement contact to constrain the time of mantle exhumation; to sample sediments and pore fluids above the basement contact to investigate fluid-rock interactions; and to recover basement samples to determine the heterogeneous composition of the exhumed mantle, its degree of serpentinization and alteration, and its pattern of structural deformation.

The original Site U1612 plan called for rotary core barrel (RCB) coring an estimated 278 m of sediment and 140 m of basement to cross a possible detachment fault zone that exhumed the mantle. Coring would be followed by downhole logging. If recovery of the sediment/basement interface in the RCB hole was poor and time allowed, the plan was to drill an additional hole, washing down to 50 m above basement and then coring using the advanced piston corer (APC)/extended core barrel (XCB) systems in the lowermost sediment column to the top of the basement.

### 3.1.2. Operations

*JOIDES Resolution* departed Napoli, Italy, on 14 February 2024, with the pilot boarding at 0651 h and the last line released at 0724 h. The pilot disembarked at 0755 h, and the ship completed the 86.6 nmi transit to Site U1612. The ship arrived on site at 1530 h and transitioned from cruise mode to dynamic positioning (DP) mode. The precision depth recorder (PDR) reading determined seafloor to be at 3572.6 meters below sea level (mbsl). Hole U1612A was spudded at 0800 h on 15 February, and the water depth was determined to be 3573.8 m.

RCB drilling in Hole U1612A advanced through the sediment column with a formation change to basement at 333 meters below seafloor (mbsf) in Core 35R. Core recovery throughout the sediment column was poor: 72.5 m or 22%. Seventeen cores had no recovery or recovery of <0.5 m core material, including Cores 1R and 2R at the seawater/sediment interface. Recovery improved near basement; Cores 32R–34R had an average 98% recovery. During sediment coring, the Sediment Temperature 2 (SET2) tool was run three times, following Cores 11R, 17R, and 21R. The

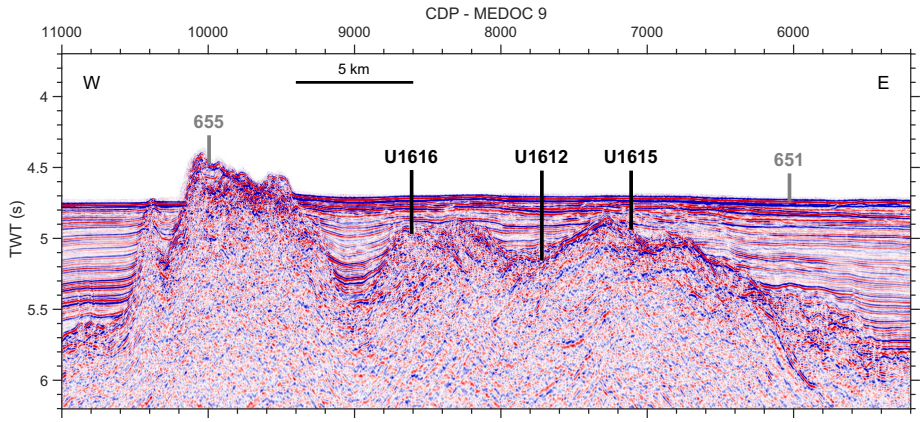


**Figure F2.** Sites U1612, U1615, and U1616 (Vavilov Basin) and ODP Sites 651 (projected) and 655B on Seismic Line MEDOC 9 (location in Figure F1). TWT = two-way traveltime, CDP = common depth point.

measurement attempted after Core 17R did not provide a good reading, likely because of a poor contact between the probe and the formation. Cores 35R–39R advanced into basement. Including the ~0.5 m of basement recovered in Core 34R, we penetrated 15.7 m into basement, recovering 3.45 m of material (22%).

The drill pipe became stuck while coring Core 402-U1612A-40R, losing rotation and vertical movement. After prolonged unsuccessful attempts to free the drill string, the decision was made to sever the pipe at the bottom-hole assembly (BHA). A severing charge was lowered into the hole to 207 mbsf and detonated. A decrease in string weight was not observed, indicating that the pipe was stuck farther up in the sediment column. A second severing charge was lowered just below the sediment/water interface and detonated at 0235 h on 19 February. An immediate drop in string weight indicated the pipe was successfully severed and free. Pipe was tripped back to the surface. The decision was made to discontinue operations at Site U1612.

At the very end of the expedition, however, the site was revisited in the final 48 h of operations. Logging operations in Hole U1616E ended abruptly when the logging bit became briefly stuck while reaming the hole. With the remaining time available, we revisited Hole U1612 with the goal of drilling down through the sediment column to recover as much of the basement as possible. The vessel began the 3 nmi transit between Sites U1616 and U1612 in DP mode while still tripping pipe up from seafloor. The logging bit used in Hole U1616E was recovered onto the rig floor at 0630 h on 6 April. A new RCB BHA was made up, and pipe was tripped toward seafloor while the vessel continued the transit. We arrived on location at 1242 h, picked up the top drive, filled the pipe, and deployed the center bit. Hole U1612B was spudded at 1921 h on 6 April.

The drill ahead in Hole U1612B (drilled interval 402-U1612B-11) reached 318.1 mbsf before contacting a hard layer. The center bit was recovered, and RCB coring proceeded with Cores 2R–4R. These three cores advanced 16.8 m to a total hole depth of 334.9 mbsf and recovered 3.80 m of breccia, granitoids, and peridotite (23% recovery). Rate of penetration was ~5.0 m/h. Following recovery of Core 4R, pipe was tripped back to the surface and the rig floor was secured for the transit to Napoli, Italy. At 2126 h on 7 April, the vessel transitioned from DP to cruise mode, ending Hole U1612B and operations for Expedition 402.

### 3.1.3. Principal results

#### 3.1.3.1. Lithostratigraphy

Core 402-U1612A-1R through Section 35R-1 were described both macroscopically and microscopically (using smear slides), and three lithostratigraphic units were defined. Unit I is composed of gray nannofossil ooze with variable content of volcaniclastic material. Contacts between lithologies are mostly gradational and marked by subtle color changes. Bioturbation is sparse to moderate. Unit II extends from Section 27R-1 through 34R-5 and is composed of nannofossil chalk with siltier horizons rich in Radiolaria. Bioturbation is moderate and occasionally abundant. There are few shell fragments and pyrite precipitates, as well as black organic matter patches. Several sapropel and tephra layers were noted, included a faulted sapropel. Much of the cored material was slightly to severely disturbed, including biscuiting and cracking. Unit III extends to the basement contact and consists of dolomite-rich mud with abundant bioturbation. Sediment lithologies encountered at Expedition 402 sites are summarized in Figure **F3**.

#### 3.1.3.2. Biostratigraphy

The biostratigraphy of planktic foraminifera and calcareous nannofossils was analyzed in core catcher samples from Hole U1612A. Both microfossil groups are abundant in the nannofossil ooze lithologies, and preservation is good in general. Some core catcher samples with significant amounts of volcanogenic clastic materials, as well as lithic fragments and volcanic glass, did not contain foraminifera. A total of 26 core catcher samples were collected as a part of sediment drilling, with additional toothpick samples for nannofossil analysis taken from Cores 33R and 34R to refine the age of the oldest sediments recovered.

From planktic foraminifera assemblages, four biosubzones from the Holocene through Pleistocene were identified, coinciding with the most common occurrences of marker species. The top three cores recovered from the site are estimated to be younger than 0.53 Ma in age, followed by a thick

volcanogenic sediment sequence at 27–165 mbsf that lacked any prominent biozone marker species. Calcareous oozes are more prevalent beneath that sequence, with occasional volcanogenic layers, permitting biozone assignments.

According to nannofossil data, Cores 402-U1612A-1R through 17R are late Calabrian–Holocene in age. Samples 19R-CC to 26R-CC are late Calabrian–Gelasian in age. Core 31R to Sample 33R-6, 127 cm, contains well-preserved nannofossil assemblages of Piacenzian age. In the core below, nannofossils are absent and dolomite granules are present. Nannofossil biostratigraphy follows Di Stefano et al. (2023).

The biostratigraphy data indicate a high sedimentation rate, especially in the upper part of Hole U1612A, where about 240 m of sediments were deposited over 1.60 My (sedimentation rate ~15 cm/ky). Two hiatuses are preliminarily identified, corresponding to ~0.5 and 0.6 Ma. A lower sedimentation rate of ~7 cm/ky is observed in the deeper part of the hole.

### 3.1.3.3. Paleomagnetism

The superconducting rock magnetometer (SRM) and spinner magnetometer (AGICO JR-6A) were tested with a variety of parameters to determine proper measurement sequences for archive-half sections and discrete samples, respectively. Alternating field (AF) demagnetization of natural remanent magnetization (NRM) of a 1.5 m archive-half section was set up to 20 mT in four steps to remove secondary magnetization such as drilling overprint. AF demagnetization of NRM of discrete samples was up to 100 mT in eight steps to reveal characteristic remanent magnetization (ChRM). Measurements on archive-half sections of Cores 402-U1612A-1R through 31R (0–294 mbsf) were completed. Although several geomagnetic reversals were expected over this interval, all inclinations show normal polarity. The ChRM of discrete samples suggests that a secondary component, likely drilling overprint, can be removed around 20 mT, confirming the results for the archive-half sections. However, recovery in Hole U1612A was very low, which may account for the fact that no reversals were measured.

Following a more in-depth discrete sample demagnetization analysis, a possible reversal in Section 402-U1612A-31R-1 was identified. Although limited data points for this reversal are found, it correlates strongly with shipboard biostratigraphy. The unit directly overlying this interval is a volcaniclastic tuff, which could be responsible for the loss of preservation of a larger portion of this reversal.

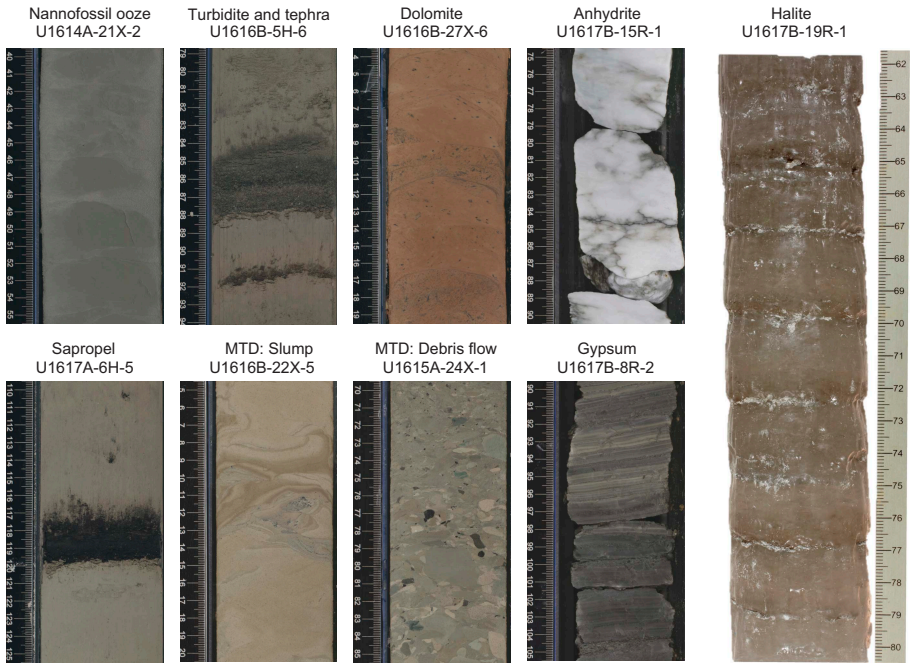


**Figure F3.** Main sedimentary lithologies sampled during Expedition 402, including MTDs and Messinian evaporites.

### 3.1.3.4. Igneous and metamorphic petrology

Hole U1612A recovered a variety of igneous rocks, ranging from volcaniclastics within the sediments to basalts to intrusive rocks interpreted to represent the local geologic basement. Volcaniclastic layers encountered within the sediment were poorly recovered. Recovery was sufficient to define unit boundaries but not contacts or transitions. In Core 31R (~284 mbsf), a basalt clast marks the transition between a volcaniclastic layer and sediments.

The sediment/basement interface was encountered at ~324 mbsf, beginning with an unconsolidated breccia containing clasts of diverse lithologies including basalt, peridotite, granite, and gneiss. The nature of this basal breccia (e.g., a sedimentary deposit or the result of displacement along a fault) remains uncertain due to poor recovery. However, the primary contact with the sediments is exceptionally well preserved in a 10 cm thick interval of pillow basalt that still contains slightly altered rims. Below the breccia, a crystalline interval was penetrated from ~333 to ~345 mbsf. These rocks consist mainly of a single unit of a variably deformed granitoid with a predominantly quartz-diorite composition (Figure F4). Two peridotite pebbles were in the basal breccia of Core 402-U1612A-35R, and an 8 cm long mantle serpentinized peridotite cobble was recovered at the bottom of Core 37R without a preserved contact with the granitoids. These observations suggest that mantle peridotites were exposed on the seafloor prior to sedimentary deposition.

### 3.1.3.5. Structural geology

Sediments cored at Site U1612 mostly show subhorizontal, parallel lamination; below 220 mbsf, bedding dip increases slightly to an average of 10°. Observed deformation structures include faulted and folded lamination, normal and reverse faulting, and boudinage. Clasts just below the sediment/basement interface suggest a polymictic breccia underlain by variably deformed gneiss. The mylonitic and ultramylonitic fabric in the gneiss progressively decreases to a weak foliation downhole.

### 3.1.3.6. Sediment and pore water geochemistry

Samples collected for sediment and pore water geochemistry in Hole U1612A include (1) sediment plugs and small pieces of concretions and/or rocks for measuring hydrocarbon gas concentrations and distribution to ensure safety (Cores 1R–35R), (2) 5 cm long whole-round samples

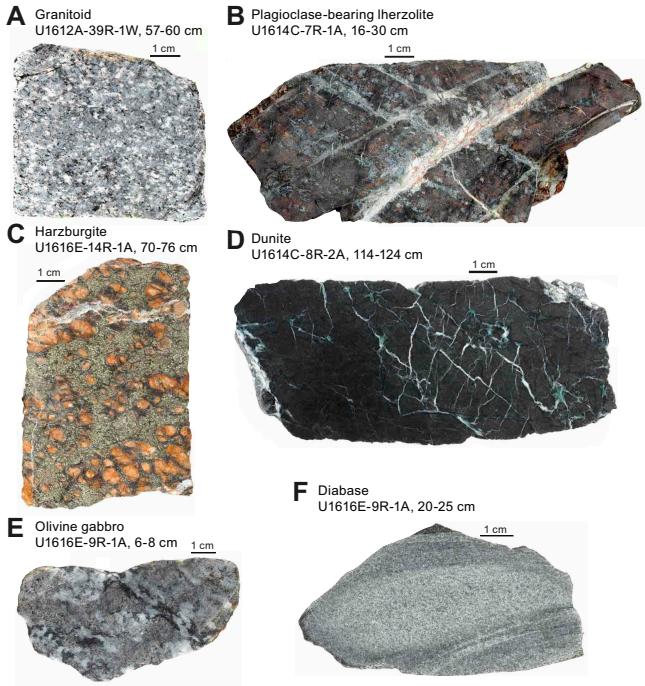


**Figure F4.** Basement lithologies, Expedition 402. A. Granitoid. B. Plagioclase-bearing lherzolite with pyroxene-rich veins crosscut by a tremolite vein. C. Harzburgite with dispersed carbonate veins and typical mesh-texture formed as a result of serpentinization. D. Dunite with serpentine veins. E. Fresh olivine gabbro. F. Diabase with ophitic texture.

taken from 13 cores to extract the interstitial water (IW) by squeezing, and (3) sediments from different layers identified by sedimentologists during shipboard discrete sampling.

Only very small concentrations of methane were measured between 0 and 323.7 mbsf, varying from 0.20 to 3.06 ppmv. Although pH values of IW are relatively stable with depth, a slight increase in salinity and chloride concentrations occurs between 143.9 and 208.9 mbsf. This same trend is observed for other anions and cations, possibly reflecting mineral dissolution. Sulfate concentrations are stable in the first few cores and then increase downsection to 319.8 mbsf. A slight decrease in alkalinity and magnesium between 20.8 and ~150.0 mbsf could indicate precipitation of authigenic dolomite.

All sediments, including squeeze cakes and an additional discrete samples chosen according to changes in lithology, were freeze-dried, ground to a fine powder, and homogenized using an agate pestle and mortar then analyzed for (1) total inorganic carbon (TIC) content; (2) percentage of total carbonate content; (3) total carbon (TC), total nitrogen (TN), and total sulfur (TS) content; and (4) total organic carbon (TOC) and total organic matter content. Atomic TOC/TN ratios range widely from 1.5 to 28.6, indicating changes in organic matter origin (marine versus terrestrial) and/or diagenetic processes. Very low ratios can also be explained by the occurrence of inorganic nitrogen fixed onto mineral surface.

### 3.1.3.7. Igneous geochemistry

At Site U1612, igneous geochemistry analyses were made on recovered core using portable X-ray fluorescence (pXRF) and inductively coupled plasma–atomic emission spectroscopy (ICP-AES). Three samples representing the range of igneous rocks were analyzed using ICP-AES, and additional intervals were selected for pXRF measurements. For pXRF rock standards, it was observed that lighter elements were measured as being lower in concentration than their known values. For instance, when analyzing pure $SiO_2$, the pXRF indicated that the material was only 80 wt% $SiO_2$. To compensate, shipboard standards were measured with the pXRF instrumentation and a correction curve was generated for each reported element.

Loss on ignition (LOI) is higher in the basalt than in the felsic rocks. High MgO content in the basalt determined by ICP-AES may indicate a primary origin. The two samples of felsic rock analyzed using ICP-AES are granite to granodiorite in composition based on a total alkali-silica diagram (Figure F5). We also conducted pXRF analyses on IW squeeze cake residues and sediment section halves adjacent to IW samples to better interpret sediment geochemical records.

### 3.1.3.8. Physical properties

A complete set of physical properties measurements were made on core recovered from Hole U1612A, including density, MS, and *P*-wave velocity ($V_P$) using the Whole-Round Multisensor

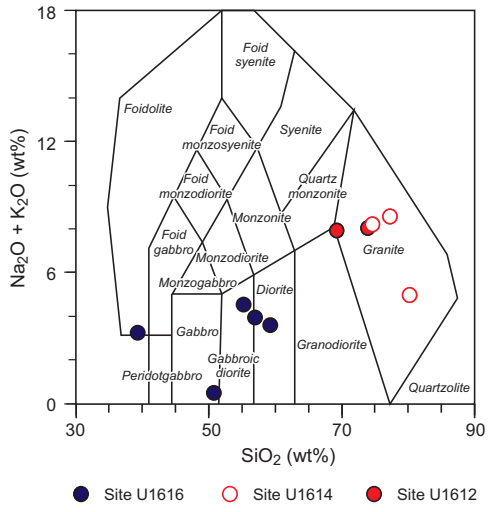


**Figure F5.** Felsic rocks compositions plotted on a total alkali-silica classification diagram for plutonic rocks, Sites U1612, U1614, and U1616. Classification is after Middlemost (1994).

Logger (WRMSL) (71 core sections), X-ray imaging, and natural gamma radiation (NGR) (62 core sections). X-ray and NGR analyses were made immediately after core recovery, whereas cores were not run on the WRMSL until they had equilibrated to room temperature for at least 4 h. In addition, the group performed 51 discrete $V_P$ measurements, collected and processed 30 moisture and density (MAD) samples, and performed 23 measurements of thermal conductivity, 4 of which were unsuccessful due to poor contact between the probe and sample.

For X-ray imaging, the group compared results from 71 whole-round sections scanned at multiple angles (0°, 45°, 90°, and 135°) as well as from 62 section halves. The multiple-angle scans provided quality images of low-density fractures and their orientations. However, indentations on the core exterior left by the core catcher during the coring process obscured some of these images. In contrast, X-ray scans of section halves at a single overhead angle yielded better images of sedimentary structures. Because core recovery is faster in sediments than in hard rocks and scanning at multiple angles is time consuming, we decided to only scan section halves in sediment and scan whole rounds at multiple angles in hard rock. It was later decided that scanning section halves for hard rocks was also clearly optimal, and near the middle of the cruise we abandoned scanning whole rounds of hard rocks.

Despite poor core recovery, the physical properties data show notable variations that can be associated with lithologic changes. Seismic velocities measured on the WRMSL are consistent with discrete $V_P$ measurements from the Gantry system. The overall increasing trend downhole from ~1500 to ~1700 m/s in the sedimentary section coincides with the bulk density change from ~1.6 to ~2.0 g/cm$^3$ and a porosity decrease from ~75% to ~45%, which we interpret as a general compaction trend in sediments. $V_P$ increases dramatically at ~333 mbsf to values greater than 4000 m/s, supporting the designation of this depth as the basement contact (Figure **F6**). MS is generally low, with values near 50 IU and local peaks up to 2143 IU associated with volcaniclastic material in sediments or with serpentinized peridotites in the polymictic breccia above the basement. NGR varies from 10 to 223 counts/s, with higher values generally in volcanic-rich sedimentary intervals

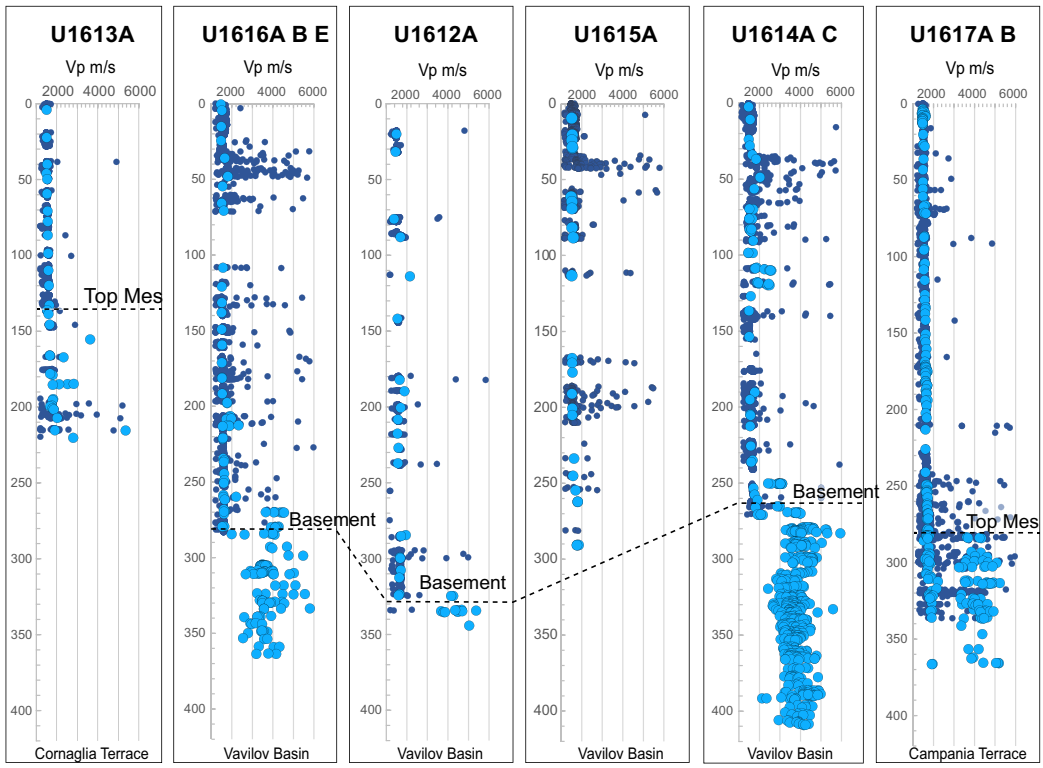


**Figure F6.** $V_P$ measurements, Expedition 402. Sites are ordered from west (Site U1613, Cornaglia Terrace) to east (Site U1617, Campania Terrace). $V_P$ trends highlight the boundary between sediments and basement in the Vavilov Basin and between Early Pliocene and Messinian sediments and evaporites in the conjugate terraces. Dark blue dots = WRMSL $V_P$, light blue dots = $V_P$ measured on discrete samples with the Gantry system.

and in the basement. Thermal conductivity increases with depth and varies from 0.9 W/(m·K) at the top of the sediment column to 2.9 W/(m·K) in the basement rocks. Three MAD measurements show that the basement rocks have a high density (~2.63 g/cm$^3$) and low porosity (~1%).

#### 3.1.3.9. Downhole measurements

The SET2 downhole instrument was deployed three times in Hole U1612A to measure in situ sediment temperatures. Two measurements appeared successful at 103.4 mbsf (above Core 12R) and 198.4 mbsf (above Core 22R), with equilibrium temperatures (after onboard calibration of the probes) of 32.3° and 48.26°C, respectively. A third temperature measurement at 160.4 mbsf (above Core 18R) gave a reading of 15.92°C. However, given the coarse-grained lithology recovered in the core below, this data point is interpreted as an erroneous measurement caused by poor contact between the probe tip and the formation. The loss of the drill string in Hole U1612A did not permit any additional downhole measurements.

#### 3.1.3.10. Microbiology

For Hole U1612A, whole-round samples and syringe plugs of core were collected on the catwalk for metagenomic analyses (5 cm whole round), 16S rRNA (10 cm$^3$ plug), viral counts (1 cm$^3$ plug), and microbial enrichments (5 cm whole round). Metagenomic and 16S rRNA samples were bagged and frozen at –86°C immediately after collection. Samples for viral counts were fixed in 4% formaldehyde. Viral activity incubations were initiated, and subsamples were taken at 0h, 4h, 8h, 12h and 24h in triplicate. Incubation subsamples were fixed in 4% formaldehyde and frozen at –86°C, and microbial enrichments were initiated (2 samples) and kept in the dark.

Oxygen profiles for Hole U1612A were taken from Cores 3R, 4R, 9R, 10R, 16R, and 22R in either or both Sections 2 and 3, which were typically the least disturbed. The remainder of the cores between Cores 1R and 22R had little or no recovery, preventing oxygen profiling. Oxygen measurements were made on whole-round core sections immediately after core recovery and prior to temperature equilibration by drilling two small holes in the core liner and inserting the oxygen and temperature probes into the undisturbed core center. Oxygen concentrations in Core 3R were undetectable, but continued measurements were made once per core through Core 22R to verify the absence of oxygen. A total of 2.7 µM oxygen was measured in Core 16R. Occasionally, observed higher oxygen concentration values may indicate intrusion of oxygenated drill fluid or air into the sample through core disturbance or cracking during probe insertion.

## 3.2. Site U1613, Cornaglia Terrace

### 3.2.1. Background and objectives

Site U1613 (water depth = 2707 m) is located in the Cornaglia Terrace in the lower continental slope of the Tyrrhenian margin of Sardinia and at the western end of the planned east–west transect across the Tyrrhenian Sea (Figures **F1**, **F7**). The basement of this margin has been generally

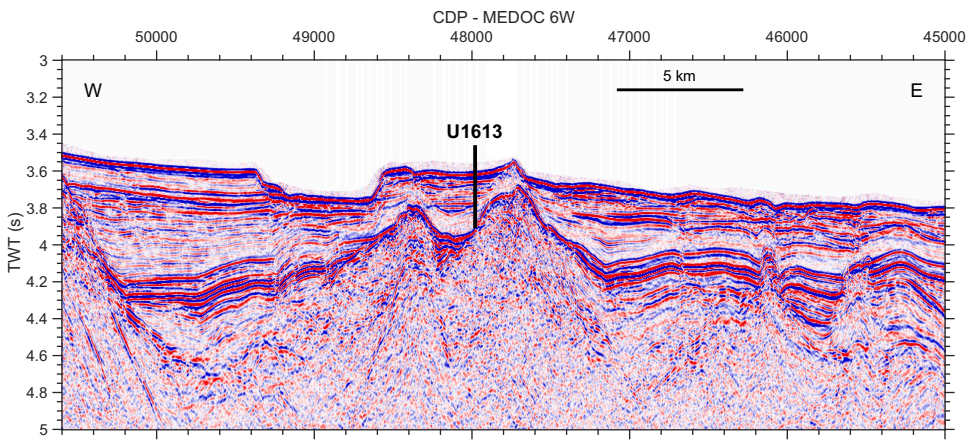


**Figure F7.** Site U1613 (Cornaglia Terrace) on Seismic Line MEDOC 6 (location in Figure F1). TWT = two-way traveltime, CDP = common depth point.

considered to be extended continental crust on the basis of subdued magnetic anomalies and extensive outcrops of continental basement rocks sampled by dredging. An alternative hypothesis presented recently is that the crust of the Cornaglia Terrace is oceanic because of its seismic velocity structure (Prada et al., 2014, 2015). The scientific objectives for Site U1613 were to recover a sequence of hemipelagic Pliocene–Pleistocene sediments and possible Messinian evaporites and establish the age of the sediment/basement interface using tephrochronology, biostratigraphy, and magnetostratigraphy as well as determine whether the basement is rifted continental material or basalt formed by magmatic accretion.

We followed the original plan at Site U1613, which was to core a single RCB hole to a total depth of 265 mbsf, including an estimated 195 m of sediment and 70 m of basement, followed by downhole logging.

### 3.2.2. Operations

The ship completed the 76.4 nmi transit to Site U1613 at an average speed of 11.75 kt, arriving at 1930 h on 19 February 2024 and transitioning to DP mode over the coordinates for Hole U1613A at 2007 h. A new BHA with a C7 RCB bit was made up to better recover hard formations such as the basalt basement lithology anticipated at Site U1613. Pipe was tripped to seafloor, and Hole U1613A was spudded at 0830 h on 20 February, with a seafloor depth of 2706.8 mbsl. Coring reached a total depth of 223.6 mbsf in Core 24R, recovering 99.63 m of material (45%).

Core 402-U1613A-2R had 0 m of recovery, which was later attributed to a malfunctioning core catcher that was removed and repaired. A hard layer identified as conglomerate was encountered in the core catcher of Core 16R. The rate of penetration decreased substantially below that depth, varying between 14.7 m/h for Core 17R and 1.2 m/h for Core 22R, relative to the average 80.2 m/h for Cores 1R–16R. The conglomerate in Section 16R-CC was preliminarily determined to be continental basement, suggesting that the targeted basalt layer is not present at this site, and the decision was made to stop coring after Core 24R.

Temperature measurements using the SET2 tool were made at 67.1, 95.6, and 125.9 mbsf, following Cores 402-U1613A-7R, 10R, and 13R. The third-generation advanced piston corer temperature (APCT-3) tool was also run to seafloor depth to verify the calibration of the SET2 tool. Nonmagnetic core barrels were used on all cores in Hole U1613A.

Logging was planned in Hole U1613A to better characterize intervals of low recovery and borehole physical properties. To prepare for logging, we swept the hole with 90 bbl of high-viscosity sepiolite. We then ran the rotary shifting tool to drop the RCB bit at the bottom of the hole. The knobbies were laid out, the top drive was set back, and pipe was tripped up to 74 mbsf. A first logging run was made with the triple combination (triple combo) tool string starting at 1430 h on 22 February. The tool string encountered a ledge at 127 mbsf but was able to eventually pass through it. A second ledge at 197 mbsf could not be worked through. Given the poor hole conditions, only a single pass was made with the triple combo. As a consequence of the poor hole conditions, the Formation MicroScanner (FMS) was removed from the standard FMS-sonic tool string and a single additional run was made with just the Dipole Sonic Imager (DSI). This modified tool string was deployed at 2100 h and reached 182 mbsf. The tool string was recovered by 0100 h on 23 February, and pipe was tripped back to the surface. Hole U1613A and Site U1613 ended at 0935 h on 23 February as the vessel transitioned into cruise mode and began the transit to Site U1614. Operations at Site U1613 took 3.6 days in total.

### 3.2.3. Principal results

#### 3.2.3.1. Lithostratigraphy

Four lithostratigraphic units were preliminarily defined for the sediments from Hole U1613A. The first two units transition from soupy, nannofossil-rich very fine sand to nannofossil ooze with mud. Several organic-rich layers with a coarser texture as well as glauconite-rich layers are encountered in Unit I. Multiple finely laminated intervals with erosive bases are present, as well as color changes to lighter or darker tones reflecting foraminifera-rich and siliciclastic-rich intervals. Soft-sediment deformation structures (convoluted beds) are observed. Reddish brown layers in Unit II are attributed to an increased content of iron-rich minerals. Contacts are either sharp ero-

sive or defined by a color change. Bioturbation is absent to sparse. Unit III encompasses Messinian facies underlain by oxide-rich sand, matrix-supported polymict sand, and sandy mudstone. Unit IV contains sandy mudstone and silty-rich black shale.

Basement at Site U1613 is defined as a potential Triassic to Paleozoic succession. Based on analogies with similar formations in Sardinia, three main lithostratigraphic basement units were identified and described: conglomerates (Unit IV), green/red shales (Unit V), and black shales (Unit VI). The probable difference in depositional ages of the different units indicates the occurrence of unconformities in the basement. The Unit IV conglomerates consist of rounded to subrounded clasts of quartz and volcanic material in a reddish fine-grained matrix. Unit V contains sandy mudstone and a layer of polymictic conglomerate. The black shale of Unit VI is crosscut by thin carbonate veins and additionally contains clay minerals, pyrite, and Ti-bearing phases observable in thin section. Pollen spores identified in thin section provide a preliminary late Permian age for Unit VI.

#### 3.2.3.2. Biostratigraphy

A total of 14 out of the 22 core catcher samples (402-U1613A-1R-CC to 15R-CC) from Hole U1613A were used for biostratigraphic analyses. According to planktic foraminifera data, nine biosubzones from the Holocene to Lower Pliocene (Zanclean) were identified. According to nannofossil data, the upper part of the recovered succession (down to Section 11R-CC) is Middle Pleistocene–Gelasian in age and is characterized by a sedimentation rate of ~5 cm/ky. Both foraminifera and nannofossil data indicate a temporal hiatus ~1.2 My long that is latest Zanclean/earliest Gelasian in age. Samples from Sections 12R-CC through 14R-CC are of Zanclean age (Early Pliocene). In Section 15R-2, an 8 cm horizon comparable to one of the late Messinian Salinity Crisis Onset Events was identified and is 5.97–5.85 Ma in age. Sediments and sedimentary rocks below Core 16R were correlated to units outcropping on Sardinia and correspond to continental basement.

#### 3.2.3.3. Paleomagnetism

Core recovery in Hole U1613A was higher (45%) than at Site U1612, resulting in a more continuous paleomagnetic profile. Cores 1R–5R were measured on the SRM; however, the material is reworked and the observed irregular polarity changes are not reliable for magnetostratigraphy. Alternatively, some reversal records correspond to lithologic variations in these cores, suggesting an influence of diagenesis on the NRM. A deeper normal-reversed sequence is reliable and suggests an age of ~5 Ma at 125 mbsf. The NRM of the continental basement rocks is lower than that of other stratigraphic units at this site, reflecting a low concentration of magnetic minerals or drilling disturbance.

#### 3.2.3.4. Structural geology

The main structural observations of Site U1613 are from the documented Messinian unit in the sediment and a thick incohesive, cataclastic zone in the basement below, between volcanoclastic deposits and black shales. Interestingly, the dip of the structures increases with depth, shifting from 1°–20° in the sediments to 21°–70° in the basement. The number of fractures and reverse faulting also increases with depth. The change in bedding dip at the base of Lithostratigraphic Unit II indicates an angular unconformity or the transition from a high energy depositional environment to a relatively low energy depositional environment. We interpret the cataclastic zone (Unit V) above the black shales in Unit VI as a fault gouge, either related to normal faulting or reactivation of a normal fault in reverse shearing.

#### 3.2.3.5. Sediment and pore water geochemistry

In Hole U1613A, sediment IW salinity shows an increasing trend with depth and is higher than 45 below 100 mbsf. A maximum salinity value of 50.5 is reached at 166.2 mbsf (Section 18R-1). The $Ca^{2+}$ concentration exhibits a similar trend, which may suggest the formation of evaporites. Dissolved Li and Sr have higher concentrations in the lower part of the cored interval, consistent with precipitation of authigenic minerals in dry environments.

The percentage of sediment calcium carbonate varies from 0.6 wt% (Section 402-U1613A-19R-1; 176.4 mbsf) to 69.3 wt% (Section 12R-3; 170.6 mbsf). Low TOC (0.07–0.39 wt%), TN (0.00–0.05 wt%) and TS (0.0–0.2 wt%) contents were measured in sediments collected from this site. Higher

atomic TOC/TN ratios (15.0–37.0) occurred at 61.6, 77.9, 119.1, and 130.3 mbsf, indicating higher inputs of terrestrial organic matter and/or diagenetic processing of organic matter.

Chemical analysis of sediments also included 37 samples analyzed using pXRF and 9 samples analyzed using ICP-AES. The chemical composition of sediments shows a drastic change between Cores 402-U1613A-14R and 15R, where oxide abundances increase and lithology changes from muddy ooze to silt or sand downhole. The $SiO_2$, $Al_2O_3$, Fe, and Rb contents increase downhole starting at Cores 14R–15R, whereas the CaO, MnO, and Sr contents decrease. The black shale of Core 24R is higher in Ca and Mn (~21 wt% CaO; ~0.12 wt% MnO) compared to the above sections composed of silt and sand (~10 wt% CaO; 0 wt% MnO).

#### 3.2.3.6. Physical properties

Cores recovered from Hole U1613A were measured for gamma ray attenuation (GRA) bulk density, MS, and $V_P$ on the WRMSL, as well as X-ray imaging and NGR. Discrete samples were taken for MAD analysis in addition to discrete measurements of thermal conductivity and $V_P$ made on the Gantry system. Our measurements highlight the changes in physical properties between the sedimentary cover and the pre-Messinian basement and allow us to identify various heterogeneities within the sediments, such as coarse-grained layers or changes in the organic content. For example, a thin gypsum layer just above basement is evident from changes in all measured parameters. Measured physical properties within the basement show trends consistent with the presence of alternating layers of sandy mudstone and conglomerate.

Across Lithostratigraphic Unit I, GRA bulk density increases and porosity decreases downhole from ~ 70% to ~56%. A layer of medium-grained sand with higher bulk density, $V_P$, NGR, and MS is observed in Sections 402-U1613A-3R-6 through 3R-7 (Figure **F6**). Physical properties remain relatively constant throughout Unit II and then change sharply in Unit III, with increased density, thermal conductivity, $V_P$, and NGR and decreased porosity. $V_P$, thermal conductivity, and density increase substantially in the basement units, and MS is low and constant.

#### 3.2.3.7. Downhole measurements

Downhole measurements conducted in Hole U1613A included three runs of the SET2 tool and downhole logging runs with two tool strings. The SET2 tool was deployed three times to measure in situ sediment temperatures. Two measurements were successful at 67.1 mbsf (above Core 8R) and 125.9 mbsf (above Core 14R), with equilibrium temperatures of 22.80° and 30.22°C after onboard calibration, respectively, after applying a correction factor determined using shipboard measurements. These temperatures are consistent with an equilibrium seafloor temperature of 13.40°C recorded by the Schlumberger sensor.

The first logging tool string deployed in Hole U1613A was the triple combo, including the logging equipment head-tension and mud temperature (LEH-PT) for borehole fluid temperature; the Hostile Environment Natural Gamma Ray Sonde (HNGS); the Hostile Environment Litho-Density Sonde (HLDS) for bulk density, photoelectric factor, and a one-arm caliper; the High-Resolution Laterolog Array (HRLA) electrical resistivity tool; and the Magnetic Susceptibility Sonde (MSS). Because of poor hole conditions, only a single pass was carried out with this tool string and with a second string that included just the DSI.

Logging data from Hole U1613A may be more qualitative than quantitative because of the single passes made with each tool string in addition to the large hole size. Spectral gamma ray, density, and MS profiles are in good agreement with core data when not affected by the hole size.

#### 3.2.3.8. Microbiology

Whole-round samples and syringe plugs of core were collected on the catwalk for metagenomics, 16S rRNA, microbial experiments, and viral counts in sediment from Site U1613. Metagenomic and 16S rRNA samples were frozen at −86°C immediately after collection. Samples for viral counts were fixed in formaldehyde. Microbial experiments were initiated in anaerobic conditions, including enrichment cultures in a sample from Section 402-U1613A-5R-5 and viral incubations and prophage induction experiments in Sections 1R-2 and 11R-2.

Oxygen measurements were made on whole-round cores from Hole U1613A immediately after core recovery and prior to temperature equilibration by drilling two small holes in the core liner and inserting the oxygen and temperature probes into the undisturbed core center. Core 1R exhibited significant disturbance, particularly in Sections 1R-1 and 1R-3, which hindered the generation of reliable data. From Core 3R downward, the oxygen profile declines to low or zero concentration levels. In Cores 11R and 13R, oxygen levels increase marginally. To confirm these results, measurements in Cores 11R and 13R were repeated in at least one additional section of each core, yielding similar values, which were associated with the presence of a void space in the core liner.

## 3.3. Site U1614, Vavilov Basin

### 3.3.1. Background and objectives

Site U1614 (water depth = 3579 m) is one of four drill sites in the Vavilov Basin that target exhumed mantle peridotites. Site U1614 is near the center of the planned north–south transect across the Vavilov Basin and is located on the flank of a basement high interpreted to be the uplifted footwall of a low-angle detachment fault that exhumed the mantle (Figures **F1**, **F8**). As for the other sites in the Vavilov Basin, the scientific objectives for Site U1614 were to date with biostratigraphy and magnetostratigraphy the oldest sediment above the basement contact to constrain the time of mantle exhumation; to sample sediments and pore fluids above the basement contact to investigate fluid-rock interactions; and to recover basement samples to determine the heterogeneous composition of the exhumed mantle, its degree of serpentinization and alteration, and its pattern of structural deformation.

The original Site U1614 drilling plan was modified after the drill string became irremediably stuck in the previously drilled Hole U1612A (located in the Vavilov Basin approximately 10 km southwest of Site U1614), likely due to material falling into the hole from thick intervals of unconsolidated volcaniclastic sediments in the upper part of the sediment column. The modified drilling plan was to drill first an APC/XCB hole to sample the sediments, tag the basement (expected at ~200 mbsf), and determine the vertical extent of unstable volcaniclastics that could cause drilling problems. We would then install casing over these problematic intervals in a second hole, to be cored with the RCB at least 140 m into basement that was expected to consist of exhumed mantle peridotite. After coring, we planned to run downhole logging to supplement core recovery and assist the interpretation of the drilled basement interval.

### 3.3.2. Operations

The 80.4 nmi transit to Site U1614 from Site U1613 on the Cornaglia Terrace took 7.6 h at an average speed of 10.6 kt. We arrived on site and transitioned to DP mode at 1755 h (UTC + 1 h) on 23 February 2024. The PDR estimated the seafloor as 3580.1 mbsl. An APC/XCB BHA with a 9⅞ inch polycrystalline diamond compact (PDC) bit was assembled and deployed to 5 m above seafloor. Prior to spudding, we pumped enough microbial contamination tracer with circulating drilling fluid to fill the drill string.

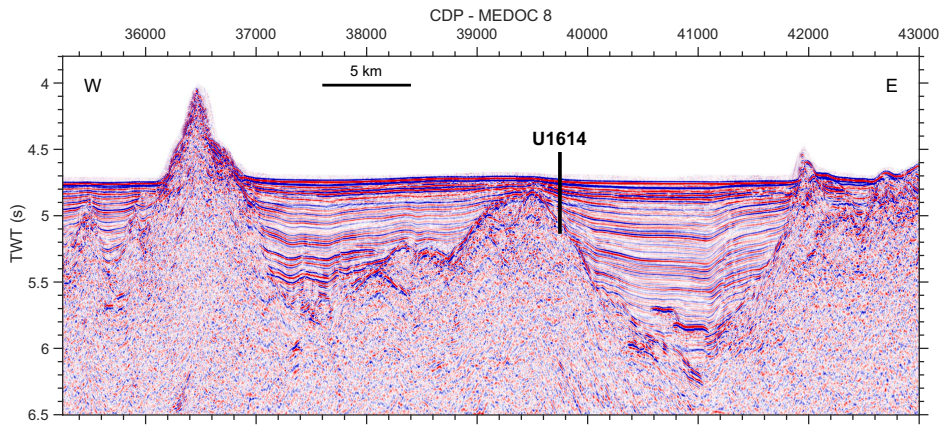


**Figure F8.** Site U1614 (Vavilov Basin) on Seismic Line MEDOC 8 (location in Figure F1).

Hole U1614A was spudded at 0645 h on 24 February, with the first core recovering 5.7 m of sediment as well as the mudline. Based on this recovery, seafloor is calculated at 3579.0 mbsl. Cores 1H–9H were full-length APC cores that advanced 77.3 m and recovered 76.21 m of sediment (98%). Measurements with the APCT-3 tool were made during Cores 4H and 7H, and all full-length APC cores were oriented. Cores 7H and 9H were partial strokes, where Core 9H experienced 30 klb of overpull. As a result, Cores 10F–14F were taken using the half-length APC (HLAPC) system. These cores advanced 16.4 m to a total depth of 93.7 mbsf and recovered 12.72 m of sediment (78%). Gravel recovered in the tops of multiple cores is interpreted as fall-in.

Cores 402-U1614A-15X through 34X advanced 186.4 m to a total depth of 280.1 mbsf and recovered 90.41 m core material (49%). Recovery across this interval ranged 0%–103%. The basement contact was encountered in Core 33X. Core 34X penetrated another 9.8 m but only recovered 0.76 m (8%). We attempted to XCB drill an additional core, but experienced high torque after deploying the core barrel and instead recovered a ghost core, Core 35G, which contained 2.16 m of fill from an undetermined depth and ended the hole. Pipe was tripped back to the surface, and the drill collars were racked. We then laid out the upper guide horn to prepare for a jet-in test for the planned casing installation at this site. In total, the 35 cores collected in Hole U1614A recovered 179.36 m of material, or 64%, and took 3.2 days.

The planned casing installation consisted of a 13⅜ inch casing string to ~60 mbsf and a second 10¾ inch casing string extending to ~40 m above the basement interface. A jet-in test in Hole U1614B was necessary to determine if the full 60 m length of the 13⅜ inch casing string could be installed. We made up the BHA with a 14¾ inch tricone bit, tripped pipe to seafloor, and spudded Hole U1614B at 0900 h on 27 February. The jet-in test was successful, penetrating to 65.2 mbsf. We then pulled out of the hole and tripped back to the surface with the bit clearing the rig floor and ending Hole U1614B at 1900 h.

The reentry cone was then positioned in the moonpool, and the five joints of 13⅜ inch casing as well as a shoe joint were hung in the guide base, using a 16 inch casing hanger and a 16 inch to 13⅜ inch crossover. The stinger with the running tool and BHA were made up and latched into the casing and reentry cone, which was deployed through the moonpool at 0515 h on 28 February. Pipe was tripped toward seafloor, and the vibration isolated television (VIT) camera system was deployed after 60 stands of pipe to follow the reentry cone. At 1400 h, we installed the top drive and spudded Hole U1614C, jetting in casing to 66.0 mbsf. We detached the running tool from the casing by rotating the drill string 3.5 times to the right at 1550 h, began pulling out of the hole, and recovered the VIT system. We then tripped pipe back toward the surface.

To aid installation of the 10¾ inch casing string, we conducted a drill ahead to a depth ~20 m above the expected basement contact. The drilling BHA with a 12¼ inch bit was made up and deployed, reentering Hole U1614C at 1100 h on 29 February using the VIT camera system to guide reentry. After retrieving the VIT system, the drill ahead successfully penetrated to 250.0 mbsf, after which the hole was displaced with 100 bbl of heavy mud and pipe was tripped back to the surface.

The Conductivity-Temperature-Depth (CTD) sensor and a Niskin bottle water sampler were attached to the VIT camera system frame and deployed during the first two VIT runs, generating temperature and conductivity profiles of the water column and collecting bottom seawater samples for chemistry and microbiology.

The final casing step involved the installation of the 10¾ inch casing string. The running tool and drill collars were made up, and a standard slip and cut of drill line was performed prior to running the 20 joints of casing. With the casing hanging off the moonpool doors, we made up the BHA and latched into the casing hanger and then began tripping toward seafloor. The VIT camera system was launched and lowered to guide reentry. The second reentry into Hole U1614C occurred at 0030 h on 2 March. We washed in the casing to 227.3 mbsf, working through an obstruction at 172.7 mbsf by picking up the top drive and using the rig pumps. The casing was latched and released at 0345 h. We recovered the VIT camera system and tripped pipe back to the surface, with the bit clearing the rig floor at 1300 h. After racking the drill collars in the derrick and reinstalling

the upper guide horn, we prepped the RCB core barrels and made up the BHA with a C7 RCB drill bit for coring basement in Hole U1614C.

The third reentry into Hole U1614C to begin RCB drilling occurred at 0135 h on 3 March, guided by the VIT camera system. We then picked up the top drive, recovered the VIT system, and dropped a core barrel with the bit at 229.7 mbsf. The core barrel was washed down to the bottom of the previous drilled interval (250.0 mbsf) before we began coring.

Cores 402-U1614C-2R through 28R advanced 160.6 m to a total hole depth of 410.6 mbsf with a 71.58 m recovery (45%). Recovery varied from 6% to 99%. Cores 8R–28R were taken as half advances to improve recovery. After drilling Core 11R, we experienced high overpull and loss of rotation but were able to work the pipe free. Recovery was relatively high (61%) in Cores 5R–19R and 22R–28R (the latter had 49% recovery) and very low in Cores 20R (9%) and 21R (21%), likely due to the differences in lithology recovered.

Following recovery of Core 402-U1614C-28R, we lost pipe rotation and became stuck. Working the pipe allowed us to regain rotation and lay out two single pieces of pipe from the drill string. The drill string became stuck again, with no rotation or vertical movement. Good circulation suggested that we were losing circulating fluids into the formation. From 1430 to 1700 h on 6 March, we worked the pipe without regaining movement. The vessel was offset to retrieve the core barrel and release the bit as a last attempt to free ourselves. When this effort failed, we made the decision to deploy a severing charge and sever the pipe just below the depth of the casing string. A severing charge was lowered to 234.7 mbsf on the Schlumberger wireline. The charges were detonated with 20 klb overpull on the pipe; an immediate drop in string weight indicated that we were free. The Schlumberger wireline was recovered, and we began pulling out of the hole. After the end of the pipe cleared the seafloor at 0500 h on 7 March, the vessel started to move in DP mode at 0.5 kt toward Site U1615. The end of the pipe reached the rig floor at 1000 h, ending Hole U1614C and Site U1614.

### 3.3.3. Principal results

#### 3.3.3.1. Lithostratigraphy

Three primary lithostratigraphic units were defined for the sediments from Hole U1614A. The first unit was split into three subunits based on the abundance of volcaniclastic gravel. Subunit IA is nannofossil-rich mud with intervals that are more sand rich or silt rich (Figure **F3**). The subunit has small, frequent turbidite deposits with erosive bases and fining-upward sequences. Subunit IB contains almost entirely volcaniclastic gravel. Drilling disturbance makes it difficult to pick out any sedimentary or structural features. Subunit IC also contains some volcaniclastic gravel, but its consistent appearance at the tops of cores suggests that it is fall-in from overlying Subunit IB. The rest of Subunit IC is composed of sandy silt and silt.

Unit II is split into two subunits. Subunit IIA consists of volcaniclastic material in the form of unconsolidated volcaniclastic breccia with a more consolidated tuff found downcore. Foraminifera-rich silt is observed between the breccia and the tuff; this lithology shows extensive drilling disturbance in the form of biscuiting. Subunit IIB is made up of nannofossil chalk with minor volcaniclastic components. Glauconite-rich and sapropel layers are present as well as pyrite nodules and fragments.

Unit III is made up of reddish dolomitic muds and nannofossil chalk overlying the basement contact. The interface is denoted by dolomite overlying a thin layer of greenish gray nannofossil chalk that directly overlays the serpentinite.

#### 3.3.3.2. Biostratigraphy

Micropaleontologists obtained and analyzed 32 core catcher samples from Hole U1614A. Most core catcher samples are volcanoclastic in nature and barren of any planktic foraminifera. When present, planktic foraminifera from volcanoclastic-dominant layers in the middle (between Samples 402-U1614A-9H-CC and 23X-CC) and the bottom of the drilled interval (Samples 29X-CC to 33X-CC) are reworked, making biozonal and age assignments difficult. The topmost Holocene sedimentary layers (Samples 1H-CC to 3H-CC) have well-preserved planktic foraminifera species.

Additional samples were taken from nannofossil ooze intervals to refine the biozone assignments. Based on the planktic foraminifera assemblage observed, sedimentary successions appear to be continuous. Sample 29X-2, 52–54 cm, the bottommost sedimentary layer to be associated with a biozone, was determined to be Early Pleistocene (late Gelasian; equal to or younger than 1.95 Ma) in age.

Calcareous nannofossils were analyzed in ~30 samples from Hole U1614A. The uppermost part of site, down to Sample 12R-CC (about 100 mbsf) is a nearly continuous succession ranging from Holocene to early Calabrian, with an average sedimentation rate of ~62 m/My. In the middle of the cored interval at this site (Samples 16R-CC to 21R-CC), the succession is partially repeated and ranges from Chibanian to early Calabrian. The calculated average sedimentation rate is of ~32 m/My, with a probable hiatus corresponding to the MNQ19b biozone, about 0.36 My in duration. The interval containing Samples 22R-CC to 28R-CC ranges from Calabrian to late Gelasian, with an average sedimentation rate of ~84 m/My. Samples 31R-CC to 33R-1, 124 cm, just above the basement, were assigned to the MNQ19a biozone of Calabrian age. The repeated intervals may be due to the presence of slumps, folds, or reverse faults.

RCB drilling in Hole U1614C captured the sediment/basement interface, including ~20 m of sediment above the contact. Two core catcher samples and two additional foraminifera samples from the core sections were analyzed to estimate the age of the sediments deposited above the basement. Sediments from three of the four samples were found to be volcanogenic in nature and were completely devoid of any planktic foraminifera. The deepest sample to which an age could successfully be assigned was Sample 3R-CC, from the deepest core above basement. Both foraminifera and nannofossil data show this sample to be late Gelasian (1.95–1.71 Ma) in age.

#### 3.3.3.3. Paleomagnetism

Paleomagnetic measurements were performed for the sediments and a small portion of basement recovered in Hole U1614A, as well as the basement recovered in the ~150 m drilled interval in Hole U1614C. Demagnetization of NRM of the archive-half sections of sediments up to 20 mT peak AF showed that the cores recorded almost exclusively normal polarity except for a few highly disturbed sections and cores (34.2–53.2 mbsf), although the biostratigraphy suggests that the time span of the sedimentary column should include multiple reversed polarities. ChRM determined from discrete samples only shows one NRM component between 15 and 80 mT.

For the serpentinized peridotites found in Hole U1614C, initial NRM is strong with a normal polarity. However, the intensity drops quickly at low demagnetization levels. After the overprint is removed by demagnetization at 20 mT peak AF, most rock segments exhibit reversed polarity. Different magnetic minerals, including magnetite, hematite and possibly iron sulfide, were found through experiments on the discrete samples.

#### 3.3.3.4. Igneous and metamorphic petrology

Basement cores from Site U1614 consist of very heterogeneous mantle lithologies that include serpentinized lherzolites, harzburgite, dunite, and pyroxenite, with a short interval of brecciated ophicarbonate (Figure **F4**). The mantle section is crosscut by mafic intrusions. The recovered basement cores show variable degrees of deformation and alteration. The degree of alteration is moderate to high. Alteration minerals include serpentine, magnetite, clays, and carbonate, with instances of various types of amphibole replacing the clinopyroxene. The primary mineralogy and alteration features were also confirmed by thin section observations.

Five lithostratigraphic units were defined in the basement based on primary igneous and alteration features. Units I–III are sedimentary. Unit IV includes the sediment/basement interface and contains a mélange of mud and serpentinized peridotite. Unit V consists of variable mantle lithologies with gabbroic intrusions; Subunit VA is lherzolite-dominated, transitioning to dunite- and harzburgite-dominated in Subunit VB. Unit VI is defined by plagioclase- and clinopyroxene-bearing peridotites with dense mafic veins increasing in concentration with depth. Unit VII contains reddish serpentinized peridotites with mafic intrusions and dense veins. The lithology in Unit VIII returns to plagioclase- and clinopyroxene-bearing peridotites and is relatively homogeneous compared to the units above.

### 3.3.3.5. Structural geology

Sediment in Hole U1614A has subhorizontal bedding throughout the succession, with local increases when related to slumping (Figure **F9**). Observed features include laminations, graded bedding in a turbidite layer in Core 26X, and normal faulting with 2 mm thick boudinage in Section 26X-6. The sediment/basement interface is marked by a sharp contact where dolomitic sediments rest on top of weathered peridotite (Figure **F9C**). The bedding of the dolomitic sediments shows higher dip values than the dip of the strata above them.

The structural geology group described and measured the orientation of ~770 deformation structures in the 150 m of mantle peridotites recovered from Hole U1614C. They include crystal-plastic and brittle fabrics, magmatic impregnations, gabbroic intrusions, and metamorphic veins (serpentine and carbonate). Figure **F9** summarizes the results of the structural geology analysis at Site U1614.

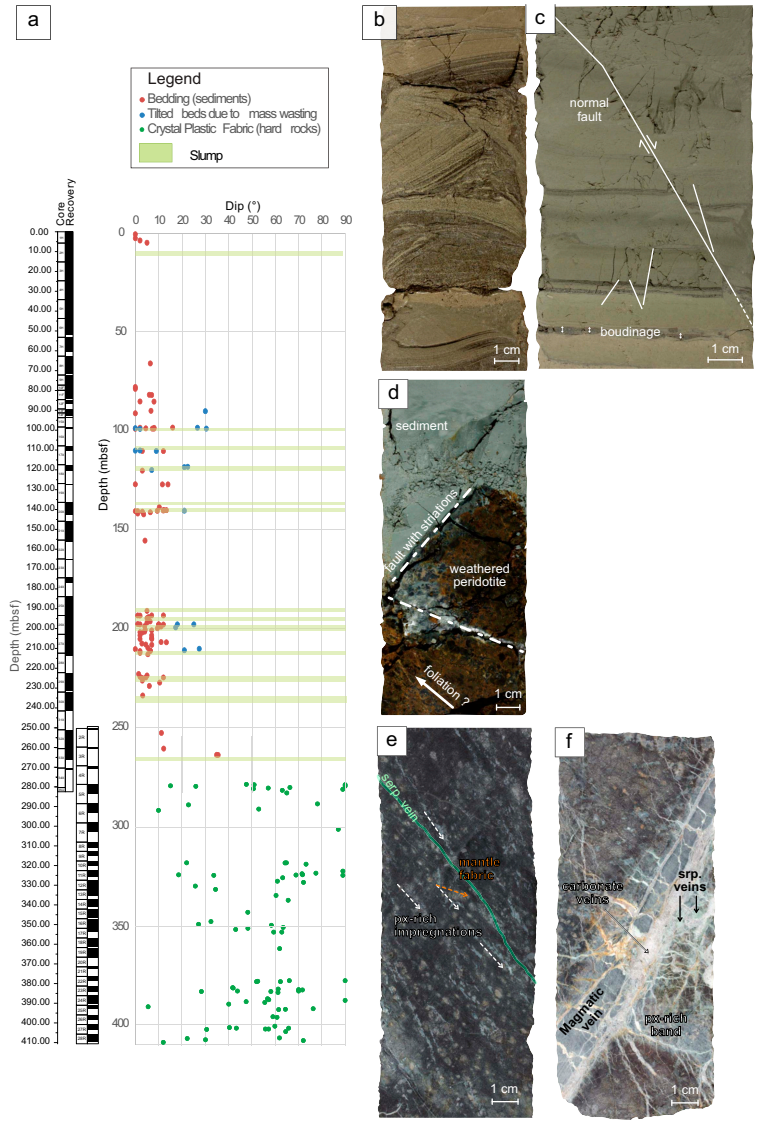


**Figure F9.** Dip and structures of sediment bedding and mantle foliation, Site U1614. A. Dip vs. depth of sediment bedding (red), MTDs (blue), and mantle foliation (green). B. Faulted and folded laminations (partially due to drilling disturbance; 402-U1614A-16X-1). C. Normal fault and boudinage in lamination. Note the higher fracture density (26X-6). D. Sediment/basement interface marked by a fault plane with striations. Peridotite is highly weathered (reddish pattern) with a weak mantle fabric (altered, black minerals) (33X-4). E. Pyroxene (px)-rich impregnations in partially serpentinized (serp) peridotite at low angle to the mantle fabric orientation (402-U1614C-24R-2). F. Weathered peridotite intruded by a magmatic vein or mylonite, rimmed and then partially replaced first by serpentine (srp) and then by a carbonate vein network (22R-1).

#### 3.3.3.6. Sediment and pore water geochemistry

A total of 23 IW samples were collected from the sedimentary succession of Hole U1614A. Although pH values show little variations with depth, IW salinity generally decreases with depth, except at 78.4 and 118.9–151.9 mbsf. IW alkalinity as well as ammonium and phosphate concentrations are characterized by greater values between 10.1 and 76.0 mbsf, probably resulting from organic matter degradation. Alkalinity decreases continuously from the seafloor to 78.2 mbsf and remains constant with depth below, whereas $Ca^{2+}$ content becomes elevated below the same depth. $Mg^{2+}$ concentrations decrease consistently with depth in the uppermost ~200 m. The sulfate concentration also shows a decreasing trend for almost the entire cored interval. The concentration of minor elements (Li, B, and Sr) increases gradually below 78.2 mbsf. In particular, the ratio of B/Cl at the base of the hole is five times the normal seawater value, suggesting the availability of organic matter is contributing to the concentration of B.

The percentage of calcium carbonate varies between 0.4 and 77.8 wt%. Total carbonate ranges from 5.7% to 77.9% and is always higher than the percentage of calcium carbonate, indicating the occurrence of other carbonates in the sediments. A positive correlation is observed between the percentages of $CaCO_3$ and the total carbonate contents. The percentage of sedimentary organic matter varies between 3.1% and 17.3% as determined by LOI. This percentage is higher than 14.7% at 23.2, 85.8, 140.6, and 228.1 mbsf. Low TOC (from below the detection limit to 0.65 wt%) and TN (0.004–0.21 wt%) are measured for sediments collected from this site. Most of sediment samples show a TOC/TN ratio less than 12, indicating that sedimentary organic matter primarily originates from a marine source, except at 29.1 and 222.6 mbsf. However, the occurrence of inorganic nitrogen could result in an overestimation of the relative contribution of the marine source. TS generally varies between undetectable and 0.27 wt% except at 222.6 mbsf, where it reaches 2.36 wt%.

Headspace samples were taken from each core to monitor $C_1$–$C_6$ hydrocarbons according to the standard safety protocol during drilling. For Hole U1614A, 32 headspace samples were analyzed. Only methane ($CH_4$) is identified with concentrations ranging 0.1–49.6 ppmv.

#### 3.3.3.7. Igneous geochemistry

The geochemistry of basement rocks from Hole U1614C was examined using pXRF (85 intervals analyzed) and ICP-AES (26 discrete samples analyzed).

Intervals for pXRF analysis were chosen in collaboration with the igneous and metamorphic petrologists to assist with core descriptions and acquire preliminary geochemical data. These data confirm the wide range of lithologies recovered in Hole U1614C, including various types of peridotite, websterite, and granitic rocks. Peridotites are generally high in Cr, as expected for mantle lithologies. Seemingly sporadic increases in $TiO_2$ occur in some dunites and gabbros; these increases will be better quantified and investigated using ICP-AES.

#### 3.3.3.8. Physical properties

Core material was recovered from Hole U1614A, which captured the sedimentary succession, and Hole U1614C, which recovered basement samples. Physical properties measurements included GRA bulk density, $V_P$, and MS on the WRMSL and NGR on more than 250 m of core from both holes. X-ray images were generated for all section halves. In addition, MAD samples were collected and analyzed from Holes U1614A (50 samples) and U1614C (55 samples). Finally, 62 discrete $V_P$ measurements were taken with the Gantry system on sediment from Hole U1614A and 644 $V_P$ measurements were made using the Gantry system on section halves from Hole U1614C. Because hard rocks did not fill the core liner, the WRMSL could not be used to measure $V_P$.

Sediment recovered in Hole U1614A varies from highly porous unconsolidated clays (porosity ~70%; density ~1.3 g/cm$^3$) to denser and sometimes consolidated volcaniclastic tuffs (density up to 2.64 g/cm$^3$; porosity = 37%). $V_P$ ranges from 1.48 km/s for mud to 2.5 km/s in tuff (Figure **F6**), and thermal conductivity is 0.655–1.657 W/(m·K), with a low value recorded over the tuff interval. Notably, each lithostratigraphic unit has characteristic K, Th, and U contents, with Subunit IIB (Cores 29X–32X) showing very high NGR values up to 400 counts/s. The basement rocks (primarily peridotites) from Hole U1614C have densities of ~2.5 g/cm$^3$ with porosities ranging 2%–19% and seismic velocities in the range of 2.4 to over 6 km/s. NGR in basement rocks is generally low,

except for in Cores 402-U1614C-20R and 21R; however, low recovery makes this interval difficult to interpret.

### 3.3.3.9. Downhole measurements

In Hole U1614A, the APCT-3 tool was deployed at 34.2 and 62.7 mbsf (Cores 4H and 7H) and collected readings of 20.43° and 27.42°C, respectively. The downhole logging planned for Hole U1614C could not be accomplished after the drill pipe was severed and the hole became inaccessible.

### 3.3.3.10. Microbiology

In Hole U1614A, whole-round samples and syringe plugs of core were collected on the catwalk for metagenomics, 16S rRNA, microbial experiments, and viral counts. Metagenomic and 16S rRNA samples were frozen at −86°C immediately after collection. Samples for viral counts were fixed in phosphate-buffered saline formaldehyde solution. Microbial experiments were initiated in anaerobic conditions, including enrichment cultures, viral incubations, and prophage induction experiments for Sample 2H-5, 137–142 cm.

Pore water dissolved oxygen measurements were made on whole-round core sections from Hole U1614A immediately after core recovery and prior to temperature equilibration by drilling two small holes in the core liner and inserting the oxygen and temperature probes into the undisturbed core center. Oxygen is detected in the upper 20 cm of Section 1H-1, with a maximum concentration of 109.5 µM, and decreases with depth (Figure **F10**). Measurements continued through the base of Section 3H-5, although most had undetectable levels of oxygen. Measurements were attempted on Cores 4H–8H; however, because these cores are very sandy and a good contact with the probe tip could not be achieved, the measurements are poor quality. Because sand can also damage the fiber optic probes, it was not feasible to proceed with oxygen measurements. A marginal increase in oxygen in Core 8H was observed, but it was associated with a possible void space in the section.

During APC/XCB coring, the microbial contamination tracer perfluorodecalin (PFD) was pumped with drilling fluid. Samples to evaluate the extent of core contamination were taken each time a microbiology sample was collected. Three samples, including drilling fluid, core exterior, and core interior, were extracted using syringes and placed in glass vials. They were then taken to the laboratory and analyzed on the gas chromatograph. The results from drilling fluid samples and core samples (inner and outer) were compared. Most of the core samples were unaffected by drilling fluid intrusion, as the gas chromatograph detected minute amounts that could be interpreted

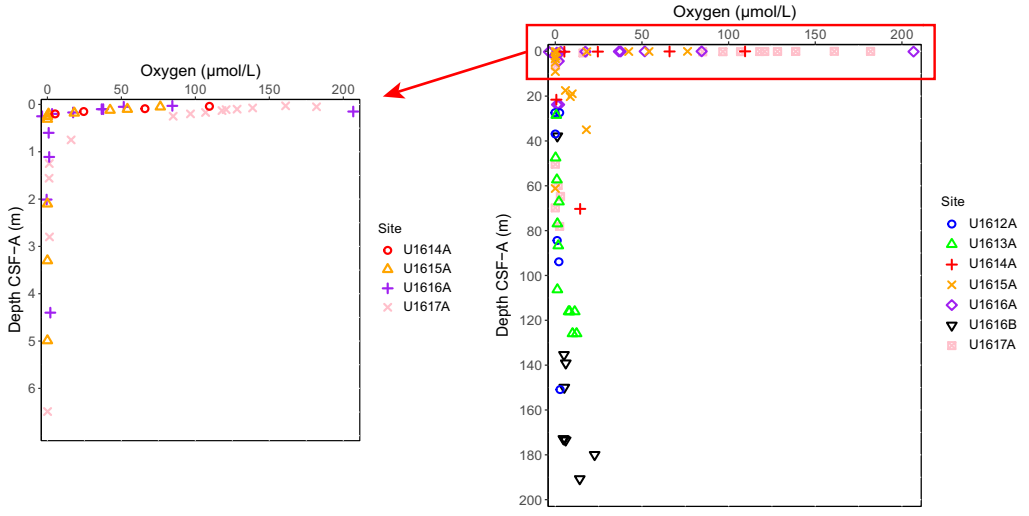


**Figure F10.** Dissolved oxygen concentration, Expedition 402 sites. Left: results from the top 6 mbsf. Right: summary view to the maximum depth where oxygen could be measured (~200 mbsf). CSF-A = core depth below seafloor, Method A (equivalent to the mbsf scale).

as clean samples. However, two of the samples showed high tracer peaks, indicating drilling fluid intrusion (from Sections 402-U1614A-1H-4 and 17X-4).

The Niskin bottle water sampler deployed on the VIT camera system frame collected 1 L of water at approximately 3550 mbsl. This sample was processed in the laboratory, with 5 mL distributed in 1 mL cryotubes and fixed with 4% formaldehyde for cell counts. The remaining water was filtered onto a 0.2 µm polycarbonate membrane filter, and the entire filter was then wrapped in an aluminum envelope and frozen at −86°C.

## 3.4. Site U1615, Vavilov Basin

### 3.4.1. Background and objectives

Site U1615 (water depth = 3569 m) is one of four drill sites in the Vavilov Basin that target exhumed mantle peridotites. Site U1615 is near the eastern end of the planned east–west transect across the Vavilov Basin and is located on an irregular basement high interpreted to be the uplifted footwall of a low-angle detachment fault that exhumed the mantle (Figures **F1**, **F2**). Like the other sites in the Vavilov Basin, the scientific objectives for Site U1615 were to date with biostratigraphy and magnetostratigraphy the oldest sediment above the basement contact to constrain the time of mantle exhumation; to sample sediments and pore fluids above the basement contact to investigate fluid-rock interactions; and to recover basement samples to determine the heterogeneous composition of the exhumed mantle, its degree of serpentinization and alteration, and its pattern of structural deformation.

After two RCB BHAs were lost when they were irremediably stuck in Holes U1612A and U1614C in the Vavilov basin, we were forced to reevaluate the drilling plan. We decided not to drill any sites at the northern end of the north–south Vavilov Basin transect (proposed Sites TYR-17A, TYR-18A, and TYR-19A) because their thick sediment cover (~500–1000 m) was likely to contain unstable volcaniclastics. We concentrated instead on Sites U1615 and U1616 (proposed Site TYR-15A), both located in the east–west transect on basement highs with a relatively thin sediment cover (estimated at ~200 m). The original order of drilling operations in these sites was reversed to core first a hole with the APC/XCB system. The expected high recovery of the sediment interval in this first hole would provide a high-quality record above the sediment/basement interface and would allow for determining the extent and depth distribution of unconsolidated volcaniclastics. We would then compare the results with those obtained in a similar APC/XCB hole to be drilled first at Site U1616, also located in the east–west transect about 10 km west of Site U1615. On the basis of the observations in the two APC/XCB holes, we would then select either Site U1615 or U1616 to drill a second hole and install a casing string that would reach below the base of the problematic volcaniclastics. This second hole would then be RCB cored starting above the sediment/basement interface with the ultimate goal of recovering the target 140 m thick basement interval. After coring, downhole geophysical logging was planned in the RCB hole with a focus on obtaining electrical and ultrasonic borehole wall imagery to supplement core recovery and provide key input to the interpretation of the drilled basement interval.

### 3.4.2. Operations

The 5.1 nmi transit from Site U1614 to Site U1615 was completed in DP mode at 1608 h on 7 March 2024. Tripping toward the seafloor began while the ship was still in transit. Hole U1615A was spudded at 2230 h with the bit positioned 5 m above the PDR water depth of 3571.4 m. Core 1H recovered the mudline and 7.49 m of material from a 7.3 m advance (103%), confirming the water depth as 3568.6 m. Coring in Hole U1615A continued through Core 34X, achieving a total depth of 300.0 mbsf and recovering 115.09 m of sediment (38%). Recovery was high in the first five cores (97%) but low throughout much of the rest of the hole, including six cores with no recovery. Formation temperature measurements using the APCT-3 tool were taken during Cores 4H, 7H, and 10H. Cores 8H and 10H experienced partial strokes, likely caused by the sandy formation; as such, Cores 11F–13F were taken as HLAPC cores before transitioning to the XCB system for the remainder of the hole. Overall, the full-length APC system was used for 10 cores over an 86.4 m interval with 79% recovery, the HLAPC system was used for 3 cores over a 14.1 m interval with 24% recovery, and the XCB system was used for 21 cores over a 199.5 m interval with 22% recov-

ery. Nonmagnetic core barrels were used for all APC and HLAPC cores, and all full-length APC cores were oriented. The microbial contamination tracer PFD was pumped along with drill fluid during coring operations.

Because of the poor core recovery in sediment, especially in the deepest four cores where sediments were expected to be relatively well consolidated (Cores 402-U1615A-31X through 34X; 262–300 mbsf; 4%–7% recovery) and because the basement contact was substantially deeper than predicted at this site, we determined it would not be a suitable location for the next casing installation and ended operations at Site U1615 at 1500 h on 9 March after Core 34X. At midnight, the vessel began the 4.8 nmi transit in DP mode to Site U1616 at a speed of 0.5 kt. Operations at Site U1615 took 2.3 days.

### 3.4.3. Principal results

#### 3.4.3.1. Lithostratigraphy

The lithostratigraphic sequence in Hole U1615A was split into two units based on lithology, with the first unit divided into three subunits. The determination was primarily made by the relative abundance of volcaniclastics and coarse-grained material, although volcaniclastics are present throughout the sediment column in varying amounts. The top of Unit I consists of alternating layers of dark gray volcaniclastic-rich silts and light brown nannofossil oozes with mud. In Subunit IB, volcaniclastic gravel becomes dominant, as has been observed at other sites. Wood fragments are present throughout the unit. Subunit IC consists of nannofossil chalk with some layers of volcaniclastic-rich material. Intervals of volcaniclastic gravel are interpreted as fall-in due to their consistent occurrence in the top of cores, but volcaniclastic-rich sands and muds are present throughout. Some intervals are also rich in foraminifera. We observe a few layers of organic-rich material that may be classified as sapropel. Unit II contains limited volcaniclastic material and mainly consists of nannofossil ooze and silts/sands. The top of Unit II shows signs of soft-sediment deformation in the form of clast-supported polymictic conglomerates and slump deposits (Figure **F3**).

#### 3.4.3.2. Biostratigraphy

Hole U1615A drilled into 300 m of sediment, recovering ~115 m (38%). The marker species assemblages of planktic foraminifera as well as calcareous nannofossils were analyzed from the core catcher samples and a few additional samples from split core sections.

The sedimentary interval at the site contains many volcaniclastic-rich mud to gravel layers along with a few interbedded nannofossil ooze layers. The volcaniclastic sediments in Samples 402-U1615A-5H-CC to 13F-CC, 18X-CC to 22X-CC, and 25X-CC to 34X-CC are barren or contain few (≤10) marker species of planktic foraminifera, making biostratigraphic assignments across these sedimentary layers challenging. However, the few core catcher and core section samples that consisted of nannofossil ooze contain relatively well preserved planktic foraminifera species that constrain the age of the sediments in Hole U1615A to Holocene–Lower Pleistocene (upper Gelasian stage; equal to or younger than 2 Ma).

Calcareous nannofossils were analyses in 25 core catcher samples of Hole U1615A. The uppermost part of the succession (Sample 1H-CC) falls within the middle Pleistocene MNQ20 biozone (0.46–0.26 Ma). All the studied samples from Sample 2H-CC to 25X-CC fall within the MNQ19d biozone (0.46–0.96 Ma) (early middle Pleistocene). The lowermost part of the succession contains reworked nannofossil assemblages, with older taxa found together with younger ones. The oldest sample studied at this site is Sample 30X-CC, which is assigned to the early Pleistocene MNQ19b biozone (1.24–1.61 Ma).

#### 3.4.3.3. Paleomagnetism

In Hole U1615A, as in previous sites, demagnetization of archive-half sections and discrete samples only show normal polarity, despite the fact that reversed polarity is expected given the age of microfossil biozones present. Low recovery and the presence of substantial volcanic material further limited the utility of this site for paleomagnetic analyses.

#### 3.4.3.4. Structural geology

Structural geology measurements included the orientation of bedding, fractures, faults, and folds throughout the recovered interval. Poor recovery at this site is partly responsible for the scatter of the acquired data. Throughout the hole, the bedding dip rarely exceeds 20°. The variation of bedding dip slightly increases in the vicinity of identified slumps. The observed bedding dips are concentrated at 59–88 and 186–209 mbsf, which correspond to intervals within the volcaniclastic-rich layer of Lithostratigraphic Unit I and the slump deposits of Unit II, respectively. Two observed faults have higher dip angles but may be related to drilling disturbance.

#### 3.4.3.5. Sediment and pore water geochemistry

In the 17 IW samples collected from Hole U1615A, the pH value is within a narrow range of 7.4 to 8.0, suggesting that the bicarbonate ion ($HCO_3^-$) is the dominant carbonate species. Alkalinity is higher (2.3–5.6 mg/L) above 65.3 mbsf and decreases to less than 2.0 mg/L toward the bottom of the cored interval. The concentrations of the major elements $Na^+$ and $Cl^-$ vary from 505.26 to 561.68 and 608.47 to 646.73 mM, respectively. Both elements reach a maximum value at 170 mbsf. Depth profiles of salinity and $Ca^{2+}$ follow the same trend as those of $Na^+$ and $Cl^-$, reaching their respective maximum values of 40.0 g/kg and 39.37 mM at intermediate depths. $Mg^{2+}$ concentrations exhibit the opposite pattern, decreasing from the highest concentration of 57.22 mM near the seafloor a minimum concentration of 17.31 mM at 190.4 mbsf and then increasing to 29.31 mM at the base of the cored interval. The minor elements B and Sr increase in concentration with depth. Sulfate accounts for the majority of TS content and ranges 23.84–30.72 mM with no obvious pattern with depth. The nutrients ammonium and phosphate decrease in concentration downhole, with ammonium (64.45–737.32 μM) significantly higher than phosphate (1.77–4.69 μM).

Methane, the only hydrocarbon gas detected in the cores at this location, shows a relatively stable concentration profile (mean value = 0.86 ± 0.42 ppmv) throughout the sediments. A small peak (maximum concentration of 5.16 ppmv) occurs near the top of Unit II.

The percentage of calcium carbonate varies from 1.9 to 47.2 wt%. Sedimentary TOC and TN contents range 0.01–1.15 wt% and 0.004–0.21 wt%, respectively. Most sediment samples show a TOC/TN ratio of less than 12, indicating that sedimentary organic matter originates from marine sources, except in the interval 12.8–22.5 mbsf. However, the occurrence of inorganic nitrogen could result in an overestimation of the relative contribution of marine source. TS generally varies between below detection and 0.90 wt%.

A total of 18 of the sediment IW squeeze cakes and intervals along their corresponding section halves were analyzed using pXRF. The data show a high degree of scatter, possibly due to frequent changes between nannofossil and/or foraminifera-rich materials and volcaniclastic-rich materials. However, general trends such as increases in $K_2O$ and Rb contents and decreases in CaO, Sr, and Ni contents downhole can be recognized in the squeeze cakes extracted from the topmost sediment layer down to ~50 mbsf. Two intervals of sediment from Site U1615 were also chosen for analysis using ICP-AES.

#### 3.4.3.6. Physical properties

Physical properties measurements were acquired on the 34 cores from Hole U1615A, including $V_P$, GRA bulk density, and MS using the WRMSL and NGR. A total of 27 discrete samples were collected for MAD analysis and calculation of density and porosity, and 17 thermal conductivity measurements were performed.

The MAD bulk density of recovered sediments in Hole U1615A varies from 1.345 to 1.957 g/cm$^3$ (average = 1.61 g/cm$^3$), and porosity decreases from 81% at the top of the hole to 45% at the bottom (average = 63%), following a typical sediment compaction trend. This trend is consistent with a corresponding increase in $V_P$ with depth (1481–1846 m/s; average = 1596 m/s; based on the Gantry measurements; Figure **F6**). NGR increases with depth from 23 to 331 counts/s with an average value of 78 counts/s. Thermal conductivity shows a general decrease with depth, ranging 1.675–0.879 W/(m·K), and has an average value of 1.15 W/(m·K). MS is highly variable in the uppermost 211 m with individual peaks reaching over 2000 IU, whereas it is more stable for the rest of the core with an average of 37 IU.

#### 3.4.3.7. Downhole measurements

The APCT-3 tool was deployed in the upper part of Hole U1615A to measure in situ sediment temperatures. Three measurements were successful at 35.8 (Core 4H), 64.30 (Core 7H), and 86.4 mbsf (Core 10H), with equilibrium temperatures of 17.86°, 21.51°, and 24.96°C, respectively, after onboard calibration. These temperatures are consistent with an equilibrium seafloor temperature of 13.61°C recorded before the second run.

#### 3.4.3.8. Microbiology

In Hole U1615A, whole-round samples and syringe plugs of the core were collected on the catwalk for viral metagenomics, 16S rRNA, microbial experiments, and viral counts. Viral metagenomics and 16S rRNA samples were double-bagged and frozen at −86°C immediately after collection. Samples for viral counts were fixed in a phosphate-buffered saline formaldehyde solution. Microbial experiments were initiated under anaerobic conditions, including enrichment cultures, viral incubations, and prophage induction incubations in the sample from Section 2H-5.

Oxygen measurements were conducted on whole-round cores from Hole U1615A immediately after recovery and prior to temperature equilibration. In Core 1H, oxygen was detected across the first 20 cm of Section 1H-1, with a maximum value of 76.31 µM at 5 cm and the lowest detectable value of 0.73 µM at 20 cm (Figure **F10**). Measured oxygen concentrations increased throughout Cores 3H and 4H to a subsurface maximum of 17.93 µM; however, this trend may be the result of drilling disturbance. An attempt was made to continue with the measurements beyond Core 7H, but the cores were either disturbed, too sandy, or had too much intruded water and drilling fluid for reliable measurements.

Additional samples were taken for PFD microbial contamination tracer analysis from each core from which a microbiology sample was collected. PFD was detected in all core exterior samples, demonstrating successful delivery of the tracer. A total of 5 out of 13 core interior samples (Sections 402-U1615A-21X-2, 24X-6, 25X-4, 29X-3, and 30X-2) contained detectable PFD, suggesting some amount of drilling fluid intrusion and microbial contamination.

## 3.5. Site U1616, Vavilov Basin

### 3.5.1. Background and objectives

Site U1616 (water depth = 3600 m) is one of four drill sites in the Vavilov Basin that target exhumed mantle peridotites. Site U1616 is near the western end of the planned east–west transect across the Vavilov Basin and is located on an irregular basement high interpreted to be the uplifted footwall of a long-offset low-angle detachment fault that exhumed the mantle (Figures **F1**, **F2**). Like other sites in the Vavilov Basin, the scientific objectives for Site U1616 were to date with biostratigraphy and magnetostratigraphy the oldest sediment above the basement contact to constrain the time of mantle exhumation; to sample sediments and pore fluids above the basement contact to investigate fluid-rock interactions; and to recover basement samples to determine the heterogeneous composition of the exhumed mantle, its degree of serpentinization and alteration, and its pattern of structural deformation.

After two RCB BHAs were lost when they were irremediably stuck in Holes U1612A and U1614C in the Vavilov basin, we were forced to reevaluate the drilling plan. We decided not to drill any sites at the northern end of north–south Vavilov Basin transect (proposed Sites TYR-17A, TYR-18A, and TYR-19A) because their thick sediment cover (~500–1000 m) was likely to contain unstable volcaniclastics. We concentrated instead on Sites U1615 and U1616, located on basement highs in the east–west transect where the estimated sediment cover was substantially thinner (~200 m). The original order of drilling operations in these sites was reversed to core first a hole with the APC/XCB system. The expected high recovery of the sediment interval in this hole would provide a high-quality record above the sediment/basement interface and would allow for determining the extent and depth distribution of unconsolidated volcaniclastics.

Because Hole U1616A gave the most favorable indications for a drilling installation, we selected Site U1616 to install a casing string that would reach below the base of problematic volcaniclastics. An additional hole would then be RCB cored starting above the sediment/basement interface,

with the ultimate goal of recovering the target 140 m thick basement interval. After coring, downhole geophysical logging was planned in the RCB hole with a focus on obtaining electrical and ultrasonic borehole wall imagery to supplement core recovery and provide key input to the interpretation of the drilled basement interval.

### 3.5.2. Operations

The vessel arrived at Site U1616 on 10 March 2024, following a 5 nmi transit from Site U1615 completed in DP mode at 0315 h. The top drive was picked up and drill pipe spaced out to spud, filling the drill string with the PFD microbial contamination tracer prior to coring. Hole U1616A was spudded at 0530 h, recovering the mudline and penetrating 2.7 m into the formation (101% recovery), placing the water depth at 3567.0 m. APC coring continued through Core 6H, reaching 50.2 mbsf and recovering 47.72 m of sediment (95%) overall. A formation temperature measurement was made with the APCT-3 tool during Core 4H. Ship heave intensified throughout the morning and, after recovery of Core 6H, the decision was made to pull out of the hole and wait on weather, thereby ending Hole U1616A.

Hole U1616B was spudded at 1500 h on 10 March after 2 h of waiting on weather. This hole began with a drilled interval (402-U1616B-11) to 31.2 mbsf, where APC/XCB coring resumed with Core 2H. Cores 2H–6H advanced 47.5 m and recovered 34.25 m of sediment (72%). An APCT-3 measurement was made during collection of Core 4H. After Core 6H, an HLAPC attempt misfired and resulted in a dropped core barrel. Two wireline runs were required to retrieve the empty barrel. Cores 7X–29X, which were taken with the XCB system, advanced the hole to a final depth of 302.6 mbsf. Recovery was poor in Cores 7X–10X (3%) but improved in Cores 11X–27X (72%). A hard contact was reached during XCB coring of Core 28X, and the rate of penetration slowed. The core advanced 8.3 m after 1 h of drilling and was retrieved with only 6% recovery, but it contained clasts identified as peridotite breccia. A final core, Core 29X, was collected to verify the basement contact. Coring was terminated, and we then began tripping pipe back to the surface. The bit cleared the rig floor at 1700 h on 12 March, ending Hole U1616B. Overall, a 271.4 m interval was cored in Hole U1616B with 156.58 m of core recovered (58%). Nonmagnetic core barrels were used for all APC cores, and all full-length APC cores were oriented. The PFD microbial contamination tracer was pumped with the drill fluid throughout coring.

Site U1616 was selected for the reentry system and casing installation because of the relatively high recovery in the sediment column compared to Site U1615 (58% in Hole U1616B compared to 38% in Hole U1615A). Additionally, the basement contact was deeper than anticipated and was not reached after 300 m of penetration in Hole U1615A. Finally, Site U1616 contains less volcaniclastic gravel than Site U1615, which can contribute to hole instability.

Following operations in Hole U1617A between 12 and 16 March, the vessel returned to Site U1616. The 40.1 nmi transit from Site U1617 was completed at 0112 h on 17 March. After arriving on site, the vessel transitioned to DP mode and preparations began for a jet-in test to verify that the full 64.64 m of 16 inch casing could be washed in. The upper guide horn was removed and a BHA with a 18½ inch tricone bit was made up. We tripped pipe toward seafloor and spudded Hole U1616C at 1115 h on 17 March. The jet-in test was successful, penetrating 76.9 m into the sediment in ~3 h. Pipe was tripped back to the surface, and the bit was recovered to the rig floor at 2215 h, ending Hole U1616C. Preparations then began for the reentry system and casing installation planned for Hole U1616D.

With the reentry cone positioned on the moonpool doors, the 64.64 m of 16 inch casing that comprised the first casing string was run through the moonpool and hung in the reentry cone. The string consisted of 5 joints of 16 inch casing in addition to several 16 inch pup joints that would extend the length of the string past a layer of volcaniclastic gravel at ~60 mbsf that could cause hole instability. The stinger with the running tool and BHA were made up and latched into the reentry cone with the DrilQuip running tool. The moonpool doors were opened, and the reentry system was lowered toward seafloor. The VIT system was launched to monitor the installation of the reentry cone on the seafloor and the release of the running tool from the reentry cone.

Hole U1616D was spudded at 2000 h on 18 March, and the casing was successfully jetted in to 64.64 m, such that the reentry cone was sitting on the seafloor. From 0430 to 0545 h on 19 March, we attempted to unlatch the running tool from the DrilQuip reentry cone and casing but were unable to rotate. We consequently made the decision to recover and inspect the reentry system and then redeploy in Hole U1616E. The casing was pulled out of the hole, experiencing strong overpull at ~10 mbsf. The VIT camera system was recovered, and pipe was tripped back toward the surface. At 1400 h on 19 March, the reentry cone was brought back up through the moonpool and landed on the moonpool doors. We observed that all of the 16 inch casing string below the 20 to 16 inch crossover was lost. It is likely that the overpull experienced while pulling out of Hole U1616D was due to the casing detaching. The bit was recovered onto the rig floor at 1800 h, ending the hole. Two bent drill collars were removed from the BHA prior to making up a new BHA and latching it back into the reentry cone.

The reentry cone with the remaining ~5 m of 20 inch casing was lowered through the moonpool, and we began tripping pipe toward the seafloor to install the reentry cone in Hole U1616E. The VIT system with the CTD sensor and Niskin bottle water sampler attached to the frame was launched at 2330 h and lowered to observe casing installation and release. Hole U1616E was offset 40 m west of Hole U1616D to avoid encountering any of the lost casing string that might be lying on the seafloor.

Hole U1616E was spudded at 0445 h on 20 March with the 20 inch casing set at 5.5 mbsf. At 0545 h, the running tool successfully unlatched from the casing. We then pulled out of the hole, recovered the VIT system, and tripped pipe back to the surface.

We began tripping pipe toward seafloor and at 2130 h launched the VIT system to guide reentry. The hole was reentered at 0120 h on 21 March, and the VIT camera system was recovered. The hole was drilled to 250 mbsf, including a 30 m rat hole to allow for fall-in from unstable layers within the sediment column. The drill ahead finished at 1130 h, and the hole was swept with sepiolite mud and then displaced with 170 bbl of barite mud to keep the hole open during casing installation. We then pulled out of the hole and began tripping back to the surface. The VIT system was deployed to monitor the bit clearing the reentry cone and the position of the cone on the seafloor given the shallow depth of the first casing string.

The 13⅜ inch casing was rigged up and run, and the casing landed on the moonpool doors. The stinger and BHA were made up, run through the casing, and the stinger latched into the casing hanger. We then began tripping pipe toward the seafloor and launched the VIT camera system to facilitate reentry in Hole U1616E. We finished tripping pipe to the seafloor and reentered Hole U1616E at 1658 h on 22 March. The casing was washed in to 219.4 mbsf, landed in the reentry cone, and released at 2045 h. This casing depth successfully sealed off the volcaniclastic gravel (~60 mbsf) and tuff (~196–206 mbsf) layers predicted to pose a risk to hole stability.

Following the recovery of the drill string, a BHA with an RCB bit was made up and tripped toward seafloor. Reentry occurred at 1628 h on 23 March, with the VIT camera system deployed to facilitate the process. The VIT system was then recovered prior to drilling. We washed down the distance from the end of the casing (219.4 mbsf) to the bottom of the drilled interval (250 mbsf), encountering fill just below the casing shoe. A center bit was deployed to aid in washing down through the fill and a 40 bbl sweep of sepiolite mud was pumped at the bottom of the hole to further clear the hole.

RCB drilling in Hole U1616E commenced at 2200 h on 23 March. Cores 2R–23R penetrated 250.0–371.0 mbsf. Cores 2R and 3R recovered 5.08 m of sediment from a 19.6 m advance (26%). A hard contact was encountered in Core 4R between sediment and a peridotite breccia, and recovery in Cores 4R–9R was very low (10%). All cores after Core 4R were taken as half advances to improve recovery. Drilling parameters and formation lithology became more consistent starting from Core 10R (303.5 mbsf), which was designated as the top of basement and marks a transition from breccia into peridotite. Cores 10R–23R advanced 67.5 m into basement and recovered 17.5 m of hard rocks (26%).

While drilling Core 402-U1616E-23R, the drill string experienced high torque and overpull at the bottom of the hole. Attempts to clean the hole bottom of any debris were unsuccessful, and coring was terminated in favor of logging after about 3 h of effort. Core 23R ultimately recovered 0.15 m of rock out of a 2.8 m advance (5%). Overall, Hole U1616E contained a 121.0 m cored interval with 25.87 m (21%) recovered. All cores were taken with nonmagnetic core barrels.

The hole was conditioned for logging with a 40 bbl sweep of sepiolite mud and reaming to flush out cuttings and debris. The VIT system was deployed, and we pulled the drill string out of the hole, clearing the seafloor at 0545 h on 26 March. The vessel was offset away from the reentry cone, and the bit was released on the seafloor. After this operation was successfully completed, we reentered Hole U1616E at 0815 h and recovered the VIT system.

The triple combo logging tool string was rigged up and deployed at 1230 h on 26 March with the end of the drill pipe set at 266.6 mbsf, ~10 m above the contact between sediment and breccia. The tool encountered an obstruction at 306.7 mbsf, directly below the breccia/basement contact at 303.5 mbsf. We made the decision to recover the triple combo tool string, lower the drill pipe past this interface to 309.8 mbsf, and attempt a second logging run. The tool string was deployed for this second logging run at 1900 h, reaching 251.8 mbsf, where it encountered an obstruction inside of the drill pipe. Attempts to clear the obstruction using circulation were not successful, with the pipe holding ~500 psi of pressure. Consequently, we ended logging operations and began pulling the triple combo string out of the hole. After recovering the tool string, the circulating head was rigged up and 1000 psi was applied to the drill pipe to clear the obstruction. The drill pipe was then recovered, with the end of pipe clearing the seafloor at 0245 h on 27 March. The end of pipe cleared the rotary, and the rig floor was secured for transit at 0925 h, ending that set of operations at Hole U1616E.

A plan to drill ahead through this interval of high torque using a tricone bit was formulated, but we decided to first drill a second hole at Site U1617 using the RCB system to attempt to recover the complete Messinian succession and reach the underlying basement. After completing operations at Site U1617, the vessel returned to Site U1616. The transit included surveying with the 3.5 and 12.0 kHz sonar systems over a region of geological interest. The addition of the survey resulted in a 43 nmi transit that was completed at 0324 h on 1 April at an average speed of 11.3 kt.

After the ship was positioned over Hole U1616E with the vessel in DP mode, a BHA with a 9⅞ inch tricone bit was made up and pipe was tripped toward seafloor. The VIT camera system was launched to observe reentry. Hole U1616E was reentered at 1400 h on 1 April, the VIT system was recovered, and drill pipe was tripped toward the hole depth of 371.0 mbsf. Ledges or obstructions in the hole were encountered starting at 254.8 mbsf; the top drive was picked up and drill fluid was circulated to clear out the hole. The hole was reamed and washed to 371.0 mbsf and then drilled from 371.0 to 400.0 mbsf (drilled interval 402-U1616E-241). We tripped pipe out of the hole, recovered the tricone bit, and made up a RCB BHA. We began tripping pipe back toward the seafloor and launched the VIT camera system to facilitate reentry into Hole U1616E. Reentry occurred at 2208 h on 2 April, and the VIT system was recovered.

Cores 402-U1616E-25R through 30R were all taken as half advances, penetrating 27.2 m deeper into basement and recovering 5.24 m of mantle rocks (19%). The final hole depth was 427.2 mbsf, including 123.7 m penetration into the basement below the peridotite breccia. Rate of penetration was 12.1 m/h, but the frequent wiper trips and mud sweeps required to keep the hole stable consumed significant time. During recovery of Core 30R, the drill pipe was pulled up above hole bottom to circulate drill fluid. For the next ~9 h, we reamed and cleaned the hole in an effort to remove cuttings and/or fill but were unable to reach hole bottom again. At 1000 h on 4 April, the decision was made to terminate coring in Hole U1616E and begin logging operations. A ghost core, Core 31G, was recovered, containing 0.78 m of rubble from an unknown depth within the hole.

Because of the challenging hole conditions, we elected to fully trip pipe back to the surface and reenter Hole U1616E with a logging bit that would give us greater ability to work through obstructions. The BHA with the logging bit was deployed and, while pipe was being tripped toward seafloor, the VIT camera system was launched to facilitate reentry. The seventh reentry into Hole

U1616E occurred at 0538 h on 5 April, and the VIT system was recovered. We picked up the top drive and used it to lower the drill string with the logging bit to 317.1 mbsf before racking the top drive again.

We deployed the standard triple combo tool string without the radioactive source in the HLDS because of concerns about hole stability. The bottom of the triple combo tool string passed ~25 m out of the logging bit, reaching 342.0 mbsf in the open hole, before an obstruction was encountered and the entire tool string was recovered. The hole was reamed from 317.1 to 417.0 mbsf, where we encountered significant fill ~10 m above the total hole depth. We then pumped a mud sweep to condition the hole prior to pulling the pipe back up for the second logging attempt; however, we lost rotation and became stuck at ~353 mbsf. We were able to work the stuck pipe and eventually back ream to the casing shoe. These unsafe hole conditions deep within the hole precluded further logging efforts. Pipe was tripped back to the surface, and the drill bit was recovered onto the rig floor at 0630 h on 6 April, ending operations at Site U1616.

Total operational time at Site U1616 was 18.0 days over the three visits to the site.

### 3.5.3. Principal results

#### 3.5.3.1. Lithostratigraphy

Sediment recovered from Holes U1616A, U1616B, and U1616E was split into four units based on lithology. Lithostratigraphic Unit I is divided into four subunits. In Hole U1616A, Subunit IA is characterized by nannofossil ooze and silty sand with volcaniclastics. Subunit IB is described from Holes U1616A and U1616B. It contains volcaniclastic-rich sandy silt, volcaniclastic-rich sand, and volcaniclastic-rich gravel in Hole U1616A but lacks the volcaniclastic-rich sandy silt in Hole U1616B. Subunit IC is composed of silt with volcaniclastics and volcaniclastic-rich sand. Subunit ID also contains silt with volcaniclastics, but with an increased abundance of foraminifera-rich silt. Volcaniclastic-rich nannofossil ooze, volcaniclastic-rich sand, tuff, nannofossil ooze, nannofossil chalk, and sapropel layers are also described in Subunit ID.

Unit II is present in Holes U1616B and U1616E; it contains nannofossil chalk, volcaniclastic-rich sand, foraminifera- and glauconite- rich nannofossil chalk, and nannofossil ooze with foraminifera. Unit III contains dolomitic-rich nannofossil ooze with foraminifera and is described in Holes U1616B and U1616E. Dolomite is present in Hole U1616E (Figure **F3**). Unit IV was also described in Holes U1616B and U1616E and is characterized by fine-grained consolidated breccia.

#### 3.5.3.2. Biostratigraphy

Operations at Site U1616 recovered sediment from Holes U1616A, U1616B, and U1616E. Samples from Hole U1616A consist of nannofossil ooze layers (Samples 1H-CC and 2H-CC) and are assigned to the Holocene–Middle Pleistocene (younger than 0.5 Ma) MPle2b foraminiferal biozone based on well-preserved planktic foraminifera marker species. The succession in the interval below (Samples 3H-CC to 6H-CC; to ~50 mbsf) predominantly contains volcanoclastic sediments that cannot be assigned to any biozones. Sediment from core catcher Samples 402-U1616B-2H-CC to 15X-CC are also predominantly volcanoclastic in nature. However, a few nannofossil ooze layers found within the sections allowed for the identification of the Middle Pleistocene MPle2a biosubzone. The lower half of the cored interval in Hole U1616B (Samples 16X-CC to 29X-CC) contains nannofossil ooze with intermittent volcanoclastic sediment layers. This succession between Samples 16X-CC and 22X-CC appears to be continuous and is assigned to the Calabrian MPle1 biozone (0.934–1.79 Ma). A ~1–1.2 Ma hiatus is found between Samples 22X-CC and 23X-CC. Below this hiatus, the sediments appear to be continuous and are Piacenzian (Samples 23X-CC to 26X-CC; MPl5 biozone; ~3.6 Ma) to Zanclean (Samples 27X-CC to 29X-CC; MPl4 biozone; ~3.85 Ma) in age. Hole U1616E was drilled using the RCB system, with the goal of recovering the sediment/basement interface and underlying mantle rocks. The layers above the basement rocks are Piacenzian (younger than 3 Ma) in age, identified by well-preserved marker foraminifera species.

A total of 5 samples from Hole U1616A, 20 from Hole U1616B, and 5 from Hole U1616E were examined for calcareous nannofossil content. The succession of the upper part of Hole U1616A is Chibanian–Holocene age of the Mediterranean zonal scheme of Di Stefano et al. (2023). The

upper part of the sediment interval sampled in Hole U1616B is volcanoclastic sediment of Calabrian/Chibanian age (Early Middle Pleistocene). It is characterized by a high sedimentation rate (~152 m/My) probably due to the presence of mass transport deposits (MTDs) and/or slumps. The ~1.2 Ma long hiatus between Samples 402-U1616B-22X-CC and 23X-CC observed in the planktic foraminifera data is also evident from examination of the calcareous nannofossils. The lower part of Hole U1616B (~235–290 mbsf) is represented by a continuous succession spanning the Piacenzian/Zanclean (2.82–3.56 Ma) and is characterized by an average sedimentation rate of ~55 m/My. In Hole U1616E, the sediments directly overlying the peridotite breccia are of Piacenzian/Zanclean age (2.51–2.82 Ma), thus highlighting a diachroneity of about 1 Ma with respect to age of sediments above the basement in Hole U1616B. However, both holes had a recovery of <10% in the cores across the sediment/breccia interface.

#### 3.5.3.3. Paleomagnetism

Sediment in Holes U1616A and U1616B shows normal inclination throughout the succession, measured both by scanning the archive halves on the SRM and from the analysis of discrete cubes. Sporadic reversals in the sediment are correlated with large deposits of volcanic gravel and the extreme drilling disturbance present in Sections 402-U1616B-25X-5 and 26X-2 and attributed to poor quality of NRM measurements across these intervals.

Mantle rocks from Hole U1616E are also of normal polarity, differing from what is observed in peridotites recovered from Hole U1614C. Isothermal remanent magnetization and anhysteretic remanent magnetization experiments were conducted to determine magnetic carriers in the peridotites. The results show that magnetic mineralogy is more homogeneous at Site U1616 than Site U1614.

#### 3.5.3.4. Igneous and metamorphic petrology

As at Site U1614, mantle peridotites in Hole U1616E were recovered in contact with the sediments, except that the sediment/peridotite interface at Site U1616 is marked by a basal breccia. The lithology of the igneous rocks differs significantly between the upper and lower sections of Hole U1616E (Figure **F4**). The boundary between the upper section and the lower section is an interval drilled without coring from 371 to 400 mbsf.

Hole U1616B recovered an intact primary contact between lithified dolomitized sediments and a 20 m thick basal breccia constituted of angular clasts of basalts and mantle peridotites. The peridotite clasts in the basal breccia at Hole U1616E are classified as lherzolites and harzburgites with the presence of minor plagioclase, embedded in a carbonate-rich matrix. A similar contact between sediments and highly serpentinized peridotites was recovered previously at Site U1614, where the basal polymictic breccia was found to be in direct contact with the dolomitic nannofossil ooze and a thin layer of lithified dolomite at 270 mbsf. In Hole U1616E, breccia was recovered in Cores 3R–9R. The clast size increases downhole, and the clasts consist mostly of harzburgites, exceptionally fresh diabase, and olivine-bearing gabbro. The top of the mantle peridotite section is at 303.5 mbsf.

Unlike in Hole U1614C, the mantle peridotites sampled from the upper section of Hole U1616E are relatively more homogeneous in composition and are dominated by harzburgites, with thin layers of lherzolites and dunites. Plagioclase-bearing peridotites were only observed as clasts in the carbonate breccia, not in the following mantle sections. Another feature that contrasts with Hole U1614C is the occurrence of diabase and gabbroic intrusives in Hole U1616E, with the gabbros altered to rodingites. Thin mica-bearing mafic intrusions are also rare in Hole U1616E compared to Hole U1614C. Additionally, Hole U1616E differs from Hole U1614C in terms of style of alteration, with the former having an overall lower degree of serpentinization but more intense oxidation. The intervals of oxidized mantle peridotites in the upper section of Hole U1616E are often rich in carbonate veins, ranging from a few centimeters to submillimeters in thickness. Peridotite alteration in the upper section of Hole U1616E is significantly different compared to Hole U1614C, with alteration being mostly static serpentinization with pervasive carbonate veins lacking any significant ductile shearing. The bottom of the upper section of Hole U1616E is characterized by two layers of tectonic breccia, showing millimeter- to centimeter-scale clasts of angular peridotite in a carbonate matrix. Brittle deformation is observed in several locations throughout

the section, mostly in between gabbroic veins and peridotites. Ductile deformation, on the other hand, is nearly absent in the upper peridotite section, whereas ductile deformed peridotites are present in the lower section.

The lower section of the hole was recovered beneath a drilled interval (371–400 mbsf). The section consists mostly of plagioclase-bearing harzburgites and lherzolites, with a substantial number of gabbroic intrusions. Notably, these plagioclase-bearing lithologies are absent in the upper section of Hole U1616E (303.5–371 mbsf). A significant portion of the peridotites in the lower section are intruded by mafic lithologies such as olivine gabbro, gabbro, diorite, and diabase/dolerite.

#### 3.5.3.5. Structural geology

Structural features were measured and described for sediment recovered in Holes U1616A and U1616B as well as the carbonate breccia and variably weathered serpentinized peridotites recovered in Hole U1616E.

The main structural featured observed in the sedimentary sequence was the finely laminated sediments interlayered by MTDs. No significant fault intersects the sedimentary section at Hole U1616B. Synsedimentary faults are locally observed to offset the bedding by about 10 mm. The sedimentary sequence is divided into two domains, based on the bedding dip: Domain I is characterized by subhorizontal bedding (average dip of 11°), and Domain II is characterized by moderately dipping beds and laminations (average dip of 30°).

The sedimentary sequence lies on top of an ultramafic igneous basement. The contact is marked by a breccia composed of carbonate cement and clasts of peridotite. The basement is characterized by weakly deformed peridotites locally intruded by mafic intrusions. The alteration pattern is mostly marked by weathering and carbonate impregnation. In the peridotite interval, we measured various deformation structures, including crystal-plastic and brittle deformation, fractures and microfaults, magmatic intrusions (gabbroic and pyroxene-rich), and metamorphic veins (mainly serpentine and carbonate).

#### 3.5.3.6. Sediment and pore water geochemistry

A total of 25 whole-round core samples were collected from Site U1616 for extraction and analysis of IW and corresponding bulk sediment chemistry. This total includes four IW samples from Hole U1616A between 1.3 and 26.2 mbsf and 18 samples from Hole U1616B between 65.2 and 280.7 mbsf.

The IW alkalinity varies from 0.9 to 8.1 mg/L, increasing sharply from 3.2 mg/L near the seafloor to a maximum value of 8.1 mg/L at 26.2 mbsf, corresponding to the boundary between Lithostratigraphic Subunits IA and IB. Alkalinity then exhibits a decreasing trend toward the base of the cored sediment interval, with values less than 2 mg/L below 138.7 mbsf. The pH and salinity values show little variation, ranging 7.2–7.9 and 37.0–40.0, respectively. Salinity increases across the lower part of Subunit IC (138.7–210.6 mbsf). The concentrations of sodium ($Na^+$) and chloride ($Cl^-$) vary from 478.28 to 557.90 mM and 590.81 to 637.20 mM, respectively. Their depth profiles follow salinity changes, with elevated concentrations at the middle to lower sections of Subunit IC. The profile of sulfate mirrors alkalinity values with depth, decreasing significantly from a maximum of 31.17 mM to a minimum of 21.30 mM at 26.2 mbsf. Below this depth, sulfate increases gradually to 30.13 mM at the base of the cored interval.

Dissolved magnesium ($Mg^{2+}$) and calcium ($Ca^{2+}$) show opposite concentration patterns with depth. $Mg^{2+}$ decreases downhole from 57.25 mM near the seafloor, reaching a minimum of 18.00 mM at 148.6 mbsf. Below that depth, it shows an increasing trend, with a peak concentration of 50.06 mM at the base of the cored sediment interval. In contrast, $Ca^{2+}$ increases downhole to a maximum of 36.94 mM at 148.6 mbsf and then decreases to 16.71 mM at the base of the cored sediment interval. Minor cation elements, including Li, B, Sr, and Mn, exhibit elevated concentrations at intermediate depths, with maximum values observed between 138.7 and 210.6 mbsf. The variation of ammonium ($NH_4^+$) from 26.61 to 783.32 µM follows alkalinity changes with depth, with a sharp increase to a maximum concentration from seafloor to 26.2 mbsf and a gradual decline to a minimum at the bottom of the hole. Phosphate decreases slightly with depth, with the highest value of 8.85 µM at 5.2 mbsf.

The percentage of calcium carbonate ($CaCO_3$) in bulk sediments varies from 16.3 to 28.4 wt% for Hole U1616A and from 1.7 to 84.5 wt% for Hole U1616B. The lower $CaCO_3$ percentages occur in layers associated with volcaniclastic materials, and higher $CaCO_3$ percentages are associated with foraminifera- and/or nannofossil-rich layers, dolomites, and the fine-grained consolidated breccia. Higher TN contents are found in TOC-rich sediments such as nannofossil ooze, nannofossil chalk, and sapropel, as confirmed by a strong positive correlation between these two parameters. Most of sediments are characterized by atomic TOC/TN ratios lower than 9, indicating higher inputs of marine derived organic matter and/or the presence of inorganic nitrogen bound to surface mineral particles. The highest TS contents (1.2–6.7 wt%) generally occur in TOC-rich layers.

The 38 headspace gas samples measured at Site U1616 (Hole U1616A = 7; Hole U1616B = 24; Hole U1616E = 7) contain only methane with a concentration varying from undetectable to 2.03 ppmv.

pXRF measurements were made on IW squeeze cakes and corresponding intervals along the archive section halves for Holes U1616A and U1616B. Trends in sediment geochemical data reflect compositional changes between volcanoclastic-rich layers and dolomite-rich nannofossil layers. Fe, $Al_2O_3$, $K_2O$, Rb, and Ni are all more abundant in volcanoclastic layers, and CaO and Sr are more abundant in nannofossil-rich layers. One interval of volcaniclastic-rich gravel was selected for analysis using ICP-AES. It shows high alkali contents up to 11.6 wt% $Na_2O$ + $K_2O$ because of the contribution of volcaniclastic materials.

#### 3.5.3.7. Igneous geochemistry

Igneous rocks collected from Hole U1616E were analyzed with pXRF, ICP-AES, and X-ray diffraction (XRD). Carbonated peridotite intervals were also analyzed for TC, TIC, and TS.

pXRF was used extensively at Hole U1616E to assist petrologists in characterizing and describing minor lithologies and veins. Analyses of intervals with high concentrations of $SiO_2$ and/or MgO yield analytical totals >100 wt% after data correction. This overestimation of $SiO_2$ and MgO stems from the pXRF instrument's internal calibration, which seems to be dependent on the relative abundance of these two oxides. Because of these data issues, pXRF data was used only qualitatively for assistance with petrographic description.

Results of ICP-AES analyses on the peridotites confirmed that there is much less chemical heterogeneity in the peridotites from Hole U1616E compared to those from Hole U1614C. However, as at Hole U1614C, the peridotites from Hole U1616E show CaO abundances higher than expected for a general mantle melting trend. This finding prompted us to analyze the peridotites using XRD and for TC and TIC, which confirmed the presence of calcium carbonates and the direct linear relationship between calcium carbonate content and CaO content measured with ICP-AES. Therefore, we can confirm that the exceptionally high CaO content of peridotites is imparted by the carbonation processes.

#### 3.5.3.8. Physical properties

Site U1616 comprises three holes: Hole U1616A, which sampled the uppermost 50 m of sedimentary cover; Hole U1616B, which cored from ~31 mbsf to the upper part of the consolidated breccia; and Hole U1616E, which cored the breccia and underlying basement rocks. Standard physical properties measurements, including GRA bulk density, $V_P$, and MS measured on the WRMSL, in addition to NGR, were performed on whole-round core sections of both sediment and hard rock. Section halves were X-ray imaged, and discrete $V_P$ measurements and thermal conductivity measurements were also made on intervals along the section halves. MAD samples were collected as cylinders or wedges from the cored material.

In Hole U1616B, GRA bulk density is variable in Cores 2H–6H and then gradually increases with depth from Core 10X. MS values are high in the uppermost cores where the concentration of volcaniclastic material is relatively high and then show spikes downhole, likely corresponding to volcaniclastic layers. NGR has intermediate values through most of the hole, peaking in Cores 19X and 20X around the occurrence of the tuff. NGR is low throughout the rest of the hole. Thermal conductivity shows a clear increasing trend with depth.

The basement at Hole U1616E contains predominantly serpentinized peridotite with intrusions of varying lithologies. MAD densities range 2.3–2.99 g/cm$^3$ in a gabbro, and serpentinized peridotites average 2.59 g/cm$^3$. Porosity ranges 1% (gabbro) to 21% (diorite) and averages ~8.1%. Discrete $V_P$ measurements range 2548 (serpentinized peridotites) to 6024 m/s (gabbro) and average ~3778 m/s (Figure **F6**). Finally, thermal conductivity varies from 2.12 to 3.79 W/(m·K) within a consolidated breccia. NGR data has an average value of 5.9 counts/s, and MS has an average value of 697 IU and a peak value of 5000 IU in the lowest unit.

#### 3.5.3.9. Downhole measurements

The APCT-3 tool was deployed at Site U1616 while coring Cores 402-U1616A-4H (31.2 mbsf) and 402-U1616B-4H (59.7 mbsf), giving temperatures of 14.98° and 17.91°C, respectively.

Two logging attempts were made in Hole U1616E during our initial drilling in the hole with the triple combo tool string, which included MS, electrical resistivity, bulk density, and NGR tools. During the first logging attempt, an obstruction was encountered at 306.7 mbsf, just below the breccia/basement contact. The MSS and the bottom of the tool string recorded data to this depth, going through the brecciated basement top and 1 m into the peridotites. Electrical resistivity, bulk density, and NGR data were also recorded over a shorter distance. During the second run, the tool string became stuck inside of the pipe, and logging operations were ended to clear the obstruction. For both runs, the NGR tool recorded data through pipe up to the mudline. The seafloor temperature was measured as 13.40°C. In all, 42 m of petrophysical data were recorded in open hole at Hole U1616E.

Logging was also attempted in Hole U1616E after we had finished coring the hole to its total depth of 427.2 mbsf. We hoped that the continued operations and additional cleaning of the hole would increase the chances of successful logging; however, the bottom of the triple combo tool string passed only ~25 m out of the logging bit, reaching 342.0 mbsf in the open hole, before an obstruction was encountered. Processing of the limited logging data from Hole U1616E is still in progress.

#### 3.5.3.10. Microbiology

At Site U1616, whole-round samples and syringe plugs of the core were collected on the catwalk for viral metagenomics, 16S rRNA, microbial experiments, and viral counts. Viral metagenomics and 16S rRNA samples were double-bagged and frozen at −86°C immediately after collection. Samples for viral counts were fixed in a phosphate-buffered saline formaldehyde solution. Microbial experiments were initiated under anaerobic conditions for a sample from Section 402-U1616A-11X-2. A viral incubation experiment was initiated for a sample from Section 402-U1616E-2R-2.

Oxygen measurements were conducted on whole-round cores from Hole U1616A immediately after core recovery and prior to temperature equilibration by drilling two small holes in the core liner and inserting the oxygen and temperature probes into the undisturbed core center. In Core 1H, oxygen was detected in the first 0.6 m of Section 1H-2, with the lowest detectable value of 0.6 μM (Figure **F10**). Thereafter, readings were maintained at very low concentrations to 179 mbsf, where there was an increase in concentration. However, only one additional measurement could be made below this depth because the compacted sediments inhibited probe insertion.

Additional samples were taken for microbial contamination analysis using PFD. These were taken each time microbiology samples were collected. Three samples, including drilling fluid, core exterior, and core interior were extracted using syringes and placed in glass vials. They were analyzed in the laboratory using a gas chromatograph. Comparison between core exterior and interior samples demonstrates successful delivery of the tracer to the core exterior and very low penetration of PFD into the core interiors, except for the sample from Section 402-U1616B-21X-5, which was identified as contaminated. The average concentration of the PDF in interior samples was 0.28 ng/g.

## 3.6. Site U1617, Campania Terrace

### 3.6.1. Background and objectives

Site U1617 (water depth = 2822 m) is located at the eastern end of the planned west–east transect across the Tyrrhenian Sea, in the Campania Terrace on the lower continental slope of the Tyrrhenian margin of peninsular Italy (Figures **F1**, **F11**). The basement in this margin has been generally considered to be extended continental crust, based on subdued magnetic anomalies and extensive outcrops of continental basement rocks sampled by dredging. An alternative hypothesis presented recently is that the crust of the Campania Terrace is oceanic because of its seismic velocity structure. The scientific objectives for Site U1617 were to recover a sequence of hemipelagic Pliocene–Pleistocene sediments and of possible Messinian evaporites and establish the age of the sediment/basement interface using biostratigraphy, magnetostratigraphy, and tephrochronology and to determine whether the basement is rifted continental material or basalt formed by magmatic accretion.

The original plan for Site U1617 was to drill a single hole with the RCB coring system through a total sediment column that was expected to be about 460 m thick and sample an additional 70 m of basement rocks. After coring, downhole geophysical logging was planned in the same hole to complement core recovery and collect in situ measurements of formation physical properties. This original plan had to be modified after the loss of two RCB BHAs in Holes U1612A and U1614C, which left us with only one remaining crossover drill collar to build a RCB BHA. As we intended to core at least one more RCB hole in the Vavilov Basin after the Campania Terrace site, we decided not to use the RCB system at Site U1617 to avoid any possibility of losing the last available RCB BHA. During Leg 107, the drill string became stuck in Hole 654A (Upper Sardinia margin) while drilling through an unstable conglomerate layer beneath Messinian evaporites and could be freed only after 3.5 h of strenuous efforts. Trying to reach the basement below the Messinian at Site U1617 would expose us to the same risk. The drilling plan at Site U1617 was therefore modified to core an APC/XCB hole as deep as possible through the Messinian deposits and possibly reaching the basement. Drilling operations would be stopped as soon as problems developed or when drilling rates became too slow. After coring, the hole would be logged as in the original plan. Later in the expedition, we drilled an additional RCB hole at Site U1617 in an attempt to reach below the Messinian evaporites.

### 3.6.2. Operations

The 40.1 nmi transit from Site U1616 to Site U1617 was completed at an average speed of 10.4 kt, with the vessel arriving at 2150 h on 12 March 2024 and transitioning from cruise to DP mode. The PDR gave a water depth reading of 2822.3 m. After tripping pipe to seafloor, we spaced out and spudded Hole U1617A at 0715 h on 13 March, confirming a water depth of 2822.3 m. The mudline Core 1H advanced 4.5 m with 100% recovery. Coring continued smoothly to Cores 15H, 16H, 20H, and 21H, which were partial strokes, and the drill bit was advanced by recovery. Cores

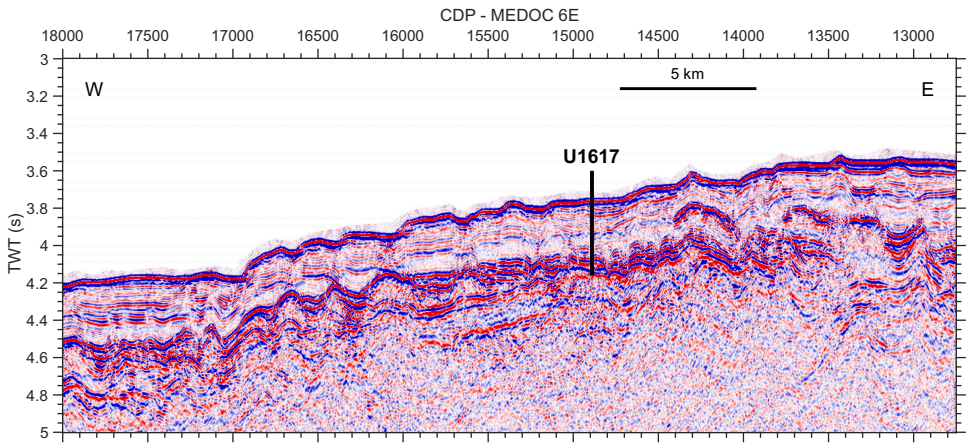


**Figure F11.** Site U1617 (Campania Terrace) on Seismic Line MEDOC 6 (location in Figure F1).

22F–27F were subsequently collected as HLAPC cores. Cores 16H–27F all experienced overpull, ranging 12–40 klb. As such, the XCB system was used starting with Core 28X. Recovery in Cores 28X and 30X–35X was over 100%, but Cores 29X, 36X, and 37X had low recovery. Rate of penetration slowed considerably starting in Core 36X, and a lithologic change into evaporite deposits was noted. All cores after Core 36X were taken as half advances to improve recovery and because of slow rates of penetration. Coring continued through Core 47X, reaching a final hole depth of 339.9 mbsf. Although we did not achieve the objective of tagging basement, the hole was ended to conserve time and because the thickness of the evaporite deposits from the seismic data was not clear.

Overall, Hole U1617A recovered 304.2 m of sediment from the 339.9 m advance (89%). APC and HLAPC cores recovered 217.74 m of sediment (104%), and XCB cores recovered 86.42 m (66%). APCT-3 tool measurements were made during Cores 4H, 7H, and 10H. Nonmagnetic core barrels were used for all APC cores, and all full-length APC cores were oriented. The perfluorocarbon microbial contamination tracer was pumped with the drill fluid throughout.

Following completion of coring in Hole U1617A, the hole was conditioned for downhole logging by pumping a sweep of high-viscosity mud. The drill pipe was tripped up with the bit at 74.6 mbsf, and the triple combo tool string was deployed to log the open hole. At 0500 h on 16 March, with the triple combo tool string at 135.4 mbsf, the tool string encountered an obstruction and this first logging attempt was ended. The tools were recovered, and three stands of drill pipe were added to the drill string, bringing the bit depth to 151.7 mbsf, past the initial obstruction. At 0845 h, the triple combo tool string was deployed a second time; however, the tool string encountered an obstruction just outside of the bit and was unable to completely exit the drill pipe. The decision was made to end logging attempts and pull out of the hole. At 2100 h, the rig floor was secured, the thrusters were raised, and we began the transit back to Site U1616, where we planned to install a reentry system and casing for RCB drilling in the basement.

Operations at Site U1616 took place 17–27 March 2024. After encountering a formation that caused high torque and overpull in Hole U1616E and attempting to log the hole, the decision was made to return to Site U1617 and drill a second hole that would penetrate past the Messinian deposits into pre-Messinian sediment and/or basement. Because of the poor recovery with the XCB system in Hole U1617A, the plan was to drill ahead to 250 mbsf with an RCB bit and then core with the RCB system until we had at least captured the sediment/basement interface. The return transit from Site U1616 to U1617 included surveying with the 3.5 and 12.0 kHz sonar systems, crossing perpendicular to a series of ridges that may have formed during the detachment faulting. In all, the transit was 57.7 nmi and took 5.3 h at a speed of 10.9 kt.

After the vessel arrived on site, we lowered the ship's thrusters and transitioned to DP mode. By 1600 h on 27 March, we were positioned over the coordinates for Hole U1617B, which was offset ~20 m north of Hole U1617A. We made up the BHA with a RCB bit and began tripping pipe toward the seafloor. Hole U1617B was spudded at 2330 h on 27 March. Drilled interval 402-U1617B-11 penetrated to 250.0 mbsf and was completed at 1030 h on 28 March before recovering the center bit so that coring could begin.

RCB drilling in Hole U1617B progressed from 250.0 to 370.4 mbsf with Cores 2R–22R. Recovery was high in Cores 2R–5R (ranging 89%–126%) but only 10% in Core 6R. Cores were drilled as half advances starting from Core 7R to improve recovery. The low recovery is attributable to the evaporite and halite lithologies. The final core, Core 22R, crossed a lithologic boundary from halite into a black shale that was observed on the catwalk to have a strong petroleum smell. Coring operations were paused while the headspace gas safety measurement for hydrocarbon content and composition was completed. The sample was found to have an anomalously low ratio of methane/ethane, indicating a thermogenic origin, halting further drilling in Hole U1617B. Overall, coring in Hole U1617B advanced 120.4 m and recovered 68.6 m of sediment, evaporites, and shale (57%).

Preparations then began for logging of Hole U1617B using the triple combo and FMS-sonic tool strings. Drill fluid was circulated through the hole, and the core barrel deployed prior to stopping coring operations was retrieved. Pipe was tripped up to 311.6 mbsf, and a 40 bbl sweep of sepiolite mud was pumped. Pipe was then tripped back to 370.4 mbsf, and the rotary shifting tool was

deployed to release the RCB bit at the bottom of the hole. Finally, pipe was set at 279.9 mbsf and the triple combo tool string was deployed at 1700 h on 30 March. The tool string encountered an obstruction at 328.4 mbsf that could not be worked through. The triple combo tool string was recovered. Because we did not reach deep enough to open the caliper on the triple combo and measure hole diameter, we could not run the FMS tool and instead ran the DSI without the FMS. The sonic tool successfully passed down to the obstruction at 328.4 mbsf and then completed an uplog. By 0445 h on 31 March, the tool had been recovered and rigged down.

We picked up the top drive and washed down past the obstruction to hole bottom and then continued to circulate while pulling pipe up to 336.8 mbsf with the goal of conducting a second logging run to total hole depth. The triple combo tool string was deployed at 1045 h on 31 March, with the caliper and density tools removed to shorten the tool string and maximize the depth of data recorded by the other tools. The triple combo tool string reached 364 mbsf, near the hole bottom at 370.4 mbsf. It was then recovered, and the hole was displaced with heavy mud due to the anomalous $C_1/C_2$ ratio.

Pipe was tripped back to the surface, and the rig floor was secured for transit at 2248 h. The vessel transitioned from DP to cruise mode, and the transit to return to Site U1616 and deepen Hole U1616E began at 2305 h on 31 March, ending Site U1617.

### 3.6.3. Principal results

#### 3.6.3.1. Lithostratigraphy

The sediment sequence at Site U1617 was divided into three lithostratigraphic units based on lithology. Tephra, sapropel and organic-rich mud layers intercalate the predominant nannofossil ooze in the upper part of Hole U1617A, defined as Unit I. Below, an intermediate unit formed by foraminifera-rich nannofossil ooze demarcates the boundary with underlying Messinian evaporitic facies recovered in Holes U1617A and U1617B. MTDs were present throughout the entire sedimentary succession, most notably in Cores 402-U1617A-4H, 7H, 8H, 10H, 15H, 27F, and 28X.

Unit I is divided into three subunits. Subunit IA is characterized by nannofossil ooze that is intercalated with tephra, sapropel and organic-rich mud layers. Subunit IB is formed by the same lithologies found in Subunit IA but is devoid of tephra layers. In Subunit IC, nannofossil ooze is still the principal component, intercalated with tephra layers and characterized by the increasing content of foraminifera. Unit II consists of a predominantly foraminifera-rich nannofossil ooze deposit, sometimes intercalated with layers characterized by minor foraminifera content. Unit III contains Messinian evaporite deposits and is also divided into three subunits. Subunit IIIA is formed by oxide-, dolomitic-, gypsum-, or organic-rich mud; gypsum; nannofossil-rich mud or silt; clay with dolomite; and black shale. Subunit IIIB contains anhydrite, organic-rich mud, gypsum with anhydrite, oxide-rich anhydrite, and mudstone. Subunit IIIC is characterized by halite, gypsum, and black shale (Figure **F3**.)

#### 3.6.3.2. Biostratigraphy

Expedition 402 drilled ~340 m of sediment in Hole U1617A. Sedimentary intervals retrieved were mostly nannofossil ooze, containing very well preserved calcareous nannofossils and planktic foraminifera species. In contrast to the other sites, the volcanogenic sediments at this site are very limited. Microfossil marker species' assemblages across the various sedimentary intervals were analyzed from the core catcher samples to decipher the biostratigraphic zonation scheme at the site.

Holocene–upper Zanclean (~4.11 Ma) sedimentary successions were recognized in Samples 402-U1617A-1H-CC to 33X-CC. A hiatus of ~0.5 My lies between Samples 13H-CC and 14H-CC because planktic foraminiferal events corresponding to the MPl6b biozone are not detected. Sedimentary successions above and below these intervals are found to be continuous. Sediments containing evaporite minerals such as gypsum are present starting with Sample 36X-CC and are interpreted to be Messinian age deposits based on previous research in and around these regions. Two core catcher samples, 34X-CC and 35X-CC, were taken to date the sediments above the Messinian deposits. However, these sediments contain entirely organic silt and oxide-rich mud, which are barren of planktic foraminifera marker species. Additional samples for postcruise analyses

were taken from Cores 34X and 35X to refine the age of the sediments deposited above the Messinian sediments. Planktic foraminifera species used for biostratigraphy in Site U1617 are illustrated in Figure **F12**.

Smear slide samples for nannofossil analysis were prepared from 35 core catcher samples. Samples from Cores 402-U1617A-1H through 6H yield abundant and well-preserved nannofossil assemblages of early Pleistocene–Holocene age (younger than 1.24 Ma). Samples 7H-CC to 13H-CC were assigned to the biostratigraphic interval spanning the MNQ19d–MNQ19a biozones (early/middle Pleistocene), highlighting a repetition in the sedimentary succession that may relate to slumping or MTDs. None of the samples were attributed ~0.2 My long MNQ18 biozone. From Sample 13H-CC downhole, we recovered an almost continuous sedimentary succession ranging

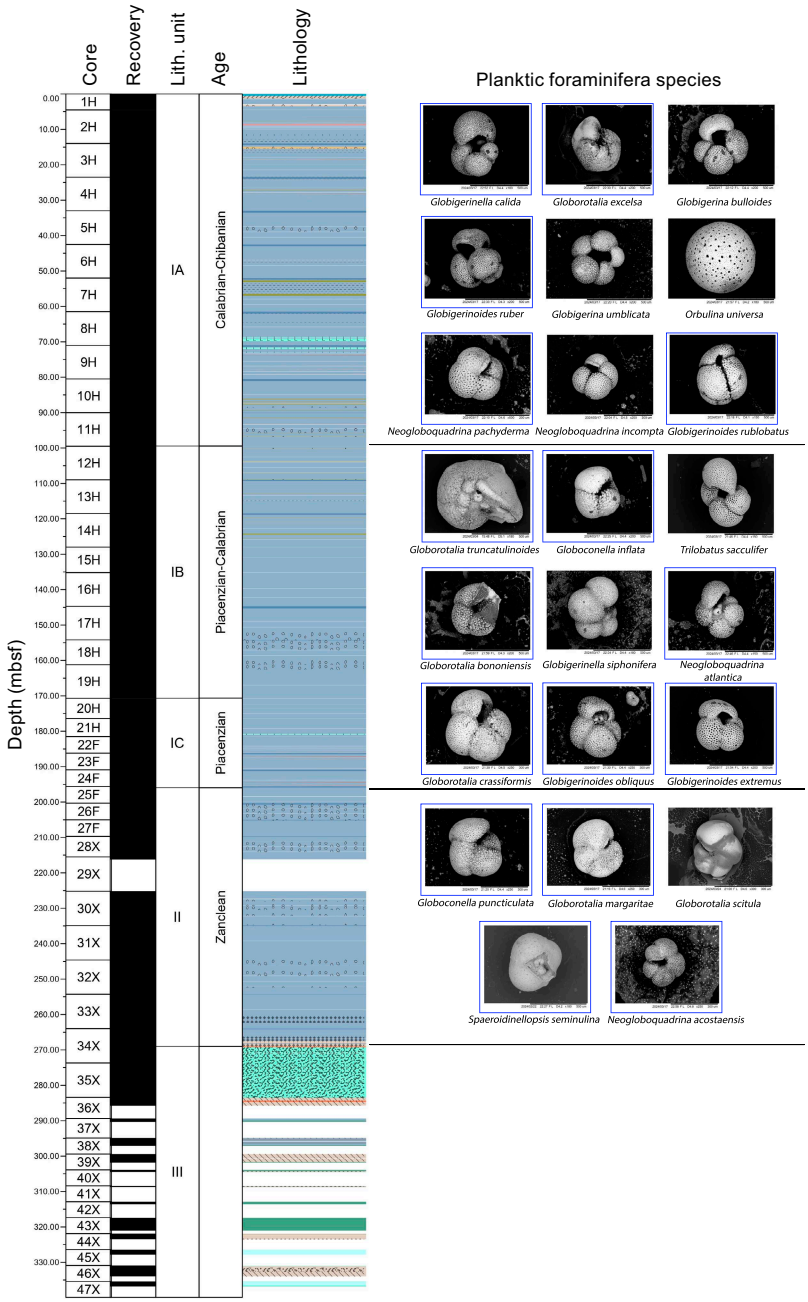


**Figure F12.** Planktic foraminifera species from different stages, Site U1617. Blue rectangles represent the important marker species within each geological stage. The rest are prominent Late Neogene species.

from the early Pleistocene–Gelasian to the early Pliocene–Zanclean. The boundary between Zanclean and Messinian sediments was detected in Section 34X-4.

Hole U1617B was drilled to capture the complete Messinian sediment succession at the site. No core catcher samples were collected from the Messinian evaporite sedimentary sequences. The core catcher samples collected above (Samples 2R-CC to 5R-CC) are stratigraphically concurrent to the sedimentary succession observed in Samples 402-U1617A-32R-CC to 35R-CC. Samples 402-U1617B-2R-CC to 5R-CC are Zanclean in age (younger than 5.332 Ma). Additional samples for postcruise analyses and age refinement were taken from the core sections.

#### 3.6.3.3. Paleomagnetism

Hole U1617A recovered 47 cores down to ~340 mbsf, ending in the Messinian evaporites. Analyses of archive-half sections on the SRM show mostly normal polarity with sporadic reversals that appear too short in length/duration to be reliable. However, one reversal is recorded for almost the entire length of Section 18H-4A and can be correlated to the Geomagnetic Polarity Time Scale (Ogg, 2020) using biostratigraphy. Rock magnetic measurements of discrete samples show abnormal magnetic fabrics that may be attributed to gravitational slumps. Magnetic properties overall correlate with lithology. Specifically, the Messinian units have a much lower magnetization.

Hole U1617B recovered 21 cores to 370.4 mbsf. Archive-half and discrete samples show normal polarity from the top of the cored interval to when evaporite deposits become predominant at ~290 mbsf. Here, the magnetic intensity is extremely low, close to the threshold that the SRM can detect. Thus, below ~290 mbsf, our inclination data are sporadic and unreliable.

#### 3.6.3.4. Structural geology

The primary structural features at Site U1617 are fine laminations of sediment interlayered by MTDs. Structural geology measurements include the orientation of bedding, fractures, faults, and folds. The high recovery allowed us to identify an angular unconformity at about 205 mbsf in Hole U1617A, which divides the succession into two structural domains. The first domain (from Cores 1H–26F) is characterized by subhorizontal bedding (average dip 9°) interlayered by MTDs. The second domain is characterized by a change in bedding dip with an average dip of 21°. Domain II also corresponds to the transition to Messinian deposits, characterized by alternation of colorful sediments with gypsum veins and evaporitic facies. Domain III is characterized by organic-rich, subhorizontal deposits. Dips do not exceed 10° for an average of 6°.

#### 3.6.3.5. Sediment and pore water geochemistry

A total of 33 IW and 55 sediment samples were collected from 1.5 to 336.7 mbsf in Hole U1617A, and 7 IW and 16 sediment samples were collected from 251.0 to 366.7 mbsf in Hole U1617B.

For IW samples, the pH value is in a narrow range of 7.3–7.6, and alkalinity (1.5–3.5 mg/L) exhibits an overall decreasing trend throughout the cored interval. Pore water salinity varies substantially, with all but one value ranging 37.5–49.0. Above the boundary between Lithostratigraphic Units I and II, salinity is approximately constant at 38.5. Below that boundary, salinity increases continuously. However, one sample at 308.1 mbsf (Section 402-U1617B-10R-1) has salinity of 73.5, deviating from the overall depth pattern. This elevated value is most likely due to the dissolution of underlying evaporite deposits. Accordingly, sodium ($Na^+$) and chloride ($Cl^-$) contents in that sample are also concentrated, with values of 1052.71 and 1169.83 mM, respectively, whereas concentrations in other samples vary from 494.87 to 620.02 mM for $Na^+$ and 604.56 to 726.98 mM for $Cl^-$. Sulfate ($SO_4^{2-}$) shows significant changes (23.54–59.85 mM), decreasing from the sediment/water interface to 85.0 mbsf and increasing downhole below that. The concentration of magnesium ($Mg^{2+}$) varies from 51.02 to 60.81 mM, a more limited range than was observed at other expedition sites. Calcium (Ca), Lithium (Li), Boron (B), and Strontium (Sr) show elevated concentrations near the bottom of the hole but different gradients, and there is a decrease in concentration downhole for potassium (K) and manganese (Mn). All major and minor elements fluctuate in concentration near the base of the cored interval. Ammonium ($NH_4^+$) varies from 0.10 µM near the seafloor to 503.89 µM at 252.67 mbsf. Phosphate ($PO_4^{3-}$), with a maximum concentration of 5.25 µM, shows fluctuations with no obvious trend downhole.

The percentage of calcium carbonate in the sediment varies from 0.3 to 75.5 wt%. Sedimentary TOC and TN contents range from nondetectable to 10.6 and 0.32 wt%, respectively. Atomic TOC/TN ratios vary between 0.3 and 79.1. Atomic TOC/TN ratios of ~10.4 or higher are found in sapropel and black shale layers, confirming that this ratio is affected by organic matter diagenesis due to more labile algal-derived organic matter rather than by higher inputs of terrestrial derived organic matter. TS contents range from nondetectable to 35.8 wt%, with the highest values occurring in these TOC-rich layers, indicating the formation of organic-S-molecules via sulfuration process that is known to protect these molecules from microbial degradation.

The 61 headspace gas samples analyzed (Hole U1617A = 40; Hole U1617B = 21) mostly contain only methane except at 336.4 mbsf (Hole U1617A) and 367.4 mbsf (Hole U1617B). In Hole U1617B, an anomalous $C_1/C_2$ relationship with temperature (~60°C) is observed, and this observation resulted in the termination of coring in Hole U1617B.

Squeeze cakes generated during the extraction of IW from Holes U1617A and U1617B were analyzed using pXRF, along with intervals from the corresponding archive section halves. A total of 32 squeeze cakes from Hole U1617A and 7 squeeze cakes from Hole U1617B were analyzed. The data generated from Site U1617 comprise the cleanest pXRF data set collected so far during Expedition 402 and show chemical changes downhole with good agreement between the IW squeeze cake and section half measurements. In the uppermost 50 m of sediment at Hole U1617A, we see corresponding increases in $Al_2O_3$, CaO, and Ni as the nannofossil oozes become richer in volcanic ash layers. Between 50 and 260 mbsf, contents for all reported elements are generally consistent. Below ~260 mbsf, we see sharp increases in Fe and Rb contents and equally sharp decreases in CaO and Sr contents, which probably result from the transition to organic- and oxide-rich silt lithologies from the oozes. These trends are observed to continue with depth in Hole U1617B. From ~275 to ~310 mbsf, we see increases in Fe, Cu, Ni, and Rb and decreases in MnO, CaO, and Sr. Because of the texture and novelty of the sediments in the evaporite layers, IW samples were not taken, and compositions for these sections were not determined using pXRF.

#### 3.6.3.6. Physical properties

Site U1617 was drilled on the Campania Terrace to the east of the Flavio Gioia Seamount. We acquired a regular set of physical properties on the 47 and 21 cores recovered from Holes U1617A and U1617B, respectively, that included $V_P$, GRA bulk density, MS, and NGR measurements. In addition, we took X-ray images of all section halves after the cores were split. We then collected 77 and 37 MAD samples for density and porosity calculations and performed 42 and 24 thermal conductivity measurements for Holes U1617A and U1617B, respectively. We made more than 250 point velocity measurements in the *X*-direction for the rocks recovered from both holes.

Our measurements show that the bulk density of sediments at Site U1617 varies from 1.343 to 2.925 g/cm$^3$ (average = 1.965 g/cm$^3$), and MAD porosity changes from 80% in the nannofossil-rich ooze at the top of Lithostratigraphic Unit I to 0% in halite layer encountered in Unit III at the bottom of Hole U1617B (average porosity for the two holes is 46%). The discrete $V_P$ values measured on the section halves from both holes vary from 1496 m/s in Unit I to 5223 m/s in Unit III (Figure **F6**). Overall, densities, porosities, and velocities reveal a typical sedimentary compaction trend in Units I and II. High density, low porosity, and fast velocity values correspond to evaporite samples from Unit III, consisting of the Messinian gypsum, anhydrite, and halite sequences.

NGR varies from 0 to 246 counts/s with an average value of 36 counts/s for both holes. In general, NGR has a decreasing trend from the seafloor to the top of Unit III, where it increases from ~20 to ~70 counts/s. Thermal conductivity is generally stable in Units I and II with an average value of 1.26 W/(m·K). In Unit III, the thermal conductivity increases dramatically to 6.605 W/(m·K) over the evaporitic section, with the highest value measured on an anhydrite nodule from Section 402-U1617B-12R-4. MS is highly variable in Unit I, with individual peaks to 800 IU measured on whole-round sections and to 1300 IU for point measurements, whereas it is more stable in Unit II (21 and 22 IU average on whole-round sections and points, respectively). MS is highly variable in Unit III, with individual peaks to 1530 IU (whole-round sections) and 5689 (point measurement) over the oxide-rich intervals.

#### 3.6.3.7. Downhole measurements

In Hole U1617A, formation temperature measurements of 17.79°, 21.47°, and 24.83°C were made with the APCT-3 tool while coring Cores 4H, 7H, and 10H at depths of 33.0, 61.5, and 90.0 mbsf, respectively.

The triple combo logging tool string, including tools for measuring MS, electrical resistivity, bulk density, and NGR, was deployed twice in Hole U1617A. During the first run, the drill bit was positioned at 74.6 mbsf and the tool string encountered an obstruction at 135.4 mbsf that could not be worked through. During the second run, the drill bit was lowered to 151.7 mbsf, past the initial obstruction, but the logging tool could not fully pass out of the drill pipe. The bottommost tool on the string, measuring MS, recorded data to 171.5 mbsf. For both runs, the NGR tool recorded data through the open hole and through the pipe up to the mudline.

Logging took place in Hole U1617B after coring operations were terminated due to the anomalously low methane/ethane ratios. The first run occurred with the triple combo tool string and the drill pipe set at 279.9 mbsf. The tool string recorded MS data to 328 mbsf, going through the gypsum-rich layers and some anhydrite near the base of the section, before encountering an obstruction. Electrical resistivity and NGR data were also recorded over a shorter distance. During the second run, the DSI and the HNGS recorded data to the same depth as the first run. The FMS was not run because the caliper was not opened during the triple combo run and the hole diameter was unknown. The hole was then cleaned, and pipe was moved past the obstruction for a final logging attempt. MS, electrical resistivity, and NGR data were recorded through the halite deposits and down to ~365 mbsf, only a few meters off hole bottom (370.4 mbsf). Because we expect the halite interval to be washed out, the sonic tool was not deployed.

#### 3.6.3.8. Microbiology

In Hole U1617A, whole-round samples and syringe plugs of the core were collected on the catwalk for viral metagenomics, 16S rRNA, microbial experiments, and viral counts. Viral metagenomics and 16S rRNA samples were double-bagged and frozen at −86°C immediately after collection. Samples for viral counts were fixed in a phosphate-buffered saline formaldehyde solution. Microbial experiments were initiated under anaerobic conditions for samples from Sections 9H-5 and 12H-7. In addition, viral incubations and prophage induction experiments were initiated for samples from Sections 3H-5 and 7H-5.

Oxygen measurements were conducted on whole-round cores from Hole U1617A immediately after core recovery. In Core 1H, oxygen was detected in the uppermost 6 m, with the lowest detected concentration of 0.1 µM (Figure **F10**). Thereafter, readings were maintained at very low concentrations to 90 mbsf, where probe insertion was no longer possible because of the compacted nature of the sediment.

While coring in Hole U1617A, the microbial contamination tracer PFD was pumped along with drill fluid. Samples for the PFD tracer were taken each time microbiology samples were collected. Three samples from each core, including drilling fluid, core exterior, and core interior, were extracted using syringes and placed in glass vials. They were measured in the laboratory using a gas chromatograph, with results compared between exterior and interior samples. PFD was detected in core exterior samples, indicating successful delivery of the tracer, and 6 out of 27 core interior samples (from Sections 8H-6, 9H-6, 10H-6, 15H-4, 31X-6, and 32X-6). However, the concentrations detected in both types of samples were very low. Most interior samples had 0 ng PFD/g sediment.

# 4. Preliminary scientific assessment

## 4.1. Operations

Coring of both sediment and basement material during Expedition 402 proved more challenging than anticipated. The original operations plan estimated 2326 m of coring in sediment and 560 m of coring in basement across six primary sites. Instead, Expedition 402 cored 1890.3 m of sediment (54% recovery) and 369.6 m of basement (35% recovery) across the six sites (Figure **F13**; Table **T1**).

Several of the sites occupied were alternates after it was determined operations would not be possible at the original primary sites. Given the pervasive, unexpected challenges, we view the drilling operations achieved as immensely successful.

Sediments within the Vavilov Basin at Sites U1612 and U1614–U1616 contain two seemingly contiguous volcanogenic layers that create hole instability. A volcaniclastic gravel at ~50–70 mbsf is ~10–40 m thick, depending on the site. Shore-based research will map its extent and origin. Deeper in the sediment column is a tuff layer that may turn to rubble when cored and fall in. At our first site, Site U1612, we became stuck while coring the granitoid basement and assumed that pieces of unconsolidated breccia or rubbly granitoid rock had trapped the drill string somewhere along the length of the BHA. As such, we first severed the drill pipe just above the BHA. This first attempt did not free us, indicating that we were stuck somewhere within the sediment column. We now presume that the gravel and/or tuff interval collapsed around the drill string and that circulating fluid was being lost to the formation along those porous layers rather than transporting material out of the hole.

In the first hole drilled during Expedition 402 (Hole U1612A), recovery of the gravel and tuff intervals was extremely low when coring with the RCB system. This low recovery prompted changes to our operational plans. The original plan involved drilling first an RCB hole that would capture the sediment column and penetrate 70–140 m into basement at each site in the Vavilov Basin, followed by an APC/XCB hole that would recapture the sediment/water and sediment/basement interfaces. The low sediment recovery prompted a reversal in order: at Sites U1614–U1617, a first APC/XCB hole sampled the entire sediment succession and determined the vertical extent of unstable volcaniclastics that could cause drilling problems. Then, at Sites U1614 and U1616, a reentry system and casing was installed to below the depths of these problematic intervals. At Site U1615, thick layers of volcaniclastic gravels as well as volcaniclastic sands made it unsuitable for casing. Proposed primary Site TYR-18A was also removed from the operational schedule because of its estimated 621 m thick sediment, which may contain problematic volcaniclastic sequences. At Site U1617, on the Campania Terrace outside of the Vavilov Basin, sediment contained little volcaniclastics, and we achieved our highest core recovery of the expedition in Hole U1617A (89%). However, the XCB system did not provide high recovery or good quality cores in the Messinian evaporites, and a second Hole U1617B was drilled with the RCB system to capture the Messinian sequence and attempt to reach the basement.

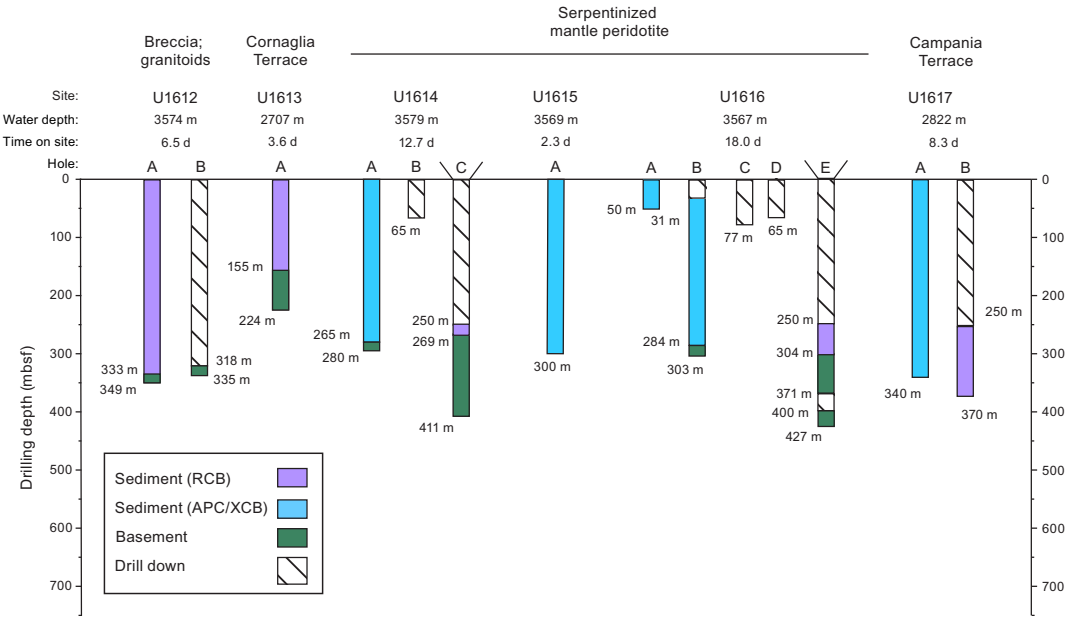


**Figure F13.** Holes drilled during Expedition 402, shaded by drilling technique.

Drilling into basement rocks presented its own challenges. In Hole U1614C, the drill pipe became stuck in basement with no prior indication of hole issues. While coring Hole U1616E, especially in the interval below the drill-ahead from 371.0–400.0 mbsf, we experienced high torque and had to use frequent wiper trips and mud sweeps to keep the hole stable. The drilled interval in Hole U1616E may contain tectonic breccia, and the underlying cored interval (400.0–427.2 mbsf) contains intrusions of lithologies such as gabbro, diorite, and diabase that are extremely hard and prone to turning to rubble during drilling. Losing circulating fluid to a possible fault zone along this interval would exacerbate the effects of rubble falling in and leave us unable to clean the hole. At Site U1612, the granitoids around the sediment/basement interface exhibited similar behavior during coring and likely contributed to our getting stuck in Hole U1612A as well as the high torque and overpull experienced in Hole U1612B.

**Table T1.** Hole summary, Expedition 402. NA = not applicable.

| Hole | Latitude | Longitude | Water depth (m) | Penetration DSF (m) | Drilled interval (m) | Cored interval (m) | Recovered length (m) | Recovery (%) | Total cores (*N*) | APC cores (*N*) | HLAPC cores (*N*) | XCB cores (*N*) | RCB cores (*N*) | Ghost cores (*N*) |
|---|---|---|---|---|---|---|---|---|---|---|---|---|---|---|
| U1612A | 40°11.0320′N | 12°37.9460′E | 3573.8 | 348.7 | NA | 348.7 | 75.41 | 22 | 39 | 0 | 0 | 0 | 39 | 0 |
| U1612B | 40°11.0329′N | 12°37.9598′E | 3573.8 | 334.9 | 318.1 | 16.8 | 3.80 | 23 | 3 | 0 | 0 | 0 | 3 | 0 |
| | | Site U1612 totals: | | 683.6 | 318.1 | 365.5 | 79.21 | 22 | 42 | 0 | 0 | 0 | 42 | 0 |
| U1613A | 40°0.0593′N | 10°59.1732′E | 2706.8 | 223.6 | NA | 223.6 | 99.63 | 44 | 24 | 0 | 0 | 0 | 24 | 0 |
| | | Site U1613 totals: | | 223.6 | NA | 223.6 | 99.63 | 44 | 24 | 0 | 0 | 0 | 24 | 0 |
| U1614A | 40°15.9781′N | 12°42.3164′E | 3579.0 | 280.1 | NA | 280.1 | 179.36 | 64 | 34 | 9 | 5 | 20 | 0 | 1 |
| U1614B | 40°15.9792′N | 12°42.3174′E | 3579.0 | 65.5 | 65.5 | 0 | 0.00 | 0 | 0 | 0 | 0 | 0 | 0 | 0 |
| U1614C | 40°15.9683′N | 12°42.3174′E | 3579.0 | 410.6 | 250.0 | 160.6 | 71.58 | 44 | 27 | 0 | 0 | 0 | 27 | 0 |
| | | Site U1614 totals: | | 756.2 | 315.5 | 440.7 | 250.94 | 57 | 61 | 9 | 5 | 20 | 27 | 1 |
| U1615A | 40°11.0430′N | 12°40.6299′E | 3568.6 | 300.0 | NA | 300.0 | 115.09 | 38 | 34 | 10 | 3 | 21 | 0 | 0 |
| | | Site U1615 totals: | | 300.0 | NA | 300.0 | 115.09 | 38 | 34 | 10 | 3 | 21 | 0 | 0 |
| U1616A | 40°11.0637′N | 12°34.0295′E | 3567.0 | 50.2 | NA | 50.2 | 47.72 | 95 | 6 | 6 | 0 | 0 | 0 | 0 |
| U1616B | 40°11.0628′N | 12°34.0381′E | 3567.0 | 302.6 | 31.2 | 271.4 | 156.57 | 58 | 28 | 5 | 0 | 23 | 0 | 0 |
| U1616C | 40°11.0491′N | 12°34.0397′E | 3567.0 | 76.9 | 76.9 | 0 | 0.00 | 0 | 0 | 0 | 0 | 0 | 0 | 0 |
| U1616D | 40°11.0520′N | 12°34.0260′E | 3567.0 | 66.1 | 66.1 | 0 | 0.00 | 0 | 0 | 0 | 0 | 0 | 0 | 0 |
| U1616E | 40°11.0506′N | 12°33.9972′E | 3567.0 | 427.2 | 279.0 | 148.2 | 31.11 | 21 | 28 | 0 | 0 | 0 | 28 | 1 |
| | | Site U1616 totals: | | 923.0 | 453.2 | 469.8 | 235.40 | 50 | 62 | 11 | 0 | 23 | 28 | 1 |
| U1617A | 40°0.0211′N | 13°24.4662′E | 2822.3 | 339.9 | NA | 339.9 | 304.20 | 89 | 47 | 21 | 6 | 20 | 0 | 0 |
| U1617B | 40°0.0317′N | 13°24.4662′E | 2822.3 | 370.4 | 250.0 | 120.4 | 68.91 | 57 | 21 | 0 | 0 | 0 | 21 | 0 |
| | | Site U1617 totals: | | 710.3 | 250.0 | 460.3 | 373.10 | 81 | 68 | 21 | 6 | 20 | 21 | 0 |
| | | Expedition totals: | | 3596.7 | 1336.8 | 2259.9 | 1153.40 | 51 | 291 | 51 | 14 | 84 | 142 | 2 |

| Hole | Date started (2024) | Time started UTC (h) | Date finished (2024) | Time finished UTC (h) | Time on hole (h) | Time on hole (days) |
|---|---|---|---|---|---|---|
| U1612A | 14 Feb | 1500 | 19 Feb | 1200 | 117.12 | 4.88 |
| U1612B | 6 Apr | 0430 | 7 Apr | 1926 | 38.88 | 1.62 |
| | | | Site U1612 totals: | | 156.00 | 6.50 |
| U1613A | 19 Feb | 1907 | 23 Feb | 0830 | 85.50 | 3.56 |
| | | | Site U1613 totals: | | 85.50 | 3.56 |
| U1614A | 23 Feb | 1700 | 26 Feb | 2000 | 75.12 | 3.13 |
| U1614B | 26 Feb | 2000 | 27 Feb | 1800 | 21.60 | 0.90 |
| U1614C | 27 Feb | 1800 | 7 Mar | 0900 | 207.12 | 8.63 |
| | | | Site U1614 totals: | | 303.84 | 12.66 |
| U1615A | 7 Mar | 0900 | 9 Mar | 1600 | 54.96 | 2.29 |
| | | | Site U1615 totals: | | 54.96 | 2.29 |
| U1616A | 10 Mar | 0215 | 10 Mar | 1200 | 9.84 | 0.41 |
| U1616B | 10 Mar | 1400 | 12 Mar | 1630 | 50.40 | 2.10 |
| U1616C | 17 Mar | 0015 | 17 Mar | 2115 | 21.12 | 0.88 |
| U1616D | 17 Mar | 2115 | 19 Mar | 1500 | 41.76 | 1.74 |
| U1616E | 19 Mar | 1500 | 1 Apr | 1230 | 309.60 | 12.90 |
| | | | Site U1616 totals: | | 432.72 | 18.03 |
| U1617A | 12 Mar | 2100 | 16 Mar | 2000 | 95.04 | 3.96 |
| U1617B | 27 Mar | 1438 | 31 Mar | 2153 | 103.20 | 4.30 |
| | | | Site U1617 totals: | | 198.24 | 8.26 |
| | | | Expedition totals: | | | 49.01 |

Planned logging efforts were more substantially impacted by difficult hole conditions and achieved limited success. At most sites, logging tool strings quickly encountered obstructions after being lowered below the base of the BHA and recovered only short intervals of data in the open hole. We could only deploy a subset of the logging tool strings that were planned and were never able to run the imaging tools (FMS or UBI).

## 4.2. Scientific objectives

### 4.2.1. Objective 1: to determine the kinematics and geometry of the extensional deformation in space and time

The deepest central part of the Tyrrhenian Sea, the Vavilov Basin (water depth = ~3600 m), is flanked to the west by the Cornaglia Terrace and to the east by the Campania Terrace, both about 600–800 m shallower. The working hypothesis to be tested during Expedition 402 was that new magmatic crust formed first before the Messinian in the Cornaglia and Campania Terraces, followed by Pliocene mantle exhumation in the Vavilov basin.

The results from Site U1613 clarified that the crust of the Cornaglia Terrace is continental and not magmatic in nature. The in situ geologic basement was reached underneath ~150 m of sediments and can be correlated to prerift rocks outcropping farther west in Sardinia. The oldest sediment resting above the basement is dated to the Messinian. In the Campania Terrace, Site U1617 crossed the Pliocene–Quaternary sedimentary succession and sampled the Messinian evaporites. Although the geologic basement could not be reached at this site, the results established that in the Messinian the Campania Terrace experienced evaporite deposition, including halite. Therefore, during the Messinian the Campania Terrace was likely connected to the Cornaglia Terrace, which contains extensive salt deposits that accumulated in the deepest parts of the Tyrrhenian at the time (Fabbri and Curzi, 1979; Malinverno et al., 1981). These observations provide robust new constraints on the extent and age of the crustal extension in the Tyrrhenian margins around the central Vavilov Basin.

Drilling at Sites U1612, U1614, and U1616 provided conclusive evidence that the basement of the Vavilov Basin consists of serpentinized upper mantle peridotites and that mantle exhumation was not followed by the formation of a magmatic oceanic crust. The sediments collected at the basement contact in these sites constrain the minimum age of the emplacement of the mantle rocks, which took place in the Pliocene after the Messinian. The oldest sediments above the basement were dated by biostratigraphy to 2.82–3.56 Ma at Site U1612 and 3.56–3.85 Ma at Site U1616. The oldest dates from biostratigraphy at Site U1614 were younger, 1.71–1.95 Ma; however, sediments directly overlying the basement at this site were reworked and could not be dated. Low recovery in this interval also limits accurate dating. Further age constraints will be provided by postcruise analyses of magnetostratigraphy and tephrochronology. Microfossil assemblage studies will also allow for estimating the paleodepths of the Tyrrhenian seafloor during the crustal thinning/exhumation phase. This information, placed in the context of knowledge of the basin, will allow us to reconstruct the geometry of the Tyrrhenian basin before, during, and after crustal extension and to follow its kinematic development over time until mantle exhumation.

### 4.2.2. Objective 2: to determine the heterogeneity of the mantle source and establish the timing and origin of the associated magmatism

Expedition 402 recovered an exceptionally varied suite of basement rocks in the Vavilov Basin at Sites U1612, U1614, and U1616 (Figures **F1**, **F4**, **F5**). At Site U1612, the sediment/basement interface (324 mbsf) is marked by an unconsolidated breccia with clasts of basalt, peridotite, and granite. Below the breccia, a crystalline basement interval (333–345 mbsf) consists of variably deformed gneisses at the top (ultramylonite to mylonite to protomylonite) with thin peridotite intervals that transition downhole to a granitoid with a predominantly quartz-diorite composition. This finding was surprising because the Vavilov Basin basement was expected to be dominantly mantle peridotite; unfortunately, drilling problems prevented us from advancing in Hole U1612 to sample the deeper basement rocks, although on the last few cores we did recover some more peridotite between granitoids.

The anticipated mantle rocks were successfully cored at Sites U1614 and U1616. The ~140 m thick interval of basement drilled at Site U1614 returned an extremely diverse set of lithologies, consisting of lherzolites, harzburgites, plagioclase-bearing lherzolites, plagioclase-bearing harzburgites, dunites, and minor amounts of pyroxenites and of mantle intrusions. The lithologies recovered from the ~125 m thick basement interval drilled at Site U1616 are much less variable, consisting primarily of harzburgites and lherzolites with some mafic intrusions. Plagioclase-bearing lherzolites and harzburgites are absent in the uppermost 70 m of basement drilled, and the Site U1616 mantle rocks are more depleted than those at Site U1614. At both sites, the vertical distribution of the various lithologies does not show distinct trends, except that depleted harzburgites and dunites seem more prevalent at shallower depths. An extraordinary characteristic of the Vavilov Basin mantle rocks is the presence of magmatic intrusions of plagioclase and phlogopite that indicate the injection of K-rich magmas.

The recovered mantle section probably represents a portion of subcontinental lithosphere that was extensively modified by melts generated before and during exhumation. Compared to mantle material recovered from mid-ocean ridges and magma-poor COTs, the samples cored during Expedition 402 are exceptionally heterogeneous, on average more fertile, and contain magmatic intrusions that may have been generated during rifting. Whole-rock and mineral chemistry, including isotopic compositions of the samples collected during Expedition 402, will elucidate the origin and timing of the peridotites/pyroxenites and magmatic events. Determinations of radiogenic isotopes, such as Nd-Hf-Os and U-Pb zircon ages, will provide insight into the timing of magmatic events and of the creation of mantle heterogeneities. Our findings will shed light on the mechanisms of mantle depletion and enrichment and their links to the tectono-magmatic evolution of COTs.

### 4.2.3. Objective 3: to establish the rheology, deformation patterns, and timing of mantle exhumation

At Sites U1612, U1614, and U1616, we recovered a suite of igneous rocks that included various types of peridotites such as harzburgite, lherzolite, and dunite, as well as mafic intrusions and sialic rocks like granitoids. These rocks carry evidence of brittle and ductile deformation distributed in bands of various widths, ranging from centimeters to meters. At times, deformation led to mylonitization (e.g., as seen at Site U1612). Veins composed of carbonates or serpentine, as well as high-temperature minerals, were frequently observed.

Strain localization for detachment formation requires strain weakening. The presence of both peridotites and granitoids with different rheological behavior provides a unique opportunity to investigate which lithologies accommodate strain and lead to weakening. Based on experimental work, weakening is reached at 550°C in felsic rocks dominated by quartz and feldspar, whereas olivine-dominated rocks need temperatures between 750° and 1200°C (e.g., Ruh et al., 2024). At Sites U1614 and U1616, mylonites are present both in the peridotites and granitoids, and at Site U1614, fault zones seem to be localized around the granitoids. This recovered material will allow for investigating the localization of stress and the deformation patterns of peridotite and granitoids. In the peridotites, deformation patterns will be explored with electron backscattering diffraction (EBSD) on olivine, pyroxenes, plagioclase, spinel, and amphibole; deformation of quartz and plagioclase can be examined in the granitoids. Comparing the rheology between the two rock types by using microstructural analyses, EBSD data, and flow laws will give insights into exhumation processes and strain localization in the mantle.

Granitoids are also ideal lithologies to obtain the ages of emplacement, deformation/fluid rock interactions, and exhumation. Zircon and apatite U-Pb, U-Th-He, and fission track analysis as well as amphibole Ar/Ar in the granitoids can be utilized. The closure temperatures of these geo/thermochronometers from ~900° to 70°C will collectively provide a depth/time evolution of the entire geologic history of the granitoids.

The magnetization of the peridotites can also provide constraints on the timing of mantle exhumation. Basement peridotites were found to be normally magnetized in Site U1616, whereas they were reversely magnetized in Site U1614 (Figure **F14**). If magnetization was acquired when ser-

pentinization formed magnetite, serpentinization (and hence exposure to seawater during exhumation) must have happened at different times in the two sites.

### 4.2.4. Objective 4: to determine the fluid-rock interactions in the peridotite basement

Significant hydration and weathering of peridotite is evident at Sites U1612, U1614, and U1616. The peridotites at these sites are locally cut by low-temperature serpentine veins and carbonate veins. Moreover, olivine in the serpentinite matrix is partly weathered into pores that are occupied by carbonate minerals. Microtextures composed of primary anhydrous minerals and secondary hydrous minerals differ between Sites U1614 and U1616, and there are also differences in hydrous mineral phases. Further study of the cored samples will reveal differences in the pressure-temperature-oxidation states between the two sites, which will contribute to understanding the exhumation history of the mantle rocks. Mineral chemistry of the serpentinite and carbonates, including stable isotopic compositions of carbon and oxygen, and metamorphic petrology will enable us to understand the fluid composition and source of hydration and carbonation.

Serpentinization is an exothermic reaction that generates hydrogen and methane if a carbon source is present (Schrenk et al., 2013). In sediment at Site U1614, we observed a downhole increase in the concentrations of pore water sulfate and of headspace methane just above the sediment/basement interface (265 mbsf). This concentration gradient suggests that sulfate and methane may be diffusing upward from the underlying peridotite. Measuring the $\delta^{13}C$ of the carbon will allow us to confirm whether the methane is abiotic (e.g., Milkov and Etiope, 2018) and derives from serpentinization-related processes.

Serpentinization reactions are a source of magnesium (Mg) when peridotite is exposed to seawater (Klein et al., 2020). The Mg pore water concentration profiles in the sediments of the Vavilov Basin sites (U1612 and U1614–U1616) show a decrease with depth from a seafloor value near the Mg content of Mediterranean deep waters (61 mM; Michard et al., 1974) to a minimum around 10–20 mM at 150–200 mbsf (Figure **F15**). Below this minimum, Mg concentrations increase with depth at Sites U1612, U1615, and U1616, where the concentration gradient may reflect variable heat flows and degrees of serpentinization processes between sites. The temperature gradients in the Vavilov Basin sites may be affected by the intensity of exothermic serpentinization reactions that can drive hydrothermal circulation, leading to transport of pore water solutes such as Mg. The data on carbonate composition, Mg concentration, and in situ temperature acquired in the Vavilov Basin sites will provide key information to investigate the complex fluid-rock interactions brought about by peridotite serpentinization.

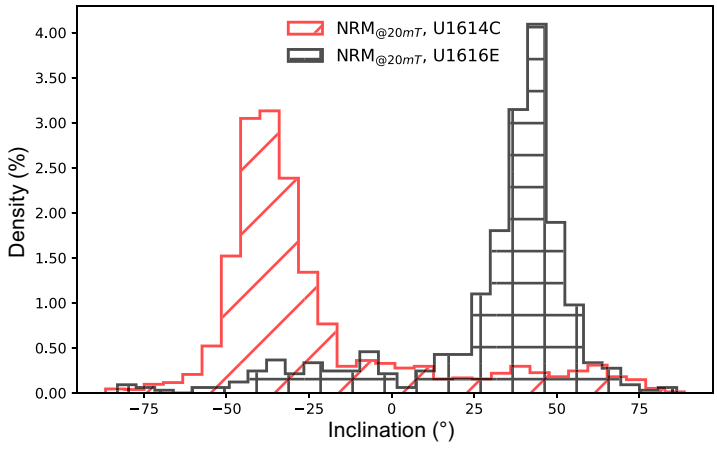


**Figure F14.** Inclination histograms of NRM after demagnetization for basement rocks, Holes U1614C and U1616E. The serpentinized peridotites from the two holes recorded opposite polarities.

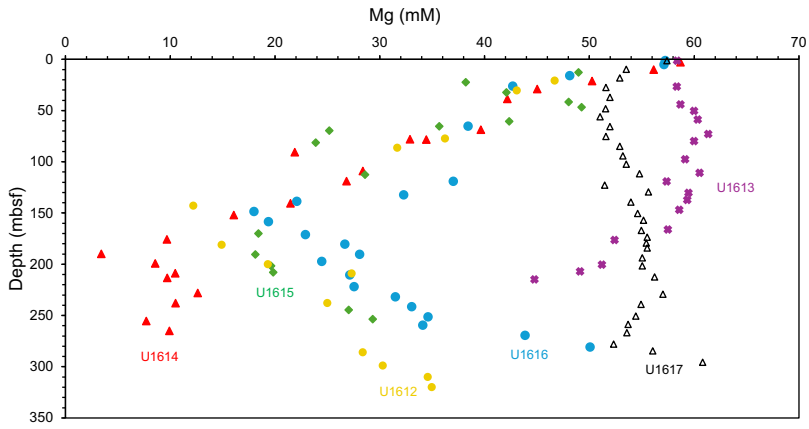


**Figure F15.** Mg concentration in sediment pore waters, Expedition 402 sites. Mg variation with depth may be attributed to the combination of the extent of basement serpentinization, reactions between carbonate minerals, and hydrothermal fluid circulation.

### 4.2.5. Objective 5: to test models of rifting and COT formation

Expedition 402 results addressing Objectives 1–4 also provide a new set of data to inform and constrain COT formation models. These new constraints include the timing of extension and subsidence on the conjugate margins surrounding the area of mantle unroofing, the timing of mantle exhumation and the rates of motion on the detachment faults, the overall geometry of the detachments (in combination with other information from seismic reflection records, bathymetry, and tectonic analysis), the spatial distribution of magmatism and alteration during the exhumation process, and the extent and effects of fluid-rock interactions. The modeling efforts will initially be focused on the Tyrrhenian system, but the insights gained can be later extended to other environments and improve our general understanding of the fundamental processes that form COTs.

# 5. Outreach

Expedition 402 had two Education and Outreach officers onboard. One outreach officer was recently a program manager for a vocational training program but previously worked in both formal and informal education spaces like museums and adult education centers. The other outreach officer came from a maritime background on research vessels where she made short, educational videos detailing data collection on board and worked with the National Science Foundation at events and on podcasts.

## 5.1. Live broadcasts

### 5.1.1. Ship-to-shore broadcasts

A total of 104 ship to shore broadcast sessions were held for over 5,317 individuals. Of the 104 sessions, 48 of them were led entirely in Italian. One event for two Chinese elementary and high school assemblies was live-streamed through Xinhua News, reaching an additional 444,000 public viewers. Weekly statistics for ship-to-shore broadcasts are listed in Table **T2**.

Other countries participating in the broadcasts included Brazil, China, Greece, Italy, France, Netherlands, Japan, Switzerland, United Kingdom, and the United States. The two most common languages for ship to shores were English and Italian, but broadcasts were additionally conducted in Japanese, Portuguese, Greek, and Chinese. The audiences for formal education spaces ranged from elementary to postdoctoral scientists, with group sizes ranging from 18 to as many as 230. Informal groups that consisted of friends, family, colleagues, or random adults ranged in size from 1 to 18. Some key groups that participated on broadcasts were the Geological Society of Italy and the Kochi Science Museum.

### 5.1.2. Collaborative broadcasts

Shadow the Scientists was a collaborative effort that happened during Expedition 401, and two more broadcasts were held for the group during Expedition 402. One was held for a "Science Fest," during which the tour was given at a booth to a shifting audience. The second broadcast was open to any of the public and their followers. Both sessions were recorded and posted on the Shadow the Scientists YouTube channel.

### 5.1.3. Reach the World broadcasts

Reach the World scheduled three livestreams through their preferred platform, StreamYard, for their audience (middle and high school groups following the expedition) to talk directly to the scientists from Expedition 402. The first broadcast was an introduction focused on questions about expedition objectives and how it was boarding the ship, the second focused on the core flow and the core laboratories, and the third focused on the chemistry, thin section, and X-ray laboratories. Scientists and technicians alike participated on the second and third calls. These broadcasts were livestreamed to the *JOIDES Resolution* YouTube channel and are available to watch as recordings.

### 5.1.4. Precruise collaboration

Before the expedition left port in Naples on 11 February, the outreach officers were invited to an European Consortium for Ocean Research Drilling (ECORD) School of Rock, where they shared what resources are available to local science teachers at **https://joidesresolution.org**. There were 30 teachers in that session. This effort appeared successful in increasing sign ups for ship to shore broadcasts.

### 5.1.5. Science and art broadcast

One outreach officer conducted a project to provide opportunities for people to merge art with science by drawing thin sections. The outreach officers collaborated with a metamorphic petrologist to co-lead two broadcasts, during which individuals were guided through drawing the scientific features while observing colors, shapes, and "what they see." The first broadcast had 7 participants, and the second broadcast had 13.

## 5.2. Expedition activities

### 5.2.1. Blog

Four blog posts were published at **https://joidesresolution.org** for Expedition 402:

- "Experiencing time or the lack of it while at sea" focuses on the adjustment it takes for someone to get onto their shift, in a different time zone, and work into the night.
- "What do soda cans, resistivity, and drilling have to do with each other?" focuses on an experiment that was completed by the Schlumberger engineer and the downhole logging specialist to determine what resistivity the drilling mud. It included a 5 min YouTube video.
- "A rock is a rock is it not" focuses on the peculiar nature of drilling for rocks and sediment all around the world and still being surprised by what you pull up. It highlights some quotes from technicians and crew about what surprises them.

**Table T2.** Statistics of ship to shore outreach, Expedition 402.

| Weeks | Number of Ship to Shores | Number of different languages | Number of Italian tours | Total number of participants |
|---|---|---|---|---|
| 1 | 2 | 1 | 2 | 31 |
| 2 | 2 | 2 | 3 | 228 |
| 3 | 18 | 5 | 7 | 649 |
| 4 | 12 | 2 | 8 | 434 |
| 5 | 15 | 4 | 8 | 570 |
| 6 | 21 | 4 | 13 | 1,920 |
| 7 | 20 | 4 | 6 | 620 |
| 8 | 9 | 3 | 1 | 444,865 |

**Table T3.** Statistics of social media engagement, Expedition 402. NA = not applicable.

| Platform | Timeframe | Number of posts | Impressions/Reach | Engagements |
|---|---|---|---|---|
| Instagram | Feb 12–Apr 6 | 190 | 8,492 | 3,903 |
| X/Twitter | Feb 12–Apr 6 | 140 | 159,789 | 7,922 |
| Threads | Feb 12–Apr 6 | 14 | NA | 199 (likes) |
| Facebook | Feb 12–Apr 6 | 176 | 3,933,378 | 49,205 |

- "Pet wall of Expedition 402" introduces the concept of the pet wall and why it is done. It also takes quotes from scientists on board and has them identify which science their pet would partake in. The purpose of this blog was to be lighthearted for the start of the expedition.

In addition to the blog posts, "Tyrrhenian Continent Ocean Transition" is the expedition summary page used to identify the expedition purpose, expedition dates, expedition Co-Chief Scientists, and Expedition Project Manager and showcase the expedition logo.

### 5.2.2. Reach the World partnership

Reach the World has been partnering with the *JOIDES Resolution* outreach team since Expedition 393. The outreach officers develop weekly blogs, and albums of pictures that are catered to prompts set by the Reach the World team. In total, 7 blogs and 7 albums were generated for the set of middle and high school groups that were following the expedition.

## 5.3. Social media

Both outreach officers posted on the *JOIDES Resolution* social media channels (X [formerly Twitter], Instagram, Facebook, and Threads). Threads was posted on less than the rest, with at least 2 posts a week, and the other channels had over 20 posts a week. Statistics for social media impact are listed in Table **T3**.

### 5.3.1. Daily videos

Daily life onboard was documented through 35–90 s videos shared on all social platforms. These videos captured not only the onboard science but also shone a light on the other operations that made the science possible and aimed to humanize all those involved in scientific drilling. A total of 49 videos were published.

### 5.3.2. LIVES on Instagram

Six Instagram Live broadcasts occurred with audience sizes ranging 30–100 throughout the 18–60 min sessions. The broadcasts took viewers to various laboratories and on deck to explain operations and data collection in real time. The audience was engaged, and the feedback on comments was positive.

# References

Argnani, A., and Savelli, C., 1999. Cenozoic volcanism and tectonics in the southern Tyrrhenian sea: space-time distribution and geodynamic significance. Journal of Geodynamics, 27(4):409–432. **https://doi.org/10.1016/S0264-3707(98)00025-8**

Beccaluva, L., Bonatti, E., Dupuy, C., Ferrara, G., Innocenti, F., Lucchini, F., Macera, P., Petrini, R., Rossi, P.L., Serri, G., Seyler, M., and Siena, F., 1990. Geochemistry and mineralogy of volcanic rocks from ODP Sites 650, 651, 655, and 654 in the Tyrrhenian Sea. In Kastens, K.A., Mascle, J., et al., Proceedings of the Ocean Drilling Program, Scientific Results. 107: College Station, TX (Ocean Drilling Program), 49–47. **https://doi.org/10.2973/odp.proc.sr.107.140.1990**

Boillot, G., and Winterer, E.L., 1988. Drilling on the Galicia margin: retrospect and prospect. In Boillot, G., Winterer, E. L., et al., Proceedings of the Ocean Drilling Program, Scientific Results. 103: College Station, TX (Ocean Drilling Program), 809–828. **https://doi.org/10.2973/odp.proc.sr.103.180.1988**

Bonatti, E., Seyler, M., Channell, J.E.T., Giraudeau, J., and Mascle, G., 1990. Peridotites drilled from the Tyrrhenian Sea, ODP Leg 107. In Kastens, K.A., Mascle, J., et al., Proceedings of the Ocean Drilling Program, Scientific Results. 107: College Station, TX (Ocean Drilling Program), 37–47. **https://doi.org/10.2973/odp.proc.sr.107.141.1990**

Cannat, M., Sauter, D., Bezos, A., Meyzen, C., Humler, E., and Le Rigoleur, M., 2008. Spreading rate, spreading obliquity, and melt supply at the ultraslow spreading Southwest Indian Ridge. Geochemistry, Geophysics, Geosystems, 9(4). **https://doi.org/10.1029/2007GC001676**

Caratori Tontini, F., Stefanelli, P., Giori, I., Faggioni, O., Carmisciano, C., 2004. The revised aeromagnetic anomaly map of Italy. Annals of Geophysics, 47(5). **https://doi.org/10.4401/ag-3358**

Colantoni, P., Fabbri, A., Gallignani, P., Sartori, R., and Rehault, J.P., 1981. Carta Litologica e Stratigrafica dei Mari Italiani, scala 1/1.500.000. Italy: Litografia Artistica Cartografica.

Davis, J.K., and Lavier, L.L., 2017. Influences on the development of volcanic and magma-poor morphologies during passive continental rifting. Geosphere, 13(5):1524–1540. **https://doi.org/10.1130/GES01538.1**

Di Stefano, A., Baldassini, N., Raffi, I., Fornaciari, E., Incarbona, A., Negri, A., Negri, A., Bonomo, S., Villa, G., Di Stefano, E., and Rio, D., 2023. Neogene-Quaternary Mediterranean calcareous nannofossil biozonation and biochronology: a review. Stratigraphy, 20(4):259–302. **https://www.micropress.org/microaccess/check/2342**

Della Vedova, B., Pellis, G., Foucher, J.P., and Rehault, J.-P., 1984. Geothermal structure of the Tyrrhenian Sea. Marine Geology, 55(1984):271–289.

Di Stefano, A., Baldassini, N., Raffi, I., Fornaciari, E., Incarbona, A., Negri, A., Bonomo, S., Villa, G., Di Stefano, E., Rio, D. (2023) Neogene-Quaternary Mediterranean calcareous nannofossil biozonation and biochronology: A review. Stratigraphy, 20/4, 259-302.

Duschenes, J., Sinha, M.C., and Louden, K.E., 1986. A seismic refraction experiment in the Tyrrhenian Sea. Geophysical Journal International, 85(1):139–160. **https://doi.org/10.1111/j.1365-246X.1986.tb05175.x**

Fabbri, A., and Curzi, P., 1979. The Messinian of the Tyrrhenian Sea: seismic evidence and dynamic implications. Giornale di Geologia, 43:215–248.

Faccenna, C., Becker, T.W., Lucente, F.P., Jolivet, L., and Rossetti, F., 2001. History of subduction and back arc extension in the Central Mediterranean. Geophysical Journal International, 145(3):809–820. **https://doi.org/10.1046/j.0956-540x.2001.01435.x**

Kastens, K.A., and Mascle, J., 1990. The geological evolution of the Tyrrhenian Sea; an introduction to the scientific results of ODP Leg 107. In Kastens, K.A., Mascle, J., et al., Proceedings of the Ocean Drilling Program, Scientific Results. 107: College Station, TX (Ocean Drilling Program), 3–26. **https://doi.org/10.2973/odp.proc.sr.107.187.1990**

Klein, F., Humphris, S.E., and Bach, W., 2020. Brucite formation and dissolution in oceanic serpentinite. Geochemical Perspectives Letters, 16:1–5. **https://doi.org/10.7185/geochemlet.203**

Lister, G.S., and Davis, G.A., 1989. The origin of metamorphic core complexes and detachment faults formed during Tertiary continental extension in the northern Colorado River region, U.S.A. Journal of Structural Geology, 11(1):65–94. **https://doi.org/10.1016/0191-8141(89)90036-9**

Malinverno, A., Cafiero, M., Ryan, W.B.F., and Cita, M.B., 1981. Distribution of Messinian sediments and erosional surfaces beneath the Tyrrhenian Sea: geodynamic implications. Oceanologica Acta, 4(4):489–496. **https://archimer.ifremer.fr/doc/00121/23232/21066.pdf**

Malinverno, A., and Ryan, W.B.F., 1986. Extension in the Tyrrhenian Sea and shortening in the Apennines as result of arc migration driven by sinking of the lithosphere. Tectonics, 5(2):227–245. **https://doi.org/10.1029/TC005i002p00227**

Michard, G., Church, T.M., and Bernat, M., 1974. The pore water chemistry of recent sediments in the western Mediterranean basin. Journal of Geophysical Research (1896-1977), 79(6):817–824. **https://doi.org/10.1029/JC079i006p00817**

Middlemost, E.A.K., 1994. Naming materials in the magma/igneous rock system. Earth-Science Reviews, 37(3–4):215–224. **https://doi.org/10.1016/0012-8252(94)90029-9**

Milkov, A.V., and Etiope, G., 2018. Revised genetic diagrams for natural gases based on a global dataset of >20,000 samples. Organic Geochemistry, 125:109–120. **https://doi.org/10.1016/j.orggeochem.2018.09.002**

Morelli, C., 1971. Physiography, gravity and magnetism of the Tyrrhenian Sea. Bollettino di Geofisica Teorica ed Applicata, 12:275–309.

Ogg, J.G., 2020. Geomagnetic Polarity Time Scale. In Gradstein, F.M., Ogg, J.G., Schmitz, M., and Ogg, G. (Eds.), Geologic Time Scale 2020. Amsterdam (Elsevier), 159–192. **https://doi.org/10.1016/B978-0-12-824360-2.00005-X**

Peccerillo, A., 2017. Cenozoic Volcanism in the Tyrrhenian Sea Region: (Springer). **https://doi.org/10.1007/978-3-319-42491-0**

Pérez-Gussinyé, M., Morgan, J.P., Reston, T.J., and Ranero, C.R., 2006. The rift to drift transition at non-volcanic margins: insights from numerical modelling. Earth and Planetary Science Letters, 244(1–2):458–473. **https://doi.org/10.1016/j.epsl.2006.01.059**

Prada, M., Sallares, V., Ranero, C.R., Vendrell, M.G., Grevemeyer, I., Zitellini, N., and de Franco, R., 2014. Seismic structure of the Central Tyrrhenian basin: Geophysical constraints on the nature of the main crustal domains. Journal of Geophysical Research: Solid Earth, 119(1):52–70. **https://doi.org/10.1002/2013JB010527**

Prada, M., Sallares, V., Ranero, C.R., Vendrell, M.G., Grevemeyer, I., Zitellini, N., and de Franco, R., 2015. The complex 3-D transition from continental crust to backarc magmatism and exhumed mantle in the Central Tyrrhenian basin. Geophysical Journal International, 203(1):63–78. **https://doi.org/10.1093/gji/ggv271**

Ruh, J., Behr, W., and Tokle, L., 2024. Effect of grain-size and textural weakening in polyphase crustal and mantle lithospheric shear zones. τεκτονικα, 2(1):91–110. **https://doi.org/10.55575/tektonika2024.2.1.68**

Sartori, R., Torelli, L., Zitellini, N., Carrara, G., Magaldi, M., and Mussoni, P., 2004. Crustal features along a W–E Tyrrhenian transect from Sardinia to Campania margins (Central Mediterranean). Tectonophysics, 383(3):171–192. **https://doi.org/10.1016/j.tecto.2004.02.008**

Sauter, D., Cannat, M., Rouméjon, S., Andreani, M., Birot, D., Bronner, A., Brunelli, D., Carlut, J., Delacour, A., Guyader, V., MacLeod, C.J., Manatschal, G., Mendel, V., Ménez, B., Pasini, V., Ruellan, E., and Searle, R., 2013.

Continuous exhumation of mantle-derived rocks at the Southwest Indian Ridge for 11 million years. Nature Geoscience, 6(4):314–320. **https://doi.org/10.1038/ngeo1771**

Schrenk, M.O., Brazelton, W.J., and Lang, S.Q., 2013. Serpentinization, carbon, and deep life. Reviews in Mineralogy and Geochemistry, 75(1):575–606. **https://doi.org/10.2138/rmg.2013.75.18**

Shipboard Scientific Party, 1978. Site 373: Tyrrhenian Basin. In Hsü, K., Montadert, L., et al., Initial Reports of the Deep Sea Drilling Project. 42(1): Washington, DC (US Government Printing Office), 151–174. **https://doi.org/10.2973/dsdp.proc.42-1.104.1978**

Shipboard Scientific Party, 1996. Site 974. In Comas, M.C., Zahn, R., Klaus, A., et al., Proceedings of the Ocean Drilling Program, Initial Reports. 161: College Station, TX (Ocean Drilling Program). **https://doi.org/10.2973/odp.proc.ir.161.104.1996**

The Shipboard Scientific Party, 1973. Gorringe Bank: Site 120. In William B.F. Ryan, K.J.H., et al., Initial Reports of the Deep Sea Drilling Project. 13: Washington, DC (US Government Printing Office), 19–41. **https://doi.org/10.2973/dsdp.proc.13.102.1973**

Tucholke, B.E., Lin, J., and Kleinrock, M.C., 1998. Megamullions and mullion structure defining oceanic metamorphic core complexes on the Mid-Atlantic Ridge. Journal of Geophysical Research: Solid Earth, 103(B5):9857-9866. **https://doi.org/10.1029/98JB00167**

Tucholke, B.E., Sawyer, D.S., and Sibuet, J.C., 2007. Breakup of the Newfoundland–Iberia rift. Geological Society Special Publication, 282(1):9. **https://doi.org/10.1144/SP282.2**

Wessel, P., Luis, J.F., Uieda, L., Scharroo, R., Wobbe, F., Smith, W.H.F., and Tian, D., 2019. The Generic Mapping Tools Version 6. Geochemistry, Geophysics, Geosystems, 20(11):5556–5564. **https://doi.org/10.1029/2019GC008515**